Yuan, G., Cao, Y., Schulz, H.-M., Hao, F., Gluyas, J., Liu, K., Yang, T., Wang, Y., Xi, K., Li, F. (2019): A review of feldspar alteration and its geological significance in sedimentary basins: From shallow aquifers to deep hydrocarbon reservoirs. - *Earth-Science Reviews*, *191*, pp. 114—140.

DOI: http://doi.org/10.1016/j.earscirev.2019.02.004

Earth-Science Reviews 191 (2019) 114–140

Contents lists available at ScienceDirect

Earth-Science Reviews

journal homepage: www.elsevier.com/locate/earscirev

A review of feldspar alteration and its geological significance in sedimentary basins: From shallow aquifers to deep hydrocarbon reservoirs

Guanghui Yuan[a,b,*], Yingchang Cao[a,b,*], Hans-Martin Schulz[c], Fang Hao[a], Jon Gluyas[d], Keyu Liu[a], Tian Yang[a], Yanzhong Wang[a], Kelai Xi[a], Fulai Li[a]

[a] Key laboratory of Deep Oil and Gas, School of Geosciences, China University of Petroleum, Qingdao, Shandong 266580, China
[b] Laboratory for Marine Mineral Resources, Qingdao National Laboratory for Marine Science and Technology, Qingdao, Shandong 266071, China
[c] GFZ German Research Centre for Geosciences, Section 4.3, Organic Geochemistry, Telegrafenberg, D-14473 Potsdam, Germany
[d] Department of Earth Sciences, Durham University, Durham DH1 3LE, UK

ARTICLE INFO

Keywords:
Feldspar alteration
Dissolution mechanisms
Rate law
Organic-inorganic interaction
Mineral assemblage
Shallow-deep reservoirs

ABSTRACT

The feldspar group is one of the most common types of minerals in the earth's crust. Feldspar alteration (including the whole processes of feldspar dissolution, transfer of released solutes, and secondary mineral precipitation) is ubiquitous and important in fields including resources and environmental sciences. This paper provides a critical review of feldspar alteration and its geological significance in shallow aquifers to deep hydrocarbon reservoirs, as assessed from peer-reviewed paper in the literature.

A variety of mechanisms such as the surface reaction-controlled dissolution mechanism, the preferential leaching-diffusion controlled mechanism, the diffusion-precipitation controlled dissolution mechanism and the interfacial dissolution-reprecipitation mechanism have been proposed to be responsible for the dissolution of feldspars. Feldspar dissolution rates can be affected by the crystal structure, Al/Si ordering, temperature, pH, surface area, organic acids, chemical affinity, and precipitation of secondary minerals. Five main dissolution rate laws have been used to describe feldspar dissolution rates, including the linear transition state theory (L-TST) rate law, non-linear TST rate law, parallel rate law, stepwave model rate law, and partial equilibrium law. The rate inconsistency between laboratory experiments and field observations is interpreted with hypotheses that include the armoring effects of the coating secondary minerals on feldspar surfaces, the possible effects of leached layers, the approach to saturation with respect to feldspars, the inhibition by absorbed Al^{3+} on the feldspar surface, and the inhibition by simultaneous slow clay precipitation rates.

The inorganic-original (meteoric water and deep hot water) and organic-original (kerogen and hydrocarbon degradation) hydrogen ion (H^+) in a fluid can probably act as a significant catalyzer of fast dissolution of feldspars in shallow aquifers and deep hydrocarbon reservoirs. Various mineral assemblages including extensively leached feldspars with a wide range of associated amounts of clay minerals and quartz cements can be identified in subsurface reservoirs under different geological conditions. Feldspar dissolution can generate enhanced secondary porosities and rock permeability in open geochemical systems at shallow depth or at a moderate-deep depth where faults develop widely. While in closed geochemical systems at moderate-deep depth, feldspar dissolution is likely to generate redistributional secondary porosities and to decrease rock permeability. Authigenic clay minerals formed following feldspar dissolution alter rock wettability and affect the charging and entrapment of hydrocarbons in reservoir. Feldspar alteration may promote hydrocarbon degradation by promoting bioactivity or by consuming low molecular weight organic acids and CO_2 produced via oil degradation. Further work should be conducted to study hydrocarbon-water-feldspar interactions in deeply buried hydrocarbon reservoirs. Feldspar alteration may promote CO_2 sequestration by consumption of H^+, generation of HCO_3^-, and pH buffering of formation water. K-feldspar alteration may also promote illitization in interbedded mudstones by supplying K^+.

* Corresponding authors at: Key laboratory of Deep Oil and Gas, School of Geosciences, China University of Petroleum, Qingdao, Shandong 266580, China.
E-mail addresses: yuan.guanghui@upc.edu.cn (G. Yuan), caoych@upc.edu.cn (Y. Cao).

https://doi.org/10.1016/j.earscirev.2019.02.004
Received 27 October 2017; Received in revised form 2 February 2019; Accepted 5 February 2019
Available online 18 February 2019

1. Introduction

Feldspars, which form the mineral series $KAlSi_3O_8$ (K-feldspar) – $NaAlSi_3O_8$ (albite) – $CaAl_2Si_2O_8$ (anorthite), constitute nearly one half of the earth's crust (Gout et al., 1997; Chardon et al., 2006; Crundwell, 2015a). Their alteration, which includes the physicochemical processes of feldspar dissolution, transfer of dissolved solutes, and concomitant secondary mineral precipitation, occurs ubiquitously from shallow to deeply buried rocks (Giles, 1987; Glasmann, 1992; Alekseyev et al., 1997; Lasaga and Luttge, 2001; Zhu et al., 2004; Fu et al., 2009; Kampman et al., 2009; Bjørlykke and Jahren, 2012; Crundwell, 2015b; Yuan et al., 2017a). Feldspar alteration plays significant roles in many aspects including surficial weathering and soil development (Berner and Holdren, 1979; Chou and Wollast, 1984; Lasaga et al., 1994; Beig and Lüttge, 2006; Maher et al., 2009; Ruizagudo et al., 2016), mass transfer in hydrothermal systems (Gout et al., 1997; Maher et al., 2009), geological carbon sequestration (Berg and Banwart, 2000; Bertier et al., 2006; Kampman et al., 2009; Liu et al., 2011; Lu et al., 2013; Wang et al., 2013; Tutolo et al., 2015), and diagenesis and evolution of porosity and permeability of sedimentary rocks (Surdam and Crossey, 1987; Glasmann, 1992; Bertier et al., 2006; Kampman et al., 2009; Bjørlykke and Jahren, 2012; Yuan et al., 2015a; Yuan et al., 2015b). As a result, feldspar alteration and its significance have been the subjects of experimental, theoretical, and practical studies over several decades.

Based on extensive experimental and theoretical studies, different dissolution mechanisms and various dissolution rate laws have been proposed to describe feldspar dissolution processes with respect to different parameters (Lagache, 1965; Berner and Holdren, 1979; Lasaga, 1984; Barth and Bjørlykke, 1993; Oelkers and Schott, 1995; Alekseyev et al., 1997; Gout et al., 1997; Lasaga and Luttge, 2001; Hellmann and Tisserand, 2006; Crundwell, 2015a; Crundwell, 2015b). In addition, different hypotheses have been proposed to explain the inconsistency between the dissolution rates obtained by laboratory experimental studies and the rates measured in natural reservoirs (Lasaga and Luttge, 2001; Zhu et al., 2004; Hellmann and Tisserand, 2006; Zhu et al., 2010). However, there are still three issues need further attention with the feldspar dissolution mechanisms and the dissolution rates when it comes to the subsurface rocks in the field. The first issue concerning secondary minerals that occuring as pore-filling minerals but not coatings on the feldspar surfaces, concomitant precipitation of such secondary minerals following feldspar dissolution has not receive enough attention. Secondly, the advective and dissuasive mass transfer processes linking feldspar dissolution and secondary mineral precipitation in porous subsurface rocks (particularly tight rocks) with fluid flows (Giles, 1987; Steefel et al., 2005) that may control the complexity of diagenetic processes including feldspar dissolution rates have not been given enough consideration. Still, the precipitation and re-dissolution of secondary minerals (eg. gibbsite, boehmite, kaolinite, illte, muscovite) in subsurface rocks under condition close to equilibrium make it difficult to distinguish the amount of dissolved feldspars in per unit of time (Thyne et al., 2001; Zhu et al., 2010). Thus, the feldspar dissolution mechanisms and the dissolution rate laws in subsurface porous rocks still require further studies with integrated consideration of leaching processes, advective and diffusive mass transfer processes, and precipitation processes, particularly at conditions close to equilibrium when secondary minerals can be precipitated and be redissolved to form other minerals (Zhu et al., 2004; Hellmann and Tisserand, 2006; Zhu et al., 2010).

In sedimentary basins, inorganic-original feldspar dissolution may originate from leaching by meteoric freshwater (Emery et al., 1990; França et al., 2003) or deep hot fluids (Taylor and Land, 1996). Organic-original feldspar dissolution in subsurface sedimentary rocks refers to leaching reactions induced by the CO_2 and organic acids originating from kerogen maturation and hydrocarbon degradation (Surdam and Crossey, 1987; van Berk et al., 2013; Yuan et al., 2015b; Yuan et al., 2017a). And the organic-inorganic interactions and the mutual impact between feldspar alteration and hydrocarbon degradation in the deeply-buried reservoirs still requires further studies. Practical studies have highlighted the geological significance of feldspar alteration with regard to several aspects including reservoir quality evolution, rock wettability, subsurface microorganism, hydrocarbon degradation, illitization and CO_2 sequestration. Feldspar alteration under different physicochemical conditions results in various diagenetic mineral assemblages (Giles and Boer, 1990; Taylor et al., 2010; Yuan et al., 2017a) and may modify rock porosity, permeability, and wettability (Barclay and Worden, 2009). The feldspar alteration in shallow aquifers and deeply buried reservoirs in sedimentary basins may represent one aspect of a successful CO_2 sequestration and may cause illitization reactions in mudstone-sandstone systems (Thyne et al., 2001; Bertier et al., 2006; van Berk et al., 2013; Tutolo et al., 2015; Yuan et al., 2015b). In summary, a wealth of data gained from experimental, theoretical, and practical studies about the mechanisms of feldspar dissolution, processes and kinetics, organic and inorganic reaction paths, and mineral assemblages have provided a platform to study ancient, modern, and future fluid-rock interactions in feldspar-rich systems ranging from shallow aquifers to deeply buried hydrocarbon reservoirs.

In this paper, we review feldspar alteration in light of the dissolution mechanisms, the dissolution rate law, the organic-inorganic interactions, and as a result of primary and secondary mineral assemblages from shallow to great depth, we also discuss existing problems to provide suggestions for future studies.

2. Feldspar dissolution mechanisms and rate laws

2.1. Dissolution mechanism

The dissolution mechanisms of feldspars have been studied extensively using various dissolution experiments and analytical techniques (Chardon et al., 2006). In summary, four main mechanisms including the (1) surface reaction-controlled dissolution mechanism (Lagache et al., 1961a, Lagache et al., 1961b; Berner and Holdren, 1979), (2) preferential leaching-diffusion controlled mechanism (Correns and Von, 1938; Correns, 1940; Chou and Wollast, 1984; Hellmann, 1994a; Oelkers and Schott, 1995; Gout et al., 1997; Chardon et al., 2006), (3) interfacial dissolution-reprecipitation mechanism (Hellmann et al., 2003; Hellmann et al., 2012; Ruiz-Agudo et al., 2012; Putnis, 2014; Hellmann et al., 2015; Ruiz-Agudo et al., 2016), and (4) diffusion-precipitation controlled dissolution mechanism (Wollast, 1967; Helgeson, 1971; Helgeson, 1972) have been proposed.

2.1.1. Surface reaction-controlled dissolution mechanism

The surface reaction-controlled dissolution mechanism was proposed in which the dissolution of feldspars is assumed to be controlled by a surface reaction, and the detachment reaction of elements at the solution/surface interface controls the overall rate of reaction (Lagache et al., 1961a, Lagache et al., 1961b; Lagache, 1965; Berner and Holdren, 1979; Chou and Wollast, 1984). This mechanism is supported by the etch pit formation at surface sites with excess energy (dislocations, twin boundaries, etc.), the stoichiometric (congruent) dissolution (Fig. 1), and linear reaction kinetics at steady state conditions far from equilibrium (Berner and Holdren, 1979; Chou and Wollast, 1984; Hellmann, 1994a; Alekseyev et al., 1997). Using X-ray photoelectron spectroscopy, Berner and Holdren (1979) showed that the outer thin surfaces of fresh feldspars and altered feldspars exhibited little differences in composition, after removing the adhering clays on the surface. The using of etch pits as a representation of surface reactions still need more discussion, as has been showed by compositions of feldspar surfaces with and without etch (Gout et al., 1997). The surface reaction-controlled feldspar dissolution was identified to occur generally in alkaline fluids, although there is still debate on this topic (Chou and Wollast, 1984). For the surface reaction-controlled dissolution, from the

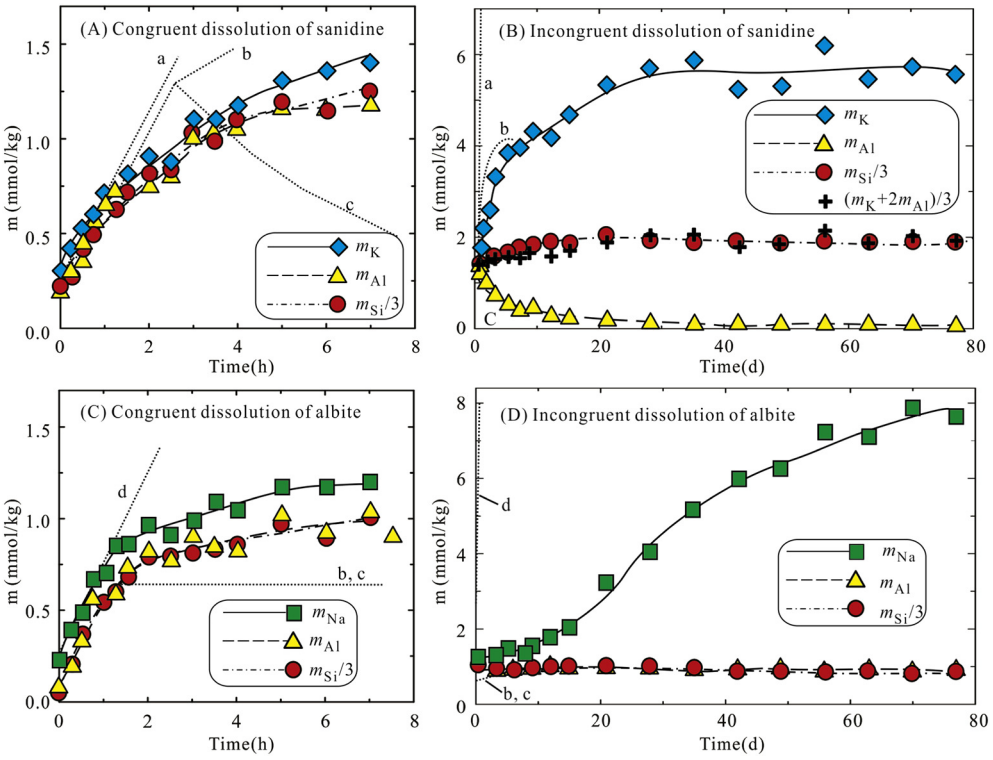

Fig. 1. Change in element concentrations as a result of the interactions between sanidine + $NaHCO_3$ (A, B) and albite + $KHCO_3$ (C, D) in the time intervals 0–7 h (a, c) and 7 h to 77 days (b, d). The filled symbols denote measured concentrations. Their averaged values are connected by polygonal lines. The open squares in Fig. 1d denote values of m_{Na} calculated from X-ray diffraction data. Dotted curved a(m_k), b($m_{Si}/3$), c(m_{Al}), and d (m_{Na}) were calculated using Eq. 6 with $n = 0$ and measured initial reaction rates in the experiments conducted in Alekseyev et al., 1997.

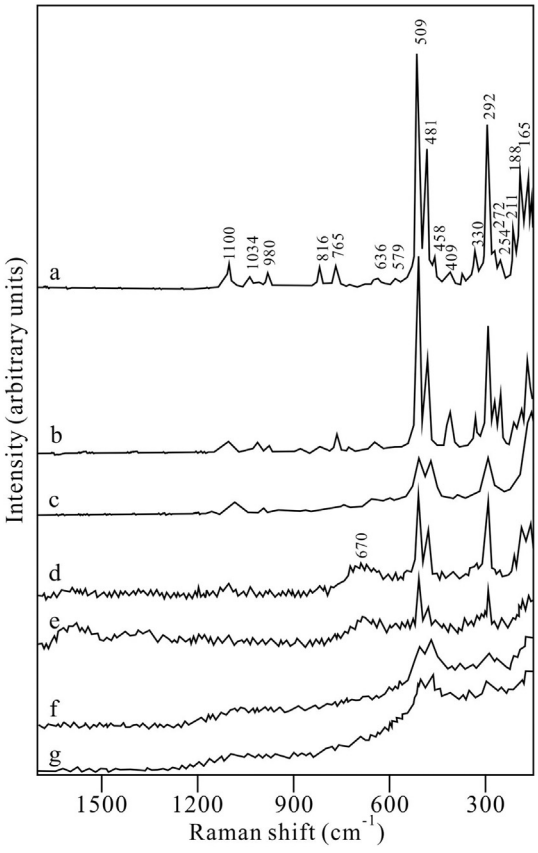

Fig. 2. Raman spectra of (a) unreacted albite and (b-g) albite after dissolution in a 0.3 *m* HCl aqueous solution at 200 °C for 2 h.
Spectra b-g are arranged in order of increasing degree of surface alteration. (after Gout et al., 1997).

congruent dissolution stage when molar ratios of the amounts of released elements to solution are in consistent with the parent feldspars to the so-called incongruent dissolution stage when the molar ratios of the released elements are different from the parent feldspars (Fig. 1), the fluid-mineral system evolves from far from equilibrium to near equilibrium, and the incongruency observed during dissolution is attributed to the consumption of aluminum and silica by secondary precipitation of aluminum hydroxide, aluminum silicate, or analcime with chemical composition distinct from the feldspar surface (Berner and Holdren, 1979; Alekseyev et al., 1997).

2.1.2. *Preferential leaching-diffusion controlled mechanism*

The preferential leaching-diffusion controlled mechanism was proposed first by Correns and Von (1938) and Correns (1940). It is initially assumed on the basis of a non-stoichiometric (incongruent) dissolution and the observed parabolic dissolution kinetics (Al and Si concentrations in fluid versus time) that the dissolution rate is controlled by the development and evolution of a leached layer built at the surface of the feldspar through which reactants and dissolution products must diffuse (Wollast, 1967; Chou and Wollast, 1984; Lasaga, 1984). As the leached layer grows, diffusion of the leachable species through the layer becomes harder and the dissolution rate will slow down, leading to generation of the parabolic concentration of Al and Si version time curve. The overall feldspar dissolution rate is jointly controlled by the ion exchange between hydrogen ion and cations (Na^+, K^+, Ca^{2+}) in the minerals, a sequential bond breaking (Al-O-Si, Si-O-Si) reaction (Muir et al., 1990; Gautier et al., 1994; Oelkers and Schott, 1995; Yang et al., 2013; Yang et al., 2014a), and the inward diffusion of reactants and/or the outward diffusion of hydrolysis products through a chemically and structurally near-surface altered layer between the fluid-solid interface and the unaltered mineral matrix (Chou and Wollast, 1984; Chou and Wollast, 1985; Hellmann, 1994a; Hellmann et al., 2003; Chardon et al., 2006), and the slowest rate of these processes controls the overall dissolution rate. This hypothesis is supported by the non-stoichiometric solute concentrations (K^+, Na^+, Al, Si) in solution (Chou and Wollast, 1984; Chou and Wollast, 1985) and the different near-surface compositions (Gout et al., 1997; Chardon et al., 2006) of feldspars from

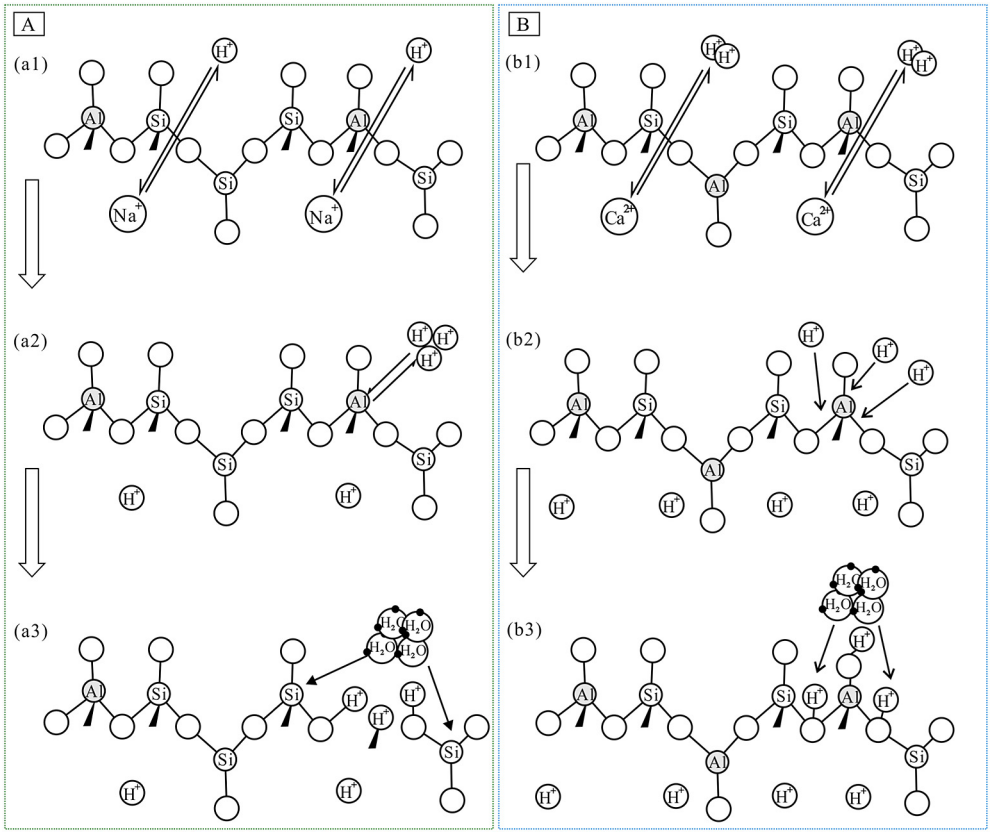

Fig. 3. (A) Schematic illustration depicting the three major steps in the dissolution of an alkali feldspar. (a1) the exchange of hydrogen with alkali ions in the feldspar structure, (a2) an exchange reaction among aqueous hydrogen ions and Al in the feldspar framework leading to the formation of Al-deficient surface precursor complexes, (a3) the irreversible detachment of the precursor complex. (B) Schematic illustration depicting the three major steps in the dissolution of anorthite. (b1) an exchange of hydrogen with calcium in the feldspar structure. (b2) the adsorption of hydrogen ions leading to the formation surface precursor complexes. (b3) the irreversible detachment of the precursor complex. (after Gautier et al., 1994; Oelkers and Schott, 1995).

unaltered to extensively altered regions (Fig. 2). However, the fractional orders of the dissolution reaction with respect to H^+ does not support this hypothesis as diffusional processes can only be first order (Crundwell, 2015a).

With different chemical bonds (Muir et al., 1990; Gautier et al., 1994; Oelkers and Schott, 1995; Yang et al., 2013), the reactions that occur within the feldspar framework structure are elementally rate-specific and each element reacts at a different rate with the reactant molecules, which diffuse into the structure; the differential rate of detachment results in the formation of the leached layers (Chou and Wollast, 1984; Hellmann, 1994a). Gautier et al. (1994) and Oelkers and Schott (1995) proposed that alkali feldspar hydrolysis under acidic conditions consists of three steps including: ① the relatively rapid exchange of hydrogen and alkali ions near the mineral surface, ② an exchange reaction between three hydrogen atoms in solution with one aluminum atom in the mineral structure resulting in the breaking of Al—O bonds, coupled with the formation of a rate-controlling Si-rich precursor complex, and ③ the hydrolysis of Si—O bonds releasing the precursor complex into solution (Fig. 3A). The removal of Si still requires the breaking of Si—O bond and thus the overall alkali feldspar dissolution rate is controlled by the decomposition of a silica-rich surface precursor in geochemical systems at far from equilibrium conditions (Gautier et al., 1994; Oelkers and Schott, 1995). Although anorthite has a different Al/Si ratio, the coordination of Al in the structure of the anorthite is identical to albite, and Oelkers and Schott (1995) proposed a similar three-step dissolution scheme for the anorthite dissolution under acidic conditions including: ① the relatively rapid exchange of hydrogen and alkali ions near the mineral surface, ② the adsorption of hydrogen ions leading to the formation of a surface precursor complex, and ③ the irreversible detachment of the precursor complex (Fig. 3B). The preferential leaching-diffusion controlled feldspar dissolution occurs in far-from-equilibrium geochemical systems, and the breaking rate of the Al—O and (or) Si—O bonds and the diffusion rate of the solutes through the altered layer control the overall feldspar dissolution rate (Oelkers and Schott, 1995).

The relatively faster release of cations (Na^+, K^+, Ca^{2+}) and certain framework elements (Al) of feldspar under acidic conditions lead to the formation of a leached layer that are enriched in Si and (or) Al (Fig. 4A) (Correns and Von, 1938; Correns, 1940; Chou and Wollast, 1984; Hellmann, 1994a). The thickness of the altered layer varies among the layers in different water systems, with different mineral chemical compositions, and for various feldspars with different Si/Al ordering (Chou and Wollast, 1984; Muir et al., 1990; Muir and Nesbitt, 1991; Nesbitt et al., 1991; Yang et al., 2013). Commonly, the depths of the residual layer range from tens to many hundreds Å, and the depth increase as temperature increase and pH decrease (Chou and Wollast, 1984; Muir and Nesbitt, 1991), maximum depths on the order of 1500 Å were recorded under acid pH conditions (Table 1). Lower pH tends to generate thicker leached layers, while addition of cations (eg. K+, Na, Ca, particularly Al(aq) and Si(aq)) in initial solutions tends to decrease the thickness of the leached layers (Muir and Nesbitt, 1991; Nesbitt et al., 1991). Generally, the Na^+ (K^+ or Ca^{2+}) depleted residual layer is the thickest, followed by the cation & Al depleted residual layer (Fig. 4A). Na^+ depleted leached layers developed on albite during the initial stages of dissolution due to the preferential release of Na with respect to Al and Si under all pH and temperature conditions (Chou and Wollast, 1984; Hellmann, 1994a; Oelkers and Schott, 1995). Leached layers deficient in Al (with respect to Si) were generally recorded under acid and neutral pH condition; under mildly basic pH conditions, either Al or Si was preferentially released and under more extreme basic pH conditions, only Al was preferentially retained (Chou and Wollast, 1984; Hellmann, 1994a).

Theoretically, the residual surface layers can reach a constant thickness due to the dissolution of the leached layer at its outer part (Chou and Wollast, 1984; Lasaga, 1984). Transmission electron microscopy (TEM) demonstrated that the thicknesses of the interfacial layers of plagioclases follow the order of labradorite > albite > anorthite and sanidine > microcline, consistent with their Al/Si

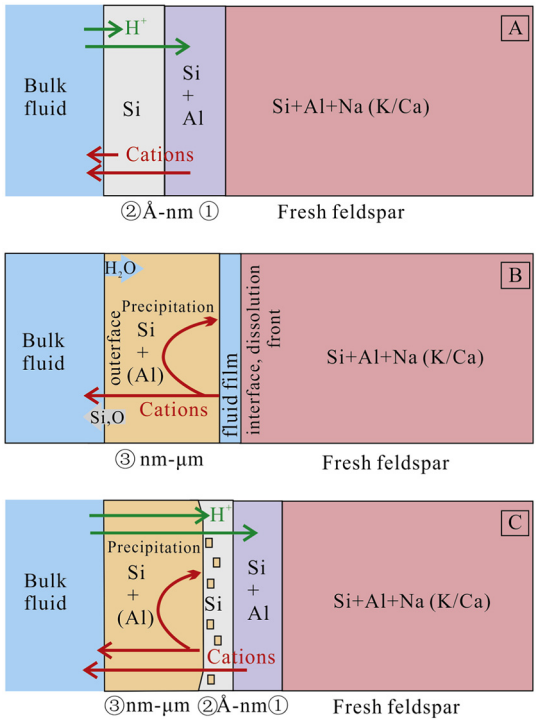

Fig. 4. (A) Schemitic illustration depicting the preferential leaching-diffusion controlled mechanism (modified from Chou and Wollast, 1984); (B) Schemitic illustration depicting the interfacial dissolution-reprecipitation mechanism with development of fluid film between the fresh feldspar surface and the re-precipitated alter layer (modified from Hellmann et al., 2012); (C) Schemitic illustration depicting the diffusion-precipitation controlled dissolution mechanism for dissolution of feldspar under acidic to neutral conditions. The area of ① represents the Na(K, Ca)-depleted residual layer, ② represents the Al-depleted residual layer, ③ represents the reprecipitated layer with Al, Si or both. Green line arrows represent the internal transfer of H^+ into altered layers, red line arrows represents the external transfer of elements into altered layer and fluid solution; red curved arrows represent reprecipitation and retention of some released elements. (For interpretation of the references to colour in this figure legend, the reader is referred to the web version of this article.)

ordering states from disordered to ordered (Yang et al., 2013; Yang et al., 2014a). This is because a more ordered structure has a chance of isolating aqueous species by a well-placed "wall" of Si (Fig. 5A), whose decomposition requires the hydrolysis of the less reactive Si–O–Si linkages, while the randomness of the Al/Si substitution in a less ordered feldspar facilitates the penetration of the aqueous species easier by making the more reactive Al–O–Si linkages available for hydrolysis (Fig. 5B) (Yang et al., 2013). However, dissolution experiments have demonstrated that the dissolution is generally non-uniform and the altered layers across the albite surface are discontinuous, for example, under the acid conditions of 0.3 HCL solution at 200 °C (Gout et al., 1997).

2.1.3. Interfacial dissolution-reprecipitation mechanism

The interfacial dissolution-reprecipitation mechanism was proposed by Hellmann et al. (2003), using an energy-filtered transmission electron microscopy/high-resolution transmission electron microscopy (EFTEM/HRTEM) high-resolution study on a labradorite dissolution at room temperature and at pH 1 and interdiffuison modeling of alkali cations and H^+ within a 500-nm-thick altered zone of the feldspar (Fig. 6). This mechanism was also supported by some recent studies with laboratory experiments conducted on dissolution of feldspars, wolastonite and glass (Hellmann et al., 2012; Ruiz-Agudo et al., 2012; Putnis, 2014; Hellmann et al., 2015; Ruizagudo et al., 2016).

The dissolution of feldspars with such a dissolution-reprecipitation mechanism was proposed to occur in a stoichiometric (congruent) dissolution pattern, the breaking of bonds and the release of interstitial cations and framework elements (Al, Si, O) to solution occur contemporaneously at an equal relative rate from the original fluid mineral interface (Fig. 4B). The released elements were precipitated as secondary minerals in altered layer almost on primary feldspar surface. Instead of a residual altered layer depleted of cations (Ca, Na) and Al due to preferential leaching, the altered layer on the feldspar surface in this dissolution-precipitation mechanism is a 500-nm-thick altered layer consisting of porous secondary amorphous minerals enriched in Si, O, and H (Fig. 6). The porous altered layers are very permeable to fluids, ensuring nondiffusion-limited transport of elements through the layer. The interface delimiting the unaltered feldspar and altered zone is characterized by a depletion of Al and Ca and an enrichment of Si and O, and the thickness of the interface can be very thin (thickness ≈ 0.5–2 nm). Modeling H^+-alkali interdiffusion within the 500-nm thick altered zone, however, suggested that the volume interdiffusion cannot be responsible for such a sharp chemical interface between the non-altered feldspar and the altered zone. This mechanism, as stressed by Hellmann et al. (2003), is interfacial in nature: bond-breaking and element release, followed by fast reprecipitation, occur directly at the original fluid-mineral interface (Fig. 5B).

Although the interfacial dissolution-reprecipitation mechanism was suggested by Hellmann et al. (2003, 2012. 2015) to be a possible universal mechanism controlling fluid-mineral interaction in laboratory experiments and natural field, the EFTEM chemical composition maps included in the relevant papers still demonstrate the possible development of the residual layers formed by preferential leaching. For example, the thickness of Ca depleted layer and the Al depleted layer in the labradorite dissolution experiment at room temperature and at pH 1 reaches up to approximately 60 Å and 40 Å (Fig. 6A, B), respectively, which is in consistent with the thickness data in Chou et al. (1984) (Table 1). Detailed analysis of naturally weathered feldspars with and without mineral coatings (kaolinite and other Al-rich amorphous materials) in Nugent et al. (1998) suggest that coatings of secondary minerals on feldspar surface may obscures the Al-depleted feature of the residual layer after preferential leaching, leading to the so called Al-rich phenomena on the weathered feldspar. The removing of the Al-rich coatings on the weathered feldspar can help to obtain the Al-depleted feature in the residual layer. As the porous Si-rich coatings on the labradorite in the work from Hellmann et al. (2003, 2012) were not removed for analysis, the abnormal abundance of Si and O in the altered layer and the interface in the EFTEM chemical maps (Fig. 6C, D) was likely due to the precipitation of these Si-rich secondary minerals close to and in the residual layer under strong acidic condition (pH) (Fig. 4C). And analysis of the mixed materials probably have obscured the Si-depleted feature in the interface zone.

That is to say, the phenomenon that have been interpreted as the result of interfacial dissolution-reprecipitation is still likely relevant to preferential leaching and element diffusion in the residual layers and can alternatively be interpreted by the following diffusion-precipitation controlled dissolution mechanism.

2.1.4. Diffusion-precipitation controlled dissolution mechanism

This mechanism was also proposed on the basis of a non-stoichiometric dissolution and is an extension of the preferential leaching-diffusion mechanism at a far-from-equilibrium state to a near- (partial-) equilibrium state. In this mechanism, the diffusion process is coupled with a subsequent precipitation reaction occurring very close to or at the feldspar surface; the precipitated layer lowers the rate of dissolution (Wollast, 1967; Helgeson, 1971; Helgeson, 1972; Chou and Wollast, 1984; Nugent et al., 1998). In such a case, the altered layer consists of two sublayers including an inner residual sublayer depleted of cations and (or) Al and an outer alumina-enriched (or Si-enriched) sublayer of slightly soluble substances (Fig. 4C). The inner residual sublayer is formed during the initial dissolution stage when the solution has a low

Table 1
Compilation of the thickness of the residual layers after dissolution of feldspars in different experiments.

Mineral	Water pH	Temperature	Time	Thickness (Å)	Method	References
Albite	5.1	Room temperature	≈ 260 h	48 Å for Al-deletion 50 Å for Na-depletion	Theoretical calculation	Chou and Wollast, 1984
	3.5	Room temperature	≈ 300 h	25 Å for Al-deletion 56 Å for Na-depletion,		
	2.5	Room temperature	≈ 300 h	20 Å for Al-deletion 57 Å for Na-depletion,		
	1.2	Room temperature	≈ 400 h	5 Å for Al-deletion 70 Å for Na-depletion,		
K-feldspar	4	Room temperature	48 h	95–160	Theoretical calculation	Wollast, 1967
K-feldspar	3	Room temperature	/	300	Theoretical calculation	Correns, 1963
Labradorite (An ≈ 54)	4	21 ± 2 °C	72 days	1500 Å for Ca depletion, decreases with addition of dissolved Al, Ca, Mg in solution	Secondary ion mass spectrometry (SIMS)	Muir and Nesbitt, 1991
Albite	3.5	Room temperature	90 days	150–300 Å for Al-depletion, 300–600 Å for Ca depletion	SIMS	Muir et al., 1990
Oligoclase				150–300 Å for Al-depletion, 200–400 Å for Ca depletion		
Andesine				150–300 Å for Al-depletion, 200–400 Å for Ca depletion		
Labradorite				60–120 Å for Al-depletion, 100–200 Å for Ca depletion		
Bytownite				75–150 Å for Al-depletion, 200–400 Å for Ca depletion		
Plagioclase	3.5	Room temperature	90 days	600–1200 Å for Al- and Ca-depletion	SIMS	Muir et al., 1989
	5.7		60 days	60–120 Å for Al-depletion, 100–200 Å for Ca depletion		
Labradorite	3	25 °C	306 h	700–1000 Å for Al depletion ≈ 1500 Å for Ca depletion	Rutherford backscattering spectra (RBS)	Casey et al., 1988
Labradorite	1	45 °C	264 h	300–500 Å for Al depletion 2000 Å for Ca depletion	RBS	Casey et al., 1989
	2	45 °C	264 h	300–500 Å for Al depletion 1500 Å for Ca depletion		
Labradorite (An ≈ 56)	5.6 distilled water 4.05 HCl solution 4.05 HCl solution with 1 mg/l of Na, Ca, K 4.05 HCl solution with 1 mg/l of Na, Ca, K, Al(aq) and Si(aq)	20 °C	72 days	No development of residual layer 1500 Å for Ca depletion 700 Å for Ca depletion < 75 Å for Ca depletion	SIMS	Nesbitt et al., 1991

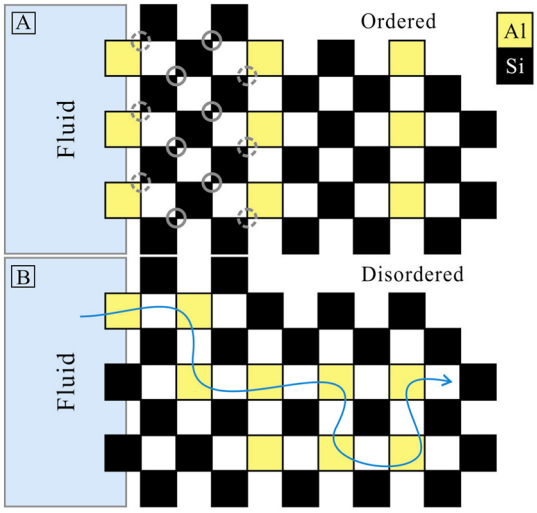

Fig. 5. The effect of Al/Si ordering on the development of an interfacial layer. (A) Ordered structure. Both Si–O–Si (solid circles) and Al–O–Si (dotted circles) need to be broken before aqueous species gain access to the fifth array of the tetrahedral sites; (B) Disordered structure. Only Al–O–Si linkages need to be broken for aqueous species to gain access to the 10th array of tetrahedral sites. (after Yang et al., 2013).

concentration of solutes; and the outer alumina-enriched sublayer is formed when the Al (Si) concentration exceeds the saturation of certain minerals. In the subsequent leaching processes, the SiO_2(aq) ($Al(OH)_3$) diffusion into the solution through the altered layers and the SiO_2(aq) ($Al(OH)_3$) removed from solution by the reactions of SiO_2(aq) and Al $(OH)_3$ jointly control the feldspar dissolution. That is, in a geochemical system at partial equilibrium state when the solution is saturated with some specific minerals but not all and equilibrium prevails in at least one process or reaction but not in others (Helgeson, 1971), the feldspar dissolution rate is not just controlled by the residual layer but depends on the concentration of silica and alumina in the solution (or secondary mineral precipitation rate) (Wollast, 1967; Helgeson, 1971, 1972). The formation of almina-enriched and Si-enriched layers likely occur under weak acidic to neutral conditions and strong acidic conditions, respectively. However, as aforementioned, the fractional orders of the dissolution reaction with respect to H^+ does not support this hypothesis either as diffusional processes can only be first order (Crundwell, 2015b).

On the whole, the surface reaction-controlled dissolution mechanism is likely to control feldspar dissolution under basic conditions. Under acidic-neutral conditions, the preferential leaching-diffusion controlled mechanism probably control the feldspar dissolution in geochemical systems at far from equilibrium conditions with low ion concentrations. The diffusion-precipitation controlled dissolution mechanism is likely to control the feldspar dissolution in laboratory geochemical systems at near (partial) equilibrium to supersaturation state.

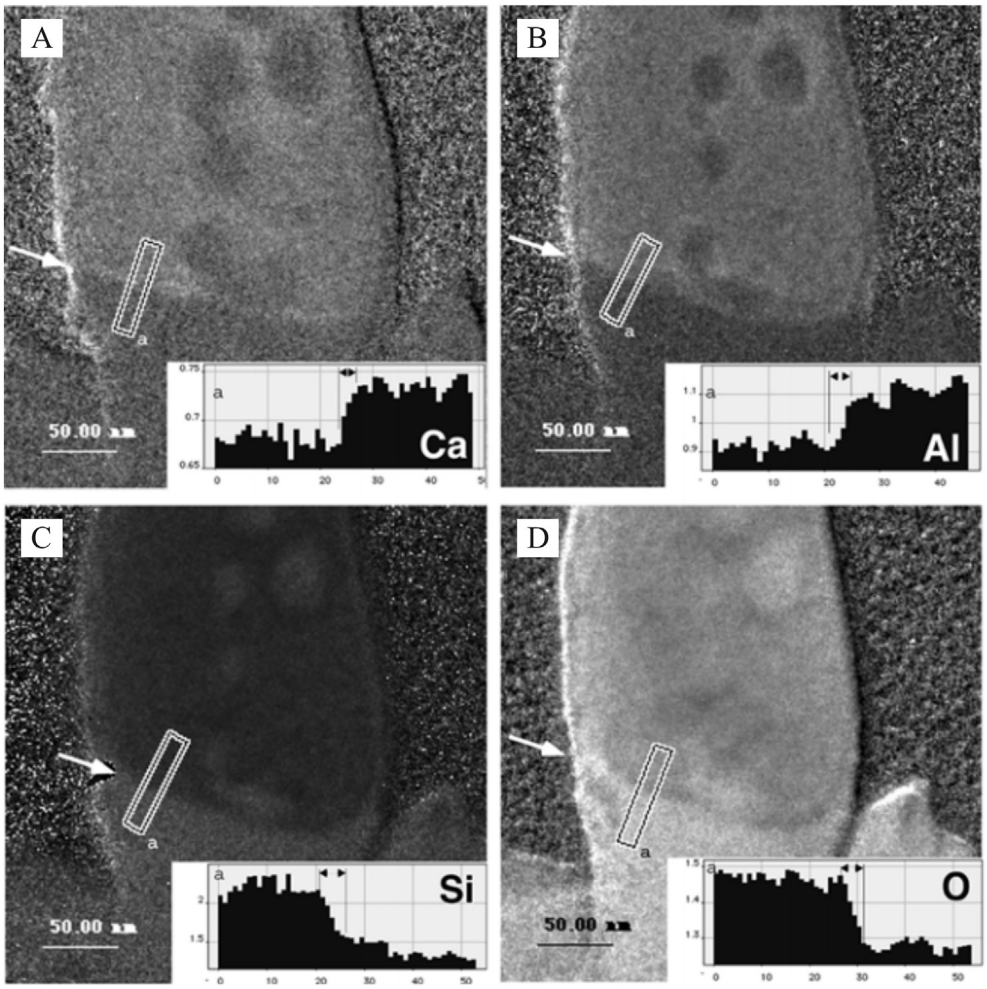

Fig. 6. Ultrathin section lamella of labradorite feldspar altered at pH 1 shows the interface between the altered zone (*bottom*) and the unaltered labradorite (*top*). EFTEM chemical maps of the interfacial boundary (white arrows) separating the altered and unaltered zones; qualitative concentrations of Ca, Al, Si, and O are shown (brightness proportional to concentration). Ca and Al are depleted in the altered zone, whereas Si and O are enriched. *Insets* show the respective chemical profiles (left to right from altered to unaltered zones); delimiting small black arrows in insets indicate estimated widths of interfacial regions (note: abscissa axes are in pixels, 1 pixel = 1.26 nm; ordinate axes have arbitrary units). The chemical gradients are very sharp, ranging from 3.8 nm (Ca) to 6.8 nm (Si). (after Hellmann et al., 2003).

When it comes to subsurface rocks with complex mineral composition, variable porosity and permeability, high ion concentrations salinity, etc., however, more consideration is required (Details in Section 2.4).

2.2. Factors affecting feldspar dissolution rate

Several factors including feldspar intrinsic features (crystal structure, Al/Si ordering, available surface) (Lasaga, 1984; Yang et al., 2013; Yang et al., 2014a) and ambient fluid chemistry (temperature, pH, initial fluid composition, chemical affinity, and rate-enhancing catalysts or rate inhibitors) (Aagaard and Helgeson, 1982; Helgeson et al., 1984; Lasaga, 1984; Bevan and Savage, 1989; Hellmann and Tisserand, 2006) can affect the feldspar dissolution rate.

2.2.1. Crystal structure and Al/Si ordering

Feldspars are tectosilicates and share similar “mirrored crankshaft-chain” frameworks of polymerized AlO_4^- and SiO_4 tetrahedra (Ribbe, 1994; Yang et al., 2013; Yang et al., 2014a) (Fig. 7). Feldspars may differ in the interstitial cation and Al content, Al-O/Si-O bond length, and/or Al/Si ordering state. Such heterogeneities result in dramatic differences in the reactivity of feldspars (e.g., plagioclases with different anorthite content). Aagaard and Helgeson (1982) proposed that “rates of feldspar hydrolysis should be a function of substitutional order/disorder among the tetrahedral sites” because of the “local surplus of negative charge in the vicinity of the Al atoms on the tetrahedral sites”. Many laboratory experiment studies have identified the phenomena that the feldspar's dissolution rate depends strongly on its anorthite content (Fig. 8) (Casey et al., 1991; Palandri and Kharaka, 2004; Yang et al., 2013). However, the investigations of the dependence of the feldspar-water interaction kinetics on the crystallographic properties of feldspar are relative scarce (Yang et al., 2013).

Until recently, the information between the atomic scale and the macro-scale (laboratory measurements) were bridged with a mechanistic model (Yang et al., 2013; Yang et al., 2014a; Yang et al., 2014b). The feldspar framework consists of interconnecting tetrahedral with one centered T-site atom and four corner oxygens. The T-site is occupied by either Al or Si. Four tetrahedra form a ring by sharing oxygens (O_r in Fig. 7A) and the ring extends into a crankshaft chain by sharing edges (two tetrahedra) with other rings. Mirrored crankshafts are connected by oxygens (O_{i1} in Fig. 7A) to form (001) crankshaft slabs, and parallel slabs are connected to each other by oxygens (O_{i2} in Fig. 7A) in the [001] direction. The O_i are located at a location of the mechanical weakness of the feldspar, while the O_r are responsible for the mineral's mechanical hardness. All oxygens are shared by two T-atoms and the dissolution of feldspar, usually measured by the release rate of T-atoms, involves the removal of the atoms from the bulk by the breakdown of all their T–O–T (SiO_iSi, AlO_iSi, SiO_rSi, AlO_rSi) linkages, reducing the connectedness of each T-site from four to zero. The T-O_i-T and T-O_r-T linkages hold different dissociation energies and hence show different reactivities, indicating that T-O_i-T break more easily than T-O_r-T, and Al—O breaks more easily than Si—O in the same reaction conditions. Yang et al. (2013, 2014a) deciphered the quantitative impact of Al occupancy, tetrahedral site–oxygen (T-O) bond length, and the Al/Si ordering on the feldspar dissolution rate employing a structure model based on a C1 space group (Fig. 7), and proposed the following equation to describe the linear correlation between the

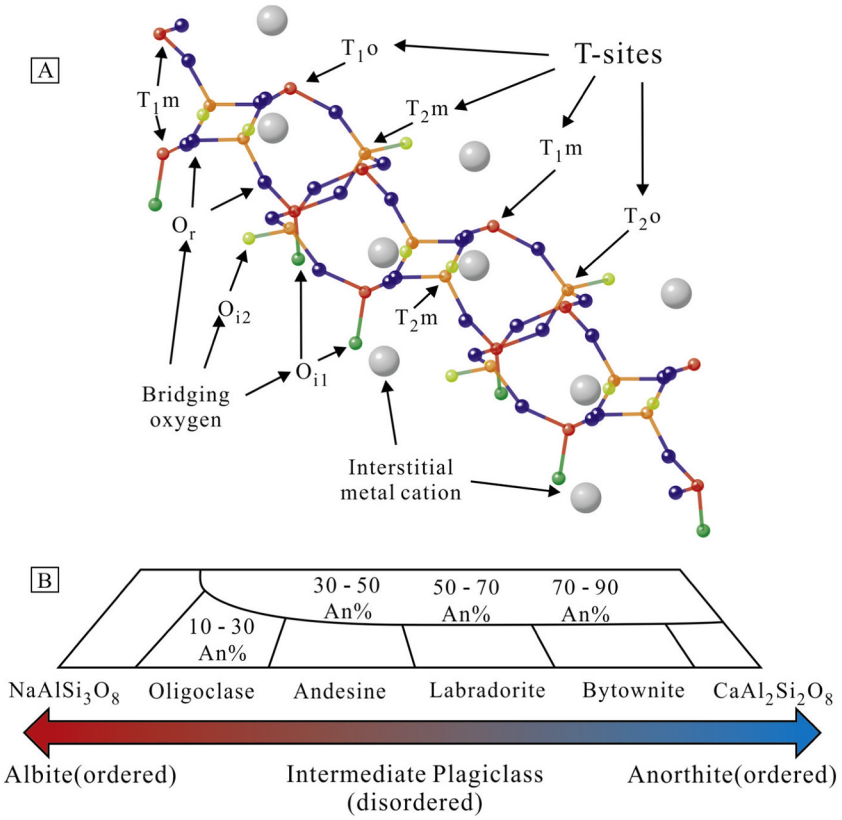

Fig. 7. (A) The crankshaft structure of the feldspar framework. C^{-}1 nomenclature is used. There are two categories of oxygen: one connects constituent tetrahedral within a tetrahedra ring (O_r, blue), and the other interconnects crankshaft chains (O_i, green). O_i can be further divided into two subcategories depending on the crystallographic plane where they are located. Interstitial cations (grey) are located between crankshaft chains and in proximity to O_i. Four T-site types (T_{1o}, T_{1m}, T_{2o}, and T_{2m}) differ in their aluminum occupancies. T_1 sites (red) are more aluminum-abundant than T_2 sites (orange) in general. The figure shows a part of a crankshaft chain, viewed from the [111] direction. Sphere size does not reflect the effective radius of an atom. (B) Part of the compositional phase diagram of feldspars (the plagioclase series). ^{16}An% stands for the corresponding anorthite content. (after Yang et al., 2013). (For interpretation of the references to colour in this figure legend, the reader is referred to the web version of this article.)

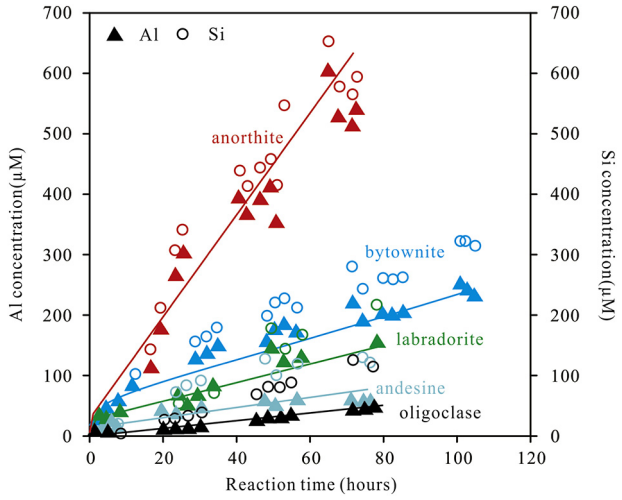

Fig. 8. Evolution of Al and Si concentration for plagioclase dissolution experiments under the conditions of 90 °C, 100 atm of CO_2, and pH 3.1. Red: anorthite; blue: bytownite; green: labradorite; aqua: andesine; black: oligoclase. Closed triangles: Al concentration; open circles: Si concentration. Lines are drawn based on the evolution of Al to guide the reader's eye. (after Yang et al., 2013). (For interpretation of the references to colour in this figure legend, the reader is referred to the web version of this article.)

logarithm of the characteristic time for the Al–O_r–Si breakdown and the anorthite content:

$$\tau_{Al} = \tau_{Al}|_{<T-O>=1.677} 1.677 \exp[\gamma_{Al}(0.0338 n_{An} - 0.034)] \quad (1)$$

where τ_{Al} denotes the characteristic time for the breakdown of Al-Or-Si, < T−O > is the average T−O bond length, the $|_{<T-O>}$ subscript indicates that τ can be affected by < T−O > . The constant 1.667 is < T−O > for pure anorthite. γAl is the single empirical coefficient that reflects the effect of < T−O > on the characteristic time for the Al–Or–Si linkage breakdown. n_{An} is the anorthite content in a plagioclase. This mechanistic interpretation of the plagioclase dissolution based on Al occupancy and T−O bond length makes it clear why the anorthite have a higher dissolution rate than other feldspars in the same chemical condition (Fig. 8).

2.2.2. Surface area

Feldspar dissolution reaction occurs at the water-feldspar interface, thus, available surface area is a critical factor controlling the overall dissolution rate, and feldspar dissolution rate increases as the available surface area increase. In general, the dissolution rate of a feldspar can be expressed by the following Eq. 2 (Lasaga, 1984).

$$\Delta c_i/\Delta t = A_m/V * k_{im} \quad (2)$$

where i represent a specific species released from feldspar, $\Delta c_i/\Delta t$ referes to the change of the concentration of species i in solution, A_m is the surface area of feldsapr m, V is the volume of solution in contact with feldspar m, and k_{im} is the dissolution rate constant of species i from feldspar m.

Specific area of mineral particles has a negative logarithmic relationship with the grain size, and detailed BET (Brunauer-Emmett-Teller) specific surface area data for different feldspars with variable grain size are available in Table 2 in Brantley and Mellott, 2000. The surface area of the loose feldspar grains used in the laboratory experiments, prior to and after the dissolution reactions, can be determined using the BET method, however, the quantitative evolution of the surface area of the reacted feldspars in the laboratory experiments need further studies. What's more, when it comes to natural rocks with variable grain sizes and porosity, development of secondary pores in grains and occupation of open pores by cementation, the surface areas of different minerals in geologic porous rocks and their evolution with on-going water-rock interactions are much more complicated (Tutolo et al., 2015; Beckingham et al., 2016; Yuan et al., 2017a).

Table 2
Compilation of the activation energy Ea of different feldspar in different studies.

Feldspar	Activation Energy E (kJ mole^{-1}) Acidic	Activation Energy E (kJ mole^{-1}) Neutral	Activation Energy E (kJ mole^{-1}) Basic	Temperature (°C)	References
Albite	88.9 ± 14.6	68.8 ± 4.5	85.2	100–300	Hellmann, 1994b
Albite	75	75	75	25–300	Crundwell, 2015a, calculate with data from Chou and Wollast (1985), Knauss and Wolery (1986) and Hellmann (1994a, 1994b)
Albite	65.3 ± 3.3	/	/	5–300	Chen and Brantley, 1997
Anorthite	18.4	/	/	45–95	Oelkers and Schott, 1995
Bytownite	/	40.6 (Distilled water)	/	5–35	Welch and Ullman, 2000
	/	45.2 (Distilled water + acetate)	/		
	/	43.5 (Distilled water + nitrate)	/		
	/	29.7 (Distilled water + nitrate)	/		
	/	27.6 (Distilled water + oxalate)	/		
Albite	65.0	69.8	71.0	25–300	Palandri and Kharaka, 2004
Oligoclase	65.0	69.8	/	25	
Andesine	53.5	57.4	/	22–250	
Labradorite	45.1	45.2	/	25–245	
Bytownite	29.3	31.5	/	5–35	
Anorthite	16.6	17.8	/	25–95	
K-feldspar	51.7	38.0	94.	25–350	
Albite	/	75 ± 14	/	7.5–20.3	Williams et al., 2010
Labradorite	42.09	/	/	30–130	Carroll and Knauss, 2005
Orthoclase	≈ 65	/	/	31–77	Fenter et al., 2014

2.2.3. Temperature

Feldspar dissolution rate increases exponentially as the temperature increases and the temperature dependence of the feldspar dissolution rates (k) follows the Arrhenius equation (Lasaga, 1984; Steefel and Lasaga, 1994).

$$k = A_f e^{-E_a/RT} \tag{3}$$

where Ea is the apparent activation energy of albite dissolution (kJ/mol), A_f is the pre-exponential factor, R is the universal gas constant (8.31J/[mol.K]), and T is the absolute temperature (K). Such a specific equation is only suitable for a specific temperature range (generally 5–300 °C) (Table 2) and changes in the activation energy often signal a change in mechanism (Lasaga, 1984; Hellmann, 1994b; Steefel and Lasaga, 1994; Chen and Brantley, 1997; Crundwell, 2015a). Additionally, the Ea values of a feldspar obtained from different laboratory experiments may differ significantly (Table 2) due to the possible chemical differences of the solution (eg. pH value, impact of organic acid) (Hellmann (1994a, 1994b); Oelkers and Schott, 1995; Welch and Ullman, 2000; Palandri and Kharaka, 2004; Carroll and Knauss, 2005; Williams et al., 2010; Fenter et al., 2014).

The most commonly used *k* values for different feldspars are those derived from laboratory experiments conducted at far-from-equilibrium conditions at approximately 25 °C (Palandri and Kharaka, 2004); it is convenient to approximate the rate constant dependency as a function of temperature with Eq. 4 (Xu et al., 2005; Yuan et al., 2017a):

$$k = k_{25} \exp\left[\frac{-E_a}{R}\left(\frac{1}{T} - \frac{1}{298.15}\right)\right] \tag{4}$$

where k_{25} is the rate constant at 25 °C (mol/cm^2/s).

2.2.4. pH

The pH dependence of feldspar dissolution rates has been studied extensively (Helgeson et al., 1984; Knauss and Wolery, 1986; Blum and Stillings, 1995; Fenter et al., 2014; Yang et al., 2014b; Crundwell, 2015a; Tutolo et al., 2015). The feldspar dissolution rate varies with different pH, which can be described by the following equation (Brantley et al., 2008; Crundwell, 2015a):

$$\text{rate} = k_{\mathrm{H}}(a_{H^+})^n + k_{\mathrm{OH}}(a_{OH^-})^m \tag{5}$$

where k_H represents the rate constant for the dissolution reaction with acid, and k_{OH} represents the rate constant for the dissolution reaction with hydroxide. The terms a_{H^+} and a_{OH^-} represent the activity of the H^+ and OH^- ions, and the constants *n* and *m* are the empirical reaction order accounting for the catalysis by H^+ and OH^- in solution, respectively.

Owing to the amphoteric nature of the feldspars in aqueous solution, feldspars exhibit a U (V)-shaped dependence of the dissolution rate on the pH value (Fig. 9) (Helgeson et al., 1984; Knauss and Wolery, 1986; Kampman et al., 2009; Crundwell, 2015a). There is consensus that the feldspar dissolution rate decreases as the pH increases from the acidic region to the neutral region and the rate increases as the pH increases from the neutral region to the alkaline region. However, a consensus has not been reached regarding the value of n and m in Eq. 5 (Table 3) (Hellmann, 1994b; Crundwell, 2015a). Available values of *n* and *m* suggest that the reaction order may be attributed to the different pH ranges over which the formulations were calibrated (Tutolo et al., 2015).

In the acidic region, values of n ranging from 0.2 to 0.6 were reported for albite based on an experimental calibration over the range of 100–300 °C (Hellmann, 1994b). Value of 0.49 was reported for albite at 25 °C (Blum and Lasage, 1991) and similar values of 0.52 and 0.45 were reported for microcline and sanidine at 25 °C, respectively (Schweda, 1990). In some other studies, however, values of n = 1 over ranges of temperatures (25–200 °C and 25–70 °C, respectively) were reported (Fig. 9) (Helgeson et al., 1984; Knauss and Wolery, 1986). Meanwhile , another study (Fenter et al., 2014) even suggest a transition from $n = 1$ at an acidic pH > 2.5 to $n = 0.37$ at pH < 2.5 at 25–80 °C for the dissolution of orthoclase. In the intermediate (neutral) region, a pH-independent region between the acid and the alkaline region was proposed by some studies and n was suggested to be zero (Helgeson et al., 1984). However, the data of Chou and Wollast (1985) and Knauss and Wolery (1986) indicate that the order of reaction with respect to H^+ in the intermediate pH region (3–6) between the acidic region and the alkaline region is 0.25 for albite dissolution (Fig. 9). In the alkaline region, the order of reaction with respect to OH^- was proposed by Knauss and Wolery (1986) to be 0.5 at 25 °C and 70 °C, which is in agreement with Hellman's (Hellmann, 1994b) data at 100, 200, and

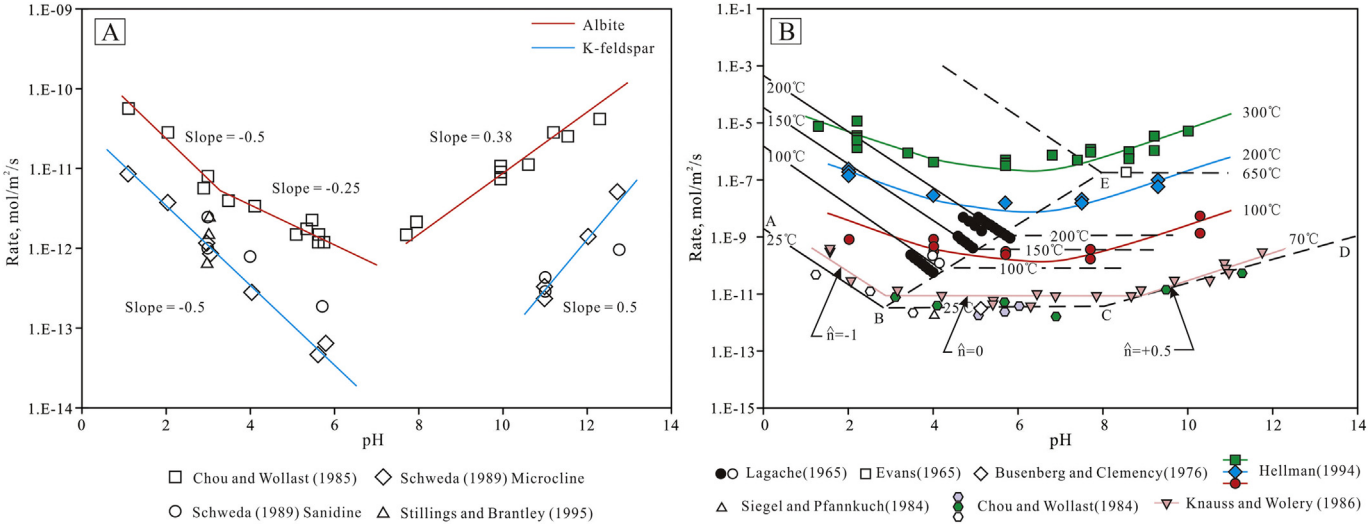

Fig. 9. (A) The effect of pH on the dissolution rate of albite and K-feldspar at 25 °C. Data from Chou and Wollast (1985), Schweda (1989) and Stillings and Brantley (1995). (B) The effect of pH on the dissolution rate of feldspars at different temperatures. Compiled data from different authors in Helgeson et al. (1984), Knauss and Wolery (1986) and Crundwell (2015a) are used here.

300 °C. However, the data from Chou and Wollast (1985) correspond to an order of reaction with respect to OH^- of 0.38 at 25 °C (Fig. 9). In a review of published laboratory data, Crundwell (2015a) proposed that the reaction order should be 0.5, 0.25, and 0.5 for the feldspar dissolution in an acidic fluid (pH < 3), an intermediate fluid (3 < pH < 7), and an alkaline fluid (pH > 7), respectively (Fig. 9A). And models based on the crossing of an activated aluminum complex through a Helmholtz layer between fresh mineral surface and a liquid were proposed to interpret the rationality of these three constants (Fig. 10) (details available in Crundwell, 2015a). The theoretical explanation based on first principles with no adjustable parameter in Crundwell (2015a) made the three constants 0.5, 0.25, and 0.5 likely to be universal for feldspar dissolution under conditions with acidic, intermediate and alkaline fluids, respectively (Table 3).

2.2.5. Organic acids

Aside from temperature and pH, organic acids may also affect the feldspar dissolution rate during both surficial and subsurface diagenetic processes (Stoessell and D, 1990; Manning et al., 1992; Drever and Stillings, 1997; Oelkers and Schott, 1998;). The rates of feldspar dissolution in solutions containing organic acids can be up to ten times greater than the rates determined in solutions containing inorganic acids at the same acidity (Welch and Ullman, 1993; Welch and Ullman, 1996). Organic acids and their anions may affect the feldspar dissolution rates mainly by affecting the speciation in solution of ions such as $A1^{3+}$ that themselves affect the mineral dissolution rate and even to form complexes at the mineral surface; the complexing of Al in solution may also affects the saturation state of the solution with respect to the feldspar minerals (Drever and Stillings, 1997; Oelkers and Schott, 1998).

The impact of organic acids on the feldspar dissolution rate varies

Table 3
Compilation of orders of reactions with respect to H^+ for the dissolution of different feldspars.

Feldspar	Temperature (°C)	Reaction order with H^+, n			References
		Acidic n (pH)	Neutral n (pH)	Basic n (pH)	
Albite	25	0.5 (< 3)	0.25 (3–7)	−0.5 (> 7)	Chou and Wollast, 1985, reaction order calculated by Crundwell (2015a)
K-feldspar	25	0.5 (0–7)	/	−0.5 (> 7)	Schweda et al., 1989, reaction order calculated by Crundwell (2015a)
Albite	100	0.2 ± 0.1 (≤5)	≈ 0 (5–8.6)	−0.3 (≥8.6)	Hellmann, 1994b
	200	0.4 ± 0.1 (≤5)	≈ 0 (5–8.6)	−0.4 ± 0.2 (≥8.6)	
	300	0.6 ± 0.2 (≤5)	≈ 0 (5–8.6)	−0.6 ± 0.3 (≥8.6)	
Albite	5	0.46 ± 0.05 (1.06–3.53)	/	/	Chen and Brantley, 1997
	50	0.54 ± 0.04 (1.06–4.40)	/	/	
	90	0.53 ± 0.06 (1.00–3.63)	/	/	
Albite	25	1.0 (0–2)	0 (2–8)	−0.5(> 8)	Knauss and Wolery, 1986
	70	1.0 (0–3)	0 (3–9)	−0.5(> 9)	
Albite	25	0.49 (0–7)	/	−0.30 (7–13)	Data from Chou and Wollast (1985), calculated by Blum and Lasaga (1991)
Orthoclase	25–80	0.37 (0–2.5) 1 (2.5–5)	/	/	Fenter et al., 2014
Albite	25	0.457	/	−0.376~ − 0.572	Palandri and Kharaka, 2004;
Oligoclase	25	0.457	/	/	Brantley et al., 2008;
Andesine	25	0.541	/	/	Crundwell, 2015a
Labradorite	25	0.626	/	/	
Bytownite	25	1.018	/	/	
Anorthite	25	1.411	/	/	
K-feldspar	25	0.500	/	−0.50~ − 0.823	
K-feldspar albite	/	0.5 (pH < 3)	0.25 (3–7)	0.5 (pH > 7)	Crundwell, 2015a

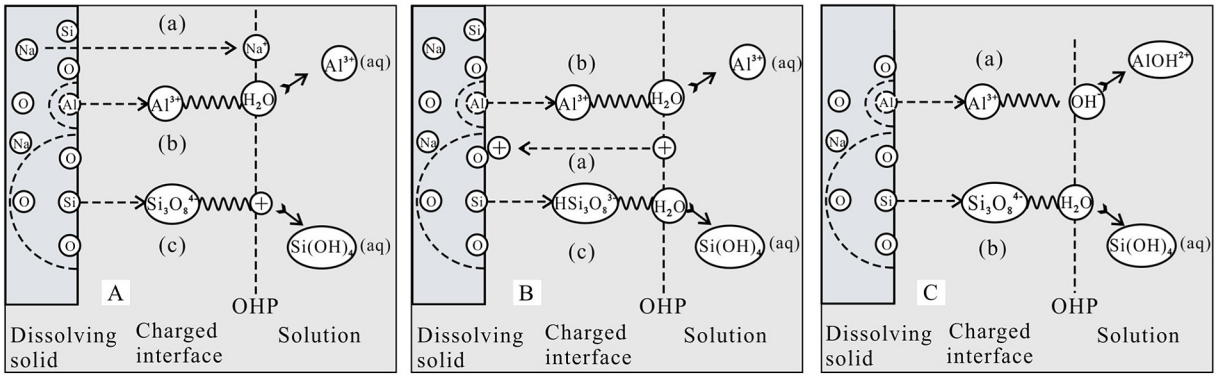

Fig. 10. (A) Schematic illustration of the mechanism of dissolution of albite in acidic solutions at a pH of < 3, showing the formation of two activated states as the aluminum and silicate group departs in independent, parallel partial reactions. (a) Sodium departs rapidly and easily from the surface. This step does not impact on the rate determining steps. (b) Aluminum at the surface reacts with water to form Al^{3+}(aq). (c) H^+ ions at the outer Helmholtz plane react with silicate groups at the surface to form $HSi_3O_8^{3-}$ (aq). (B) The proposed mechanism for the dissolution of albite and other feldspars in the intermediate region, between a pH of 3 and 7. (a) H^+ ions first adsorb at the inner Helmholtz layer at a silicate site before reacting. (b) Aluminum at the surface reacts with water to form Al^{3+}(aq) in solution. (c) Silicate group at surface together with an adsorbed H^+ reacts to form $HSi_3O_8^{3-}$ (aq) (aq) in solution. (C) Schematic illustration of the mechanism of dissolution of albite and other feldspars in alkaline solutions, showing the formation of two activated states as the aluminum and silicate group departs. (a) Aluminum at the surface reacts with OH^- ions at the outer Helmholtz plane to form $AlOH^{2+}$(aq). (b) Water reacts with silicate groups at the surface to form dissolved silica in solution. (after Crundwell 2015a).

significantly with different organic acids and different pH values. Generally, organic acids including citric, oxalic, malonic, salicylic, and succinic acids can significantly accelerate the feldspar dissolution rate (Huang and Kiang, 1972; Lasaga, 1984; Bevan and Savage, 1989; Stoessell and D, 1990; Welch and Ullman, 1993; Blake and Walter, 1999), while acetic and propionic acids have little impact on the feldspar dissolution rate (Stoessell and D, 1990; Welch and Ullman, 1993). The degree of ligand-promoted enhancement of the dissolution rate (rate in organic-containing solution/rate in inorganic solution at the same pH) decreases as the acidity increases, indicating that the ligand-promoted dissolution mechanism becomes relatively more important as the rate of proton-promoted dissolution decreases (Bevan and Savage, 1989; Welch and Ullman, 1993). For example, the presence of oxalic acid increased the dissolution rate of K-feldspar at pH 4 and 9 but decreased the rate at pH 1 at both temperatures of 70 °C and 95 °C (Bevan and Savage, 1989). The maximum increase in dissolution rate was observed at pH 4 and a temperature of 95 °C by a factor of 4. Aside from the acid type and pH region, the catalytic effect of organic acids on the feldspar dissolution rate is also affected by other solutes in fluids. For example, Blake and Walter (1999) demonstrated that the dependence of feldspar dissolution rates on organic acid concentrations in natural diagenetic environments is complicated due to the competing effects of the overall solution chemistry and ionic strength on the dissolution mechanism. The catalytic impact of oxalic acids on feldspar dissolution can be suppressed by the addition of NaCl into solution.

Surficial and subsurface microbial activity can generate various organic acids to promote feldspar dissolution in sediments and rocks (Gómez-Alarcón et al., 1994; Ehrenberg and Jakobsen, 2001; Lian et al., 2008; Seiffert et al., 2014). Overall, the role of organics may probably be important as many organics are picked up by meteoric fresh solutions passing through soils; this source of organics could influence the weathering of underlying rocks (Lasaga, 1984). A detailed review of the role of organic acids in mineral weathering is available from Drever and Stillings (1997). Acetic and propionic acids usually dominate the organic acids in pore water in deeply buried sandstones (Surdam et al., 1984; Surdam and Crossey, 1987) and the pore waters are generally close to equilibrium with respect to feldspars (Giles, 1987; Bjørlykke and Jahren, 2012). In such cases, the additional accelerating effect of organic acids on feldspar dissolution rate may be negligible (Stoessell and D, 1990).

Aside from the above factors, the impact of chemical affinity, Al^{3+}, and precipitation of secondary minerals on the feldspar dissolution rate is discussed in detail in the following Section 2.3, accompanying the review of feldspar dissolution rate laws and the relevant rate discrepancy.

2.3. Feldspar dissolution rate laws and inconsistency between laboratory and field rates

As discussed in Section 2.2, many physical and chemical parameters influence feldspar dissolution rates, both in nature and in the laboratory. The quantitative prediction and interpretation of the chemical evolution of natural water and rocks as a function of time require reliable equations describing the rates at which minerals react either congruently or incongruently with aqueous solution, and the extent to which these rates vary with pressure, temperature, pH, solution composition and chemical affinity (Aagaard and Helgeson, 1982; Thyne et al., 2001; Steefel et al., 2005; Yuan et al., 2017a). Data derived from experimental feldspar dissolution studies are generally fitted to kinetic equations that incorporate these major rate-controlling parameters. Up to now, there have been five important proposed kinetic rate law variations describing aluminosilicate dissolution stemming from both theoretical and experimental observations (Aagaard and Helgeson, 1982; Lasaga, 1984; Burch et al., 1993; Gautier et al., 1994; Lasaga and Luttge, 2001; Hellmann and Tisserand, 2006; Crundwell, 2015b). The first proposed and most commonly used kinetic law is the linear transition state theory (L-TST) rate law (Aagaard and Helgeson, 1982; Lasaga, 1984). However, a big discrepancy (2–5 orders) exists between the calculated dissolution rate using this L-TST rate law and the dissolution rate obtained from a near-equilibrium water-rock system. In order to interpret this big gap, rate laws including the non-linear transition state theory (TST) rate law (Steefel and Van Cappellen, 1990; Steefel and Lasaga, 1994; Hellevang et al., 2013), the parallel rate law (PRL) (Burch et al., 1993; Hellmann and Tisserand, 2006; Hellmann et al., 2010), the stepwave model rate law (Lasaga and Luttge, 2001), and the partial equilibrium law (Crundwell, 2015b) have been proposed.

2.3.1. L-TST rate law

The L-TST rate law, proposed first by Aagaard and Helgeson (1982) and Lasaga (1984), can be expressed by Eq. 6.

$$r_m = k_m A_m (a_{H^+})^n |1 - Q_m/K_m| = k_m A_m (a_{H^+})^n |1 - \exp(\Delta G/RT)| = k_m A_m (a_{H^+})^n |1 - \exp(-A/RT)| \quad (6)$$

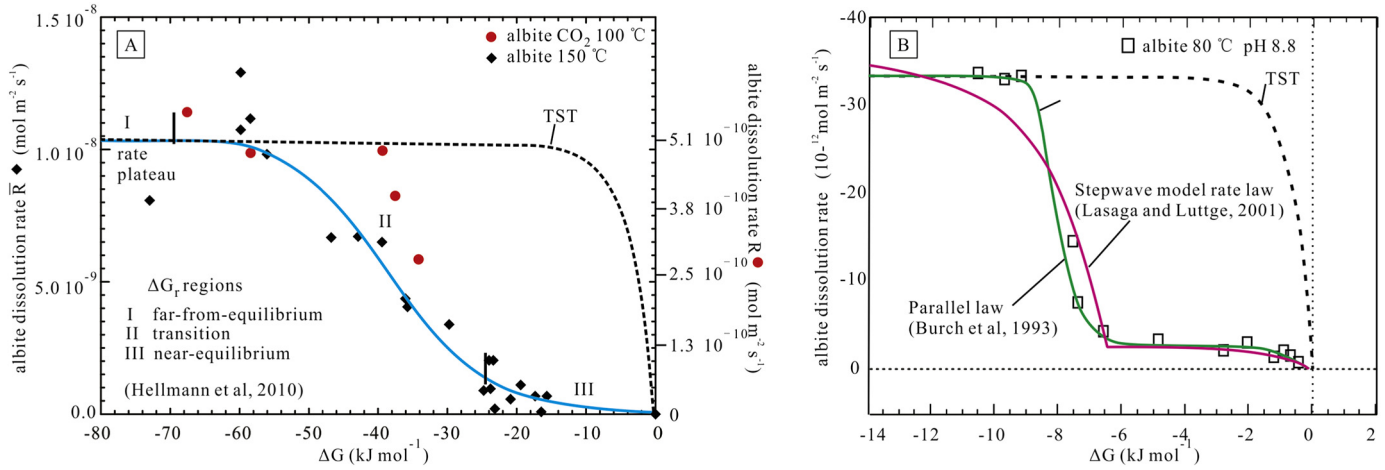

Fig. 11. (A) Dissolution rates of albite measured as a function of △G at an acid pH (filled circles) and basic pH (filled diamonds). The data and the fitted rate curve using the PRL (Eq. 10) define three R–△G regions: far-from-equilibrium (I), transition (II), and near equilibrium (III) (after Hellmann, 2010). (B) Dissolution rate of albite (at 80 °C, pH 8.8) as a function of △G. The green and red solid curves represent the rate curves using the PRL (after Burch and Lasaga, 1993) and the stepwave model rate law (after Lasaga and Luttge, 2001), respectively. The dashed lines in A and B represent the rate curve using a TST-based free energy parameter. (For interpretation of the references to colour in this figure legend, the reader is referred to the web version of this article.)

where m is the mineral index, r_m is the reaction rate (mol/s, positive values indicate dissolution and negative values precipitation), k_m is the rate constant (mol/cm^{2}sec) at temperature T, A_m is the mineral's surface area (cm^2), aH^+ is the activity of H^+, and n is the empirical reaction order accounting for catalysis by H^+ in solution. Q_m and K_m are the activity product and the equilibrium constant for the chemical reactions, respectively. △G is the change of the Gibbs free energy (kJ.mol^{-1}) of the reaction that quantifies the effect of how far from chemical equilibrium the reaction takes place, −A is the chemical affinity of the overall reaction and is reverse to △G. R is the gas constant (8.31J/[mol.K]) and T is the absolute temperature (K). This law is applicable to far-from-equilibrium water-rock systems (Fig. 11) (Aagaard and Helgeson, 1982; Hellmann and Tisserand, 2006).

2.3.2. Non-linear TST rate law

The normal non-linear TST rate law was firstly proposed by Steefel and Van Cappellen (1990) and Steefel and Lasaga (1994) and can be expressed by Eq. 7 (Steefel and Van Cappellen, 1990; Maher et al., 2009).

$$\begin{aligned} r_m &= k_m A_m (a_{H^+})^n \beta \,|1 - (Q_m/K_m)^{p|q} \\ &= k_m A_m (a_{H^+})^n \beta \,|1 - exp(\Delta G/\alpha RT)^{p|q} \\ &= k_m A_m (a_{H^+})^n \beta \,|1 - exp(-A/\alpha RT)^{p|q} \end{aligned} \quad (7)$$

where β is a term describing the inhibition or catalysis of the reaction, p and q are fitting parameters, and α is Temkin's average stoichiometric coefficient. The terms α, β, p and q are incorporated in Eq. 7 to resolve the rate gap between the L-TST law (when α, β, p and q equal to unity) rate and the dissolution rate obtained from laboratory experiments in water- mineral system near equilibrium or from natural reservoirs.

Gautier et al. (1994) considered the inhibition effect of Al on K-rich feldspar dissolution to bridge the rate gap between the L-TST rate and the laboratory rate. The Al-inhibition model (AIM) is based on the assumption that feldspar dissolution rates are controlled by the formation and destruction of an Al-deficient and Si-rich precursor complex (Gautier et al., 1994). Eq. 8 was derived by Gautier et al. (1994) to describe the steady-state K-rich feldspar dissolution rate over the full range of chemical affinity at a temperature of 150 °C and pH of 9. This is considered here by modifying the inhibition term in Eq. 7 to include a hyperbolic dependence on Al activity. The constant 3 in Eq. 8 was used for α because the dissolution of one mole of K-feldspar requires the removal of three moles of Si-rich precursor complexes.

$$r = k_m \left(\frac{1}{a_{Al}(OH)_4^- a_{H^+}} \right)^{1/3} (1 - exp(-A/3RT)) \quad (8)$$

Alekseyev et al. (1997) studied the dissolution rate of alkali feldspars as a result of secondary mineral precipitation and approach to equilibrium at 300 °C, 88 bar and a pH of 9. In the congruent dissolution stage, the authors described the dissolution rate of sanidine and albite using Eq. 9. The value of k_m (mol/m^2/s), p, and q for sanidine and albite are equal to 5.0*10^{-7}, 0.16, 1.4 and 4.5*10^{-7}, 0.76, 90, respectively. And the curves integrating r_m and ΔG with these p and q constant exhibit a sigmoidal pattern, which describes a good correlation between the theoretical rates and the laboratory rate. The p and q constants, however, vary significantly among different feldspars and different water-rock systems (Alekseyev et al., 1997).

$$r_m = k_m A_m \,|1 - (Q_m/K_m)^{p|q} \quad (9)$$

In the incongruent dissolution stage, the low dissolution rate of primary minerals is mainly controlled by a slow precipitation of the reactions of secondary minerals. However, the mineral precipitation rate law still require further studies (Alekseyev et al., 1997).

2.3.3. Parallel rate law

The third formulation, the PRL was proposed by Burch et al. (1993) and Hellmann and Tisserand (2006) to explain the discrepancy between field and laboratory dissolution rates. The PRL combines two parallel nonlinear rate laws that are summed according to Eq. 10. The PRL is based on theoretical principles and experimental data which suggest that the close-to-equilibrium dissolution behavior is fundamentally distinct from the far-from-equilibrium dissolution (Burch et al., 1993; Hellmann and Tisserand, 2006; Maher et al., 2009; Hellmann et al., 2010). One rate law describes the far-from-equilibrium dissolution behavior with a rate constant k_2 and the other rate law describes the close-to-equilibrium behavior (k_1):

$$r = k_1 [1 - exp(-ng^{m_1})] + k_2 [1 - exp(-ng^{m_2})] \quad (10)$$

Where k_1 and k_2 are rate constants that have been determined by regression, g represent | ΔG | /RT, and n, m_1 and m_2 are adjustable fitted parameters that vary significantly among different water-rock systems. For example, n, m_1, and m_2 equal to 8.4*10^{-17}, 15.0, 1.45 for albite dissolution in aqueous solutions at 80 °C and pH 8.8 (Burch et al., 1993), and 7.98 *10^{-5}, 3.81, 1.17 for albite dissolution in aqueous solutions at 150 °C and pH 9.2 (Hellmann and Tisserand, 2006). This PRL rate law describes a continuous and highly non-linear, sigmoidal

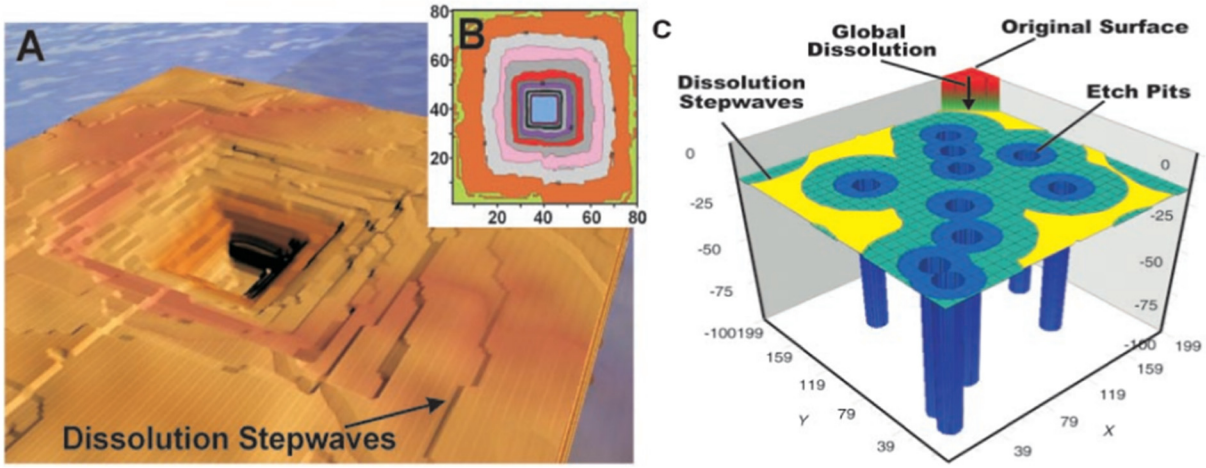

Fig. 12. (A) Monte Carlo simulation for the formation of an etch pit at the site of a dislocation defect and the generation of dissolution stepwaves. The height of the stepwaves is one molecular unit. The total distance laterally is 80 molecular units. (B) Contour plot of the topography (Monte Carlo simulation) showing circular dissolution stepwaves after 100,000 molecular units have dissolved. Each colour represents a change in depth of 5 molecular units. (C) Dissolution model that incorporates both the formation of etch pits and the far-reaching dissolution stepwaves into the overall dissolution rate. (after Lasaga and Luttge, 2001).

relation between R and ΔG that is characterized by three distinct free energy regions including a rate plateau region, a transition equilibrium region and a near equilibrium region (Fig. 11). In the plateau region, the water-rock system is at the far from equilibrium stage and the dissolution rate is high, while in the near equilibrium region, the water-rock system is at the near equilibrium stage, the dissolution rate is much lower than that in the plateau region. The significant decrease of the feldspar dissolution rate occurs in the transition region. Burcher (1993) used a critical free energy value (ΔG^{crit}) to explain the transition from the fast dissolution in the plateau region with significant undersaturation to the low dissolution rate at near equilibrium region. In the near equilibrium region where the undersaturation is low ($|\Delta G| < |\Delta G^{crit}|$), etch pits will not open up easily, suppressing the dissolution to slow dissolution rate; in constrast, in the transitional equilibrium region and rate plateau region where the undersaturtion is significant ($|\Delta G| > |\Delta G^{crit}|$), etch pits can be open up extensively on the crystal surfaces, and they also create a train of steps to form stepwaves on the mineral surfaces, accelerating the dissolution (Burch et al., 1993; Beig and Lüttge, 2006; Hellmann and Tisserand, 2006).

2.3.4. Stepwave model rate law

The stepwave model to control the bulk dissolution rate of feldspars was proposed by Lasaga and Luttge, 2001. Under large undersaturation conditions, etch pits open up easily on the feldspar surface with defect sites, and acting as the source of a train of steps (Fig. 12). These steps moving away from the defect into the surface lead to the development of dissolution stepwaves on the feldspar surface, which can travel throughout the mineral surface and eventually control the bulk dissolution rate. If the undersaturation is low, etch pits will not open up and defect sites will not lead to stepwaves forming far from the localized etch pit. Based on defect-generated dissolution etch pits and the stepwave model (Fig. 12), Lasaga and Luttge (2001) made a step forward and proposed another theoretical formulation that describes the changes in the dissolution rate resulting from changes in the degree of undersaturation (Lasaga and Luttge, 2001; Beig and Lüttge, 2006). Instead of using two distinct parallel laws (Eq. 10), the term ΔG^{crit} was directly employed in the formulation (Eq. 11).

$$\text{Rate}_{\text{diss}} = k_1(1 - e^{\Delta G/RT}) \tanh\left[\frac{B}{\left(1 - \frac{1 - e^{\frac{\Delta G_{crit}}{RT}}}{1 - e^{\frac{\Delta G}{RT}}}\right)}\right]\left(1 - \frac{1 - e^{\frac{\Delta G_{crit}}{RT}}}{1 - e^{\frac{\Delta G}{RT}}}\right) \quad (11)$$

where k_1 is a rate constant (mol m^{-2} s^{-1}), ΔG^{crit} is the Gibbs free energy that is required to form etch pits (kJ/mol), and B is a constant that depends on the surface diffusion distance. One prominent feature of this rate law is the nonlinear variation in the rate as the equilibrium is approached (Fig. 11B), which predict a substantial reduction in the rate once ΔG approaches ΔG^{crit} (Lasaga and Luttge, 2001).

The interpretation of the PRL (Eq. 10) and the stepwave model rate law (Eq. 11) using the shift between two dissolution mechanisms based on ΔG^{crit}, however, is still questionable, as etch pits are almost ubiquitous on the feldspar surface in both surficial field (Berner and Holdren, 1979) and subsurface rocks (Glasmann, 1992; Parsons et al., 2005; Bjørlykke and Jahren, 2012; Yuan et al., 2015a; Yuan et al., 2015b), where feldspar dissolution rate is extremely low.

2.3.5. Partial equilibrium law

Crundwell (2015b) did not try to resolve the rate gap between the L-TST rate law and the laboratory rate obtained at near equilibrium conditions (Crundwell, 2015b). Conversely, he argued that the chemical affinity cannot be used to describe the feldspar dissolution rate directly as only partial equilibrium has been obtained during the feldspar dissolution at conditions close to equilibrium.

Crundwell (2015a, 2015b) proposed that the feldspar dissolution reaction occurs by the parallel removal of aluminum and silica components from the surface (Fig. 10). The dissolution rate of feldspars is inhibited as the concentrations of the products, particularly aluminum and silica, increase. The parallel nature gives rise to the possibility of partial equilibrium, due to either the removal of aluminum approaching equilibrium or the removal of silica approaching equilibrium. The rate formulations for the partial equilibrium due to the removal of aluminum and silicate groups can be expressed by Eq. 12 and Eq. 13.

$$r = \vec{k}_{si}\left(\frac{\vec{k}_{Al}\,|OH^-|}{\vec{k}_{si} + \vec{k}_{Al}[Al(OH)_4^-]/(K_{Al}[OH^-]^3)}\right)^{0.5} \quad (12)$$

$$r = \vec{k}_{Al}[OH^-]\left(\frac{\vec{k}_{Si}}{\vec{k}_{Al}\,|OH^-| + \vec{k}_{Si}\vec{k}_{Na}[Si(OH)_4]^3[OH^-]^4[Na^+]/\vec{k}_{Na}/K_{Si}}\right)^{0.5} \quad (13)$$

where the symbols $k_{Si}(\rightarrow)$,$k_{Al}(\rightarrow)$ and $k_{Na}(\rightarrow)$ represent the rate constants for the forward reaction, and $k_{Si}(\leftarrow)$, $k_{Al}(\leftarrow)$ and $k_{Na}(\leftarrow)$ represent the rate constants for the reverse reaction for the removal of silica, aluminum and sodium from the surface, respectively. The square brackets, […], represent activities or concentrations of different solutes.

2.3.6. Other hypotheses

In additional to the above-mentioned rate laws and relevant interpretation of the persistent discrepancy between field and laboratory silicate mineral (e.g., feldspar) dissolution rates, other hypotheses have been used to solve the rate discrepancy; these include the armoring effects of coating secondary minerals on primary mineral surfaces by the interfacial dissolution-reprecipitation mechanism (Hellmann et al., 2003; Ruizagudo et al., 2016), the possible effects of leached layers (Section 2.1), and a shift of the rate-controlling mechanism from a primary mineral dissolution to a secondary mineral precipitation from congruent to incongruent dissolution of minerals (Alekseyev et al., 1997; Zhu et al., 2004; Zhu, 2005; Maher et al., 2009; Zhu and Lu, 2009; Zhu et al., 2010; Lu et al., 2013).

Zhu et al. (2004) and Zhu (2005) proposed that clay precipitation kinetics is the rate-limiting step in controlling feldspar dissolution reaction rates in the regional Navajo sandstones aquifer system of the Black Mesa of Arizona. Clay precipitation removes solutes from the aqueous solution, maintaining a condition of feldspar undersaturation, and makes additional feldspar dissolution possible. But the slow clay precipitation results in a steady state in which the aqueous solution is near equilibrium with feldspar (Zhu et al., 2004; Zhu, 2005; Zhu and Lu, 2009; Zhu et al., 2010; Zhu et al., 2014). The reduction of feldspar dissolution rate by slow secondary mineral precipitation has also been verified by laboratory experiments conducted by Alekseyev et al. (1997) and Lu et al. (2013). This mechanism is still difficult to explore, however, because rate laws for secondary Al mineral precipitation are relatively sparse and the surface areas of secondary minerals are especially difficult to quantify (Tutolo et al., 2015).

2.4. Existing problems and future work

Unlike laboratory feldspar dissolution at conditions far from equilibrium, feldspar dissolution and relevant secondary mineral (gibbsite, boehmite, kaolinite, illte, muscovite, paragonite, quartz) precipitation are integrated processes in experiments that have been conducted under near equilibrium conditions, and in chemical weathering and hydrothermal alteration processes in natural rocks (Giles, 1987; Alekseyev et al., 1997; Zhu et al., 2004; Steefel et al., 2005; Zhu, 2005; Maher et al., 2009; Zhu et al., 2010; Bjørlykke and Jahren, 2012; Yuan et al., 2015a; Yuan et al., 2017a). Petrographic evidences from deeply buried subsurface rocks suggest that secondary minerals originate from feldspar dissolution occur not only as some coatings on feldspar surface, but more commonly as pore filling clays and quartz cements (Glasmann, 1992; Molenaar et al., 2015; Yuan et al., 2015a; Yuan et al., 2017a). From feldspar dissolution to mineral precipitation in a natural water-rock system, four major processes have been identified (Fig. 13), including ① release of solutes (e.g., Na^+, K^+, Al^{3+}, SiO_2(aq)) from primary minerals, ② transfer of solutes across the altered layer (including residual layer and coating layer) to the solution, ③ transfer of solutes to precipitation sites across a porous medium, and ④ removal of solutes from solution by secondary mineral precipitation. One of the four processes with the lowest reaction rate probably controls the mineral dissolution rate under specific conditions (Wollast, 1967; Thyne et al., 2001; Zhu et al., 2004; Zhu, 2005; Zhu et al., 2010). For example, in a deeply-buried tight sandstone with extremely low porosity and permeability, high temperature and low pH, the extremely low diffusion coefficient of Al^{3+} and SiO_2(aq) in the pore systems of the tight rocks may critically control the low feldspar dissolution processes, although high temperature and low pH tend to accelerate the feldspar dissolution rate and secondary mineral precipitation rate. Another case is that, if the rate of chemical reaction is much higher than the diffusion rate of the ions through the residual layer, the rate of feldspar dissolution reaction is controlled by the rate of diffusion of ions through the altered layer. The diffusion rate of solutes in the altered layer was found to be very slow, approximately 10^{-19} cm^2/s (10^{-14} cm^2/day) (Correns and Von, 1938; Wollast, 1967). The hypothesis proposed in Section 2.3, however, consider only one or two of these four processes when trying to resolve the rate discrepancy. For example, the nonlinear TST rate law, the PRL, and the stepwave rate law did not consider the solute transfer in the altered layer and the solution, nor the secondary mineral precipitation; the partial equilibrium law did not consider the solute transfer in the solution and the secondary mineral precipitation; the hypothesis of clay precipitation did not consider the solute transfer processes thoroughly.

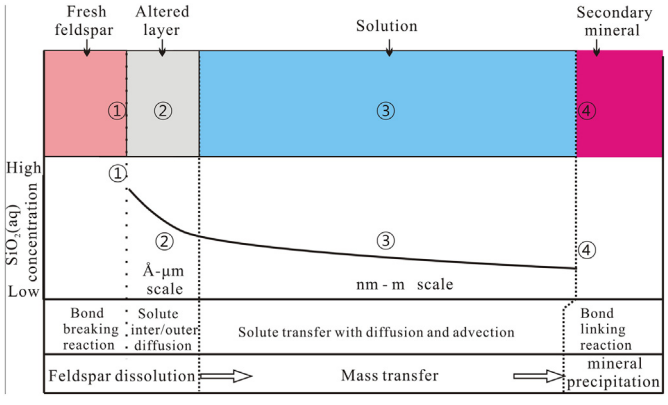

Fig. 13. Schematic illustration of the four main physicochemical processes occurring from feldspar dissolution to secondary mineral precipitation in subsurface geochemical systems. ① release of solutes from feldspars, ② transfer of solutes across the altered layer (residual layer and coating layer) to the solution, ③ transfer of solutes to precipitation sites across porous medium, and ④ removal of solutes from solution by secondary mineral precipitation.

In addition to the four processes, another annoying occurrence that makes the relevant water-rock interactions extremely complex is the fact that the precipitated minerals will dissolve again to form new minerals as the interactions proceed (Chuhan et al., 2000; Bove et al., 2002; Zhu and Lu, 2009; Franks and Zwingmann, 2010; Lander and Bonnell, 2010; Zhu et al., 2010). For example, in a K-feldspar- distilled water system, the geochemical system can evolve from the initial water-feldspar system to water-feldspar-gibbsite, to water-feldspar-gibbsite-kaolinite, to water-feldspar-kaolinite, to water-feldspar-kaolinite-quartz, to water-feldspar-kaolinite-illite-quartz and lastly to water-feldspar-illite-quartz systems. In a water-rock system with only one primary mineral and only one secondary mineral, it is still possible to test the mineral dissolution rate by determining the change in the silicon isotope composition of the water (Gruber et al., 2014; Gruber et al., 2017). In field situations, several dissolution and precipitation reactions may operate simultaneously (Zhu et al., 2010). The combination of several minerals makes it very difficult to distinguish how much feldspar has been dissolved during a given period by testing the changes in Si (Al) concentration or even the changes in the silicon isotope composition. The use of ΔG^{crit} for etch pit formation has been proposed to explain the low feldspar dissolution rate at conditions near equilibrium. Different from the stepwave model employing the ΔG^{crit} for etch pit formation, the low rate of feldspar dissolution, however, may be caused by the precipitation and re-dissolution of the secondary minerals (Zhu and Lu, 2009); and some specific ΔG^{crit} for the evolution (precipitation and re-dissolution) of these different secondary minerals may exist as the water-rock system evolves from a far from equilibrium condition to a near equilibrium condition.

Aside from laboratory experiments, reactive transport modeling, which can couple the mineral dissolution and precipitation processes to the mass transfer processes, are essential and significant tools for investigating the water-rock interactions (Steefel and Van Cappellen, 1990; Stoessell and D, 1990; Steefel and Lasaga, 1994; Steefel et al., 2005; Yuan et al., 2017a). Zhu et al. (2010) attempted to extrapolate a batch laboratory experiment (primary feldspar, secondary minerals include boehmite and kaolinite) to reactive transport modeling with

only one dissolution reaction (feldspar) and one precipitation reaction (kaolinite). In a near equilibrium system, the coupling effects of several dissolution and precipitation events in the reaction network can become extremely complex. Additionally, because of this complexity, future work should employ numerical reactive transport modeling of the reaction paths to match the experimental data and hence to quantitatively evaluate the inter-dependence of dissolution–precipitation reactions (Zhu and Lu, 2009; Zhu et al., 2010; Wigley et al., 2013).

3. Organic- and inorganic-original subsurface feldspar alteration in reservoirs

Feldspar alteration is ubiquitous from shallow to deeply buried rocks (Lasaga and Luttge, 2001; Zhu et al., 2004; Molenaar et al., 2015; Yuan et al., 2015a; Yuan et al., 2018). Due to the advances of the oil industry, variety of data (petrography, chemistry) on subsurface rocks, pore waters, natural gases, and hydrocarbons obtained during oil exploration and production have provided great opportunities for scientists to study the origin of the feldspar alteration reactions in natural water-rock systems (Carothers and Kharaka, 1978; Schmidt and A, 1979; Surdam et al., 1984; Surdam and Crossey, 1987; Glasmann, 1992; van Berk et al., 2013). Although feldspars can be dissolved by acidic, neutral, or basic fluids (Fig. 9) (Crundwell, 2015a), most petroleum geologists have ascribed surficial and subsurface feldspar dissolution to the presence of inorganic-original and organic-original acids in shallow to deep aquifers and hydrocarbon reservoirs (Fig. 14) (Schmidt and A, 1979; Surdam et al., 1984; Emery et al., 1990; van Berk et al., 2013; Yuan et al., 2015a).

3.1. Inorganic-original feldspar alteration

3.1.1. Meteoric water induced feldspar dissolution

Meteoric water promotes feldspar dissolution as CO_2 dissolves in the water to produce carbonic acid, and as a consequence, H^+ released from carbonic acid can catalyze the dissolution reactions (Giles, 1986; Emery et al., 1990; França et al., 2003; Bjørlykke and Jahren, 2012). The leaching capability of a meteorically derived water entering an aquifer depends upon the amount of dissolved CO_2 and the reactions that have occurred during its passage through the regolith (Giles, 1986; França et al., 2003).

Feldspar dissolution induced by meteoric water leaching and the concomitant kaolinite precipitation of surficial sediments in the Holocene have been described widely in soil science and clay mineralogical literature (Tardy, 1971; Berner and Holdren, 1979; Fitzpatrick and Schwertmann, 1982). In ancient sandstones, feldspar dissolution by meteoric water has also been described in several studies (Emery et al., 1990; França et al., 2003; Yuan et al., 2017b). Although meteoric water can penetrate to considerable depths in sedimentary basins (Mahnheim, 1967; Habermehl, 1980; Giles, 1986), most meteoric diagenetic alterations have been suggested to occur closely beneath unconformities (Emery et al., 1990; Huang et al., 2003) or at buried depths of less than a few hundred meters (Bjørlykke, 1993; Mansurbeg et al., 2006; Bjørlykke and Jahren, 2012). Generally, stable isotopic compositions of authigenic kaolinite have been used as important evidence to support the meteoric diagenesis relevant to feldspar dissolution in sandstones (Bird and Chivas, 1988; Purvis, 1995). Aside from the hydrogen and oxygen isotope signatures of authigenic kaolinite, it is difficult to obtain other direct chemical evidence for meteoric water leaching (Yuan et al., 2017b). Emery et al. (1990) sought three proofs to sustain the feldspar dissolution beneath an unconformity by meteoric water leaching: the enrichment of feldspars in the initial sandstones, the dissolution textures on the feldspar grains in the sandstones, and a regional unconformity capped on the sandstones. Few studies have tried to identify deep meteoric leaching reactions in buried sandstones. For example, França et al. (2003) reported an example of meteoric water leaching in Jurassic Botucatu eolianite sandstones of the Parana Basin in Brazil from outcrops to a burial depth of 1000–1500 m, but with petrographic evidence of mineral dissolution mainly occurring in sandstones shallower than 250 m. Findings concerning the incursion of meteoric water in deeply buried Permian Rotliegend sandstones of the North Sea during an uplift period was presented in Gluyas et al. (1997). Using seismic profiles, petrography, fluid inclusion and isotope composition of kaolinite and quartz cements, Yuan et al. (2017b) suggested that with the existence of widely developed faults and great uplift, meteoric freshwater has penetrated > 1500–1800 m to leach feldspars in subsurface Eocene Shahejie Formation sandstones in the Nanpu Sag, Bohai Bay Basin.

3.1.2. Deep hot water induced feldspar dissolution

Reverse weathering reactions of silicate minerals in deeply-buried layers with high temperature were proposed to be potentially important sources of acids during burial metamorphism of sediments (Smith and Ehrenberg, 1989; Hutcheon and Abercrombie, 1990; Land and Macpherson, 1992). For examples, the two reactions in Eq. 14 and Eq. 15 show that cations including Mg^{2+} and Na^+ are fixed in the mineral phases and H^+ are released into solution. These reactions have been recorded both in mudstones and sandstones (Hower et al., 1976; Boles and Franks, 1979; Milliken et al., 1989; Milliken, 1992; Hövelmann

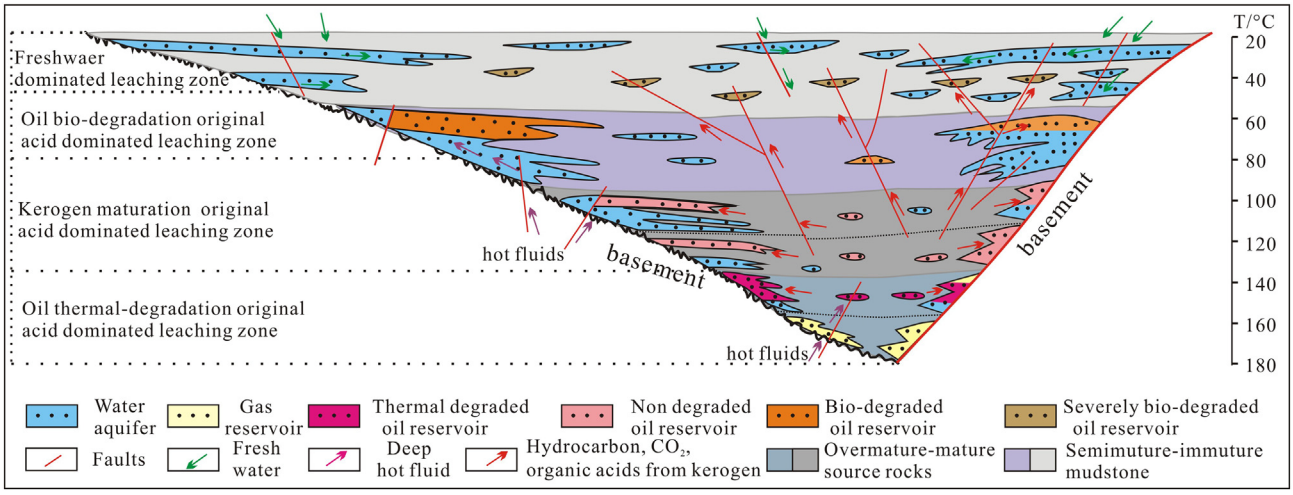

Fig. 14. A schematic shows the evolution of main fluids with increasing depth and temperature and relevant organic- and inorganic-original. feldspar alteration in a sedimentary petroliferous basin.

et al., 2010).

$$3Al2Si2O5(OH)4\ (kaolinite) + 7\ Mg2 + +9H2O \rightarrow 2\ Mg3.5Al3Si3O10(OH)8\ (chlorite) + 14H+ \quad (14)$$

$$Al2Si2O5(OH)4 + 4H4SiO4 + 2Na + \rightarrow 2NaAlSi3O8\ (albite) + 9H2O + 2H+ \quad (15)$$

The activity of H^+ in pore water residing in a deeply-buried section is presumably controlled by water-rock interactions involving these reverse weathering reactions. With increasing temperature, a metastable equilibrium between the fluids and silicate minerals buffers the water pH to progressively lower values (Hutcheon and Abercrombie, 1990; Hutcheon et al., 1993). The hot acidic fluids in the deeply-buried layers can be episodically expelled and then injected along faults into relatively shallow reservoirs, leading to the dissolution of feldspars and carbonate minerals (Taylor and Land, 1996; Taylor et al., 2010). This hypothesis, however, needs specific and extraordinary geological conditions that provide access to deep hot fluid sources, which is not common in subsurface reservoirs (Taylor et al., 2010).

3.2. Organic-original feldspar alteration

3.2.1. Kerogen maturation induced feldspar alteration

During the thermal evolution of various types of kerogen in source rocks, large amounts of water, CO_2 and organic acids can be generated prior to the main petroleum generation stage (Fig. 15) (Carothers and Kharaka, 1978; Schmidt and A, 1979; Surdam et al., 1984; Surdam and Crossey, 1987; Seewald, 2003; Yuan et al., 2015b). With identification of the CO_2 and organic acids in subsurface reservoirs, the organic-derived CO_2 leaching hypothesis and organic acid leaching hypothesis were initially proposed by Schmidt and McDonald (1979), Surdam et al. (1984), and Surdam and Crossey (1987) to be mechanisms for promoting the dissolution of labile minerals including feldspars and carbonate minerals. In addition to the available CO_2 and organic acid data from oil field, kerogen pyrolysis experiments have also verified the generation of these acids (Barth et al., 1988; Barth and Bjørlykke, 1993; Barth et al., 1996).

Schmidt and McDonald (1979) proposed that the organic-original CO_2 dissolves into pore water to generate H^+. The hydrogen ion dissolves mainly carbonate minerals but few feldspar due to the fast dissolution rate of carbonate minerals and a large number of secondary pores were generated during the mature stage. Due to bacterial consumption at low temperatures (< 80 °C) and thermal decarboxylation at higher temperatures (> 120 °C), the highest concentrations of organic acids in oil-field waters occur in the temperature range of 80–120 °C. The organic acid concentrations decrease sharply as temperature decreases to be lower than 70–80 °C or increases to be higher than 120 °C (Carothers and Kharaka, 1978; Surdam and Crossey, 1987). Unlike organic acids, the partial pressure of CO_2 (pCO_2) generally increases with increasing temperature (depth) (Smith and Ehrenberg, 1989; Seewald, 2003;). Based on the pH buffering effect of organic acids and CO_2 in CO_2-organic acid-water- feldspar-calcite systems, complex reaction pathways were proposed by Surdam et al. (1984) and Surdam and Crossey (1987) to describe the dissolution of feldspars and carbonate minerals in the temperature range of 80–120 °C and 120–200 °C (Fig. 7 and Fig. 8 in Surdam et al., 1987). With these pathways and the idea that organic acids may promote feldspar dissolution by forming aluminum-organic complexes, Surdam and Crossey et al. (1987) proposed that there is one potential carbonate dissolution episode and one feldspar dissolution episode in the range of 80–120 °C in a geochemical system with relatively high concentrations of organic acids and low pCO_2; feldspar dissolution is not preferred in zones with higher temperatures where organic acids were decomposed.

Since the leaching hypothesis by CO_2 and organic acids was proposed, doubts as to their efficiency have been raised (Bjørlykke, 1984; Lundegard et al., 1984; Giles, 1986; Taylor et al., 2010; Bjørlykke, 2014). Most counterviews argue that these hypotheses failed to explain the quantities of CO_2 or acid pore water that may have migrated through source rocks and pathways to reservoirs because CO_2 and organic acids generated in source rocks would be consumed quickly by extensive internal carbonate dissolution in the source rocks themselves.

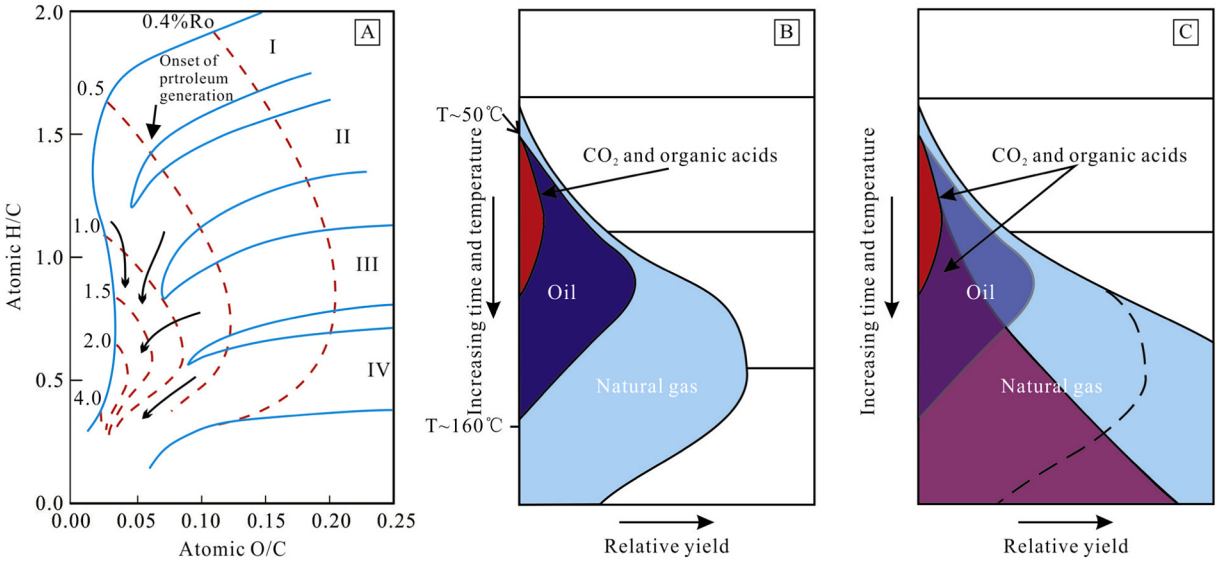

Fig. 15. Chemical evolution of kerogen and petroleum during thermal maturation in sedimentary basins. (A) Van Krevelen diagram showing the chemical evolution of immature kerogen of varying composition (type I, II, III and IV) at increasing levels of thermal maturity. Levels of thermal maturity are indicated by isochors of vitrinite reflectance (%R_o), a widely used geochemical indicator that integrates the effects of time and temperature during thermal maturation of sediments. In general, kerogen composition moves from the upper right regions of the figure to the lower left with increasing maturity. (B) Traditional model of the amount and timing of organic alteration products generated during progressive burial in sedimentary basins that assumes oxygen and hydrogen in organic alteration products are derived only from kerogen. The form of this figure is constrained by the maturation trends shown in the Van Krevelen diagram. (C) Schematic illustration of the amount and timing of organic alteration products generated if water and minerals are allowed to contribute the requisite hydrogen and oxygen for the formation of hydrocarbons and oxygenated compounds such as carbon dioxide and carboxylic acids. Ultimately, production of oxygenated products and methane will cease owing to exhaustion of a reactive carbon source. The depth at which this occurs is unknown. (after Seewald, 2003).

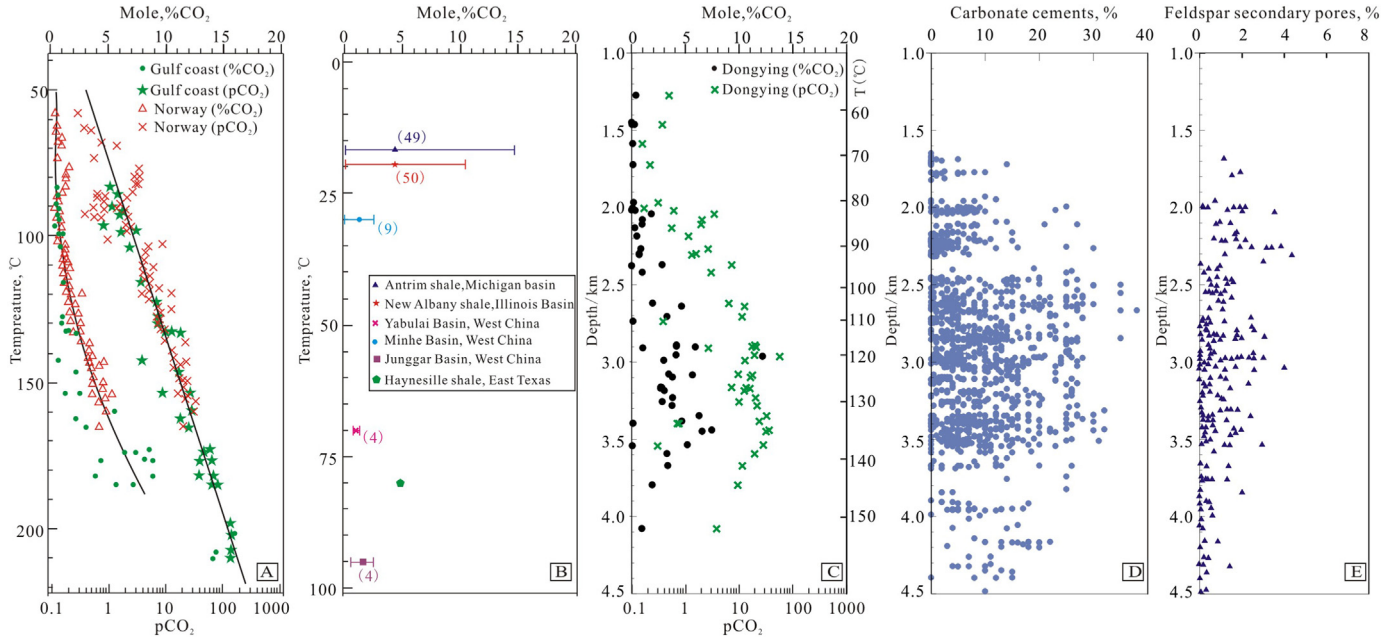

Fig. 16. (A) Mol %CO_2 and pCO_2 in hydrocarbon reservoirs from the US Gulf Coast and the Norwegian continental shelf; (B) Mol %CO_2 in organic-rich shales from global basins; Mol % CO_2 and pCO_2 (C), carbonate cements (D), and feldspar secondary porosities (E) in the Eocene sandstones in the northern Dongying Sag, China. (after Yuan et al., 2015b).

Moreover, the present concentrations of organic acids in most formation waters are too low to generate large numbers of secondary pores. Additionally, as mentioned in Section 2.2, geochemical studies have failed to substantiate meaningful levels of Al-complexing by organic acids, a potentially instrumental factor for significant feldspar dissolution (Bevan and Savage, 1989; Stoessell and D, 1990; Manning et al., 1992; Harrison and Thyne, 1994). The modeling work by van Berk et al. (2015), however, suggests that saturated fluids from source rocks may still trigger a continuous mineral dissolution along their migration path following a decreasing pressure and temperature regime.

With the inspiring and widespread phenomena of the selective dissolution of feldspars in the presence of carbonates in both sandstones (Cao et al., 2014) and organic-rich mudstones (Turchyn and Depaolo, 2011; Macquaker et al., 2014), Yuan et al. (2015b) revisited the chemistry of secondary pores formed by feldspar dissolution using evidences from sandstone petrography, numerical simulation of chemical reactions in K-feldspar-calcite-CO_2-H_2O systems and the isotopic composition of CO_2 in reservoirs and shales (Fig. 16). In subsurface layers with carbonate and silicate minerals and a limited pore water volume, the water pH is buffered by silicate minerals to a relatively high level (Hutcheon and Abercrombie, 1990; Hutcheon et al., 1993; Yuan et al., 2015b). The calcite dissolution is suppressed due to the high pH and the much lower equilibrium constants of the calcite dissolution reactions than the feldspar dissolution reactions; what's more, the selective dissolution of feldspars can even promote some carbonate mineral precipitation (Yuan et al., 2015b). Without an extensive internal consumption of the acids produced by the kerogen maturation in the source rocks, the CO_2 acids were likely transferred to the sandstone reservoirs (Fig. 16) to selectively dissolve large amounts of feldspars and form the authigenic quartz and clays (Yuan et al., 2015b). Similarly, organic acids can also be preserved and transferred to reservoirs to dissolve feldspars. Thus, the selective dissolution of feldspars, rather than carbonates, in sedimentary rocks is likely a general mechanism for deciphering the chemistry of secondary porosity.

3.2.2. Hydrocarbon degradation induced feldspar alteration

The mineral dissolution induced by organic-original CO_2 and organic acids originating from kerogen maturation has been proposed to occur mainly before or during the oil charging processes (Schmidt and A, 1979; Surdam and Crossey, 1987). Elevated temperature and pressure increase the solubility of hydrocarbons in water, and lead to organic-inorganic interactions among hydrocarbons, water and rocks in reservoirs, which are critical in the ongoing evolution of petroleum and rock quality over geological time after hydrocarbon emplacement (Lewan, 1997; Seewald, 2001; Seewald, 2003; van Berk et al., 2013). Studies on deeply-buried sandstone reservoirs have verified that feldspar alteration also occurs after hydrocarbon emplacement; this was verified using petrographic analyses of diagenetic mineral assemblages, oil phases in secondary pores, and fluid inclusions in quartz cements originating from feldspar dissolution (Yuan et al., 2018). After the emplacement of hydrocarbons in reservoirs, oil degradation may proceed by biodegradation at relatively low temperatures of < 80 °C (Meredith et al., 2000; Ehrenberg and Jakobsen, 2001; Head et al., 2003) or by thermal degradation at elevated temperatures of generally higher than 140 °C (Seewald, 2001; Hill et al., 2003; Seewald, 2003) (Fig. 14). Biodegradation is known to be associated with an increased acidity of petroleum, caused by the generation of both CO_2 and organic acids as the products of bacterial metabolism (Hiebert and Bennett, 1992; Meredith et al., 2000; Ehrenberg and Jakobsen, 2001). Oil degradation in anhydrous systems has been suggested to form lower molecular hydrocarbons via free-radical thermal cracking reaction and pyrobitumen via free-radical cross linking reaction, respectively (Lewan, 1997; Hill et al., 2003; Tian et al., 2006). Seewald (2001, 2003) proposed that in the presence of pore water in hydrocarbon reservoirs, the thermal degradation pathways of aqueous *n*-alkanes differ from the anhydrous thermal cracking pathways. In natural reservoirs, water is always available, even in the oil zone. The oil thermal degradation will generate large amounts of organic acids by step oxidation reactions and large amounts of CO_2 through thermal decarboxylation of organic acids (Fig. 17). These organic acids and CO_2 from biodegradation or thermal degradation of hydrocarbons can dissolve in the residual pore water to generate H^+, promoting dissolution of feldspar and calcite minerals (Yuan et al., 2019). Petrographic and chemical data from the Brent Group sandstone of the Gullfaks field, North Sea (Ehrenberg and Jakobsen, 2001) and hydrogeochemical modeling results with constraints of the data from the Brent Group

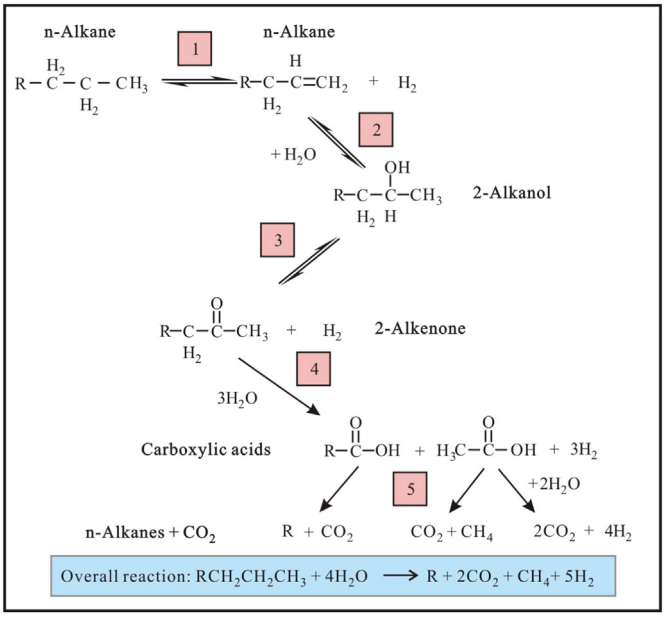

Fig. 17. Reaction pathways responsible for the stepwise oxidation of aqueous nalkanes at elevated temperatures and pressures. Mineral oxidants in the subsurface environments may consume molecular hydrogen generated by these reactions, allowing the overall reaction to proceed continuously. Saturated hydrocarbons produced in step (5) may re-enter the sequence at the top and undergo subsequent oxidation. The net effect is the conversion of long-chain alkanes in oil to short-chain hydrocarbons in natural gas. The overall reaction indicated at the bottom has been written assuming that decarboxylation is responsible for the decomposition of acetic acid in the final step of the sequence (after Seewald, 2003).

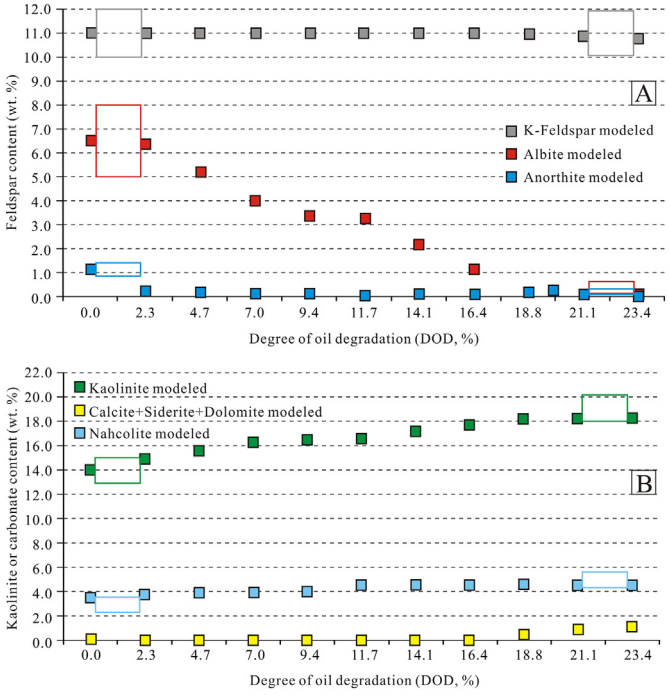

Fig. 18. Modeling results in an oil-water-rock system in comparison to measured/observed data. (A) Feldspar content versus conceptual degree of oil degradation (DOD). Measured/observed data (colored rectangle lines) are given for the lowest and highest DOD. (B) Kaolinite, Ca-Mg-Fe carbonate, and sodium carbonate content versus DOD. Measured/observed data (colored rectangle lines) are given for the lowest and highest DOD (after van Berk et al., 2013).

sandstone (Onstott et al., 2010; van Berk et al., 2013) suggested that oil degradation at the oil-water contact in the Gullfaks field probably promoted the alteration of feldspars to kaolinite and quartz (Fig. 18), and the generation of high pCO_2 in the reservoirs.

All in all, although there is still debate, the CO_2 and organic acids generated during the kerogen maturation and hydrocarbon degradation still are likely the most important acids promoting feldspar dissolution during burial diagenesis in subsurface rocks (Fig. 14).

4. Mineral assemblages of feldspar alteration

From shallow aquifers to middle-deep basinal saline or hydrocarbon reservoirs, the prevailing fluid flows in sedimentary basins evolve from downward-driven meteoric freshwater with a high velocity to upward-driven compaction flows with a low velocity and high salinity, although episodic flows through faults may dominate periodically in some cases (Giles, 1987; Bjørlykke, 1993; Bjørlykke and Jahren, 2012). Pore water saturation evolves from undersaturation to near saturation or oversaturation with most minerals after long-term contact and the geochemical system evolves from open to closed with respect to most solutes in the pore water (Giles, 1987; Bjørlykke and Jahren, 2012; Yuan et al., 2017a). As the geochemical environments change, chemical reactions and diagenetic mineral assemblages relevant to the feldspar alteration in buried feldspar-rich layers also change (Huang et al., 1986; Hayes and Boles, 1992; Bjørlykke and Jahren, 2012; Yuan et al., 2017a).

4.1. Chemical reactions from dissolution to precipitation

The dissolution of feldspars (e.g., K-feldspar) can be expressed by the following equations, providing that no precipitation of secondary minerals occurs (Giles and Boer, 1990; Zhu and Lu, 2009; Yuan et al., 2017a):

$$KAlSi_3O_8(K-feldspar) + 4\,H^+ = 2\,H_2O + K^+ + Al^{3+} + 3SiO_2(aq) \quad (16)$$

These congruent dissolution reactions can occur in an open water-rock system with high flow rates from which the solutes can be removed in time (Giles, 1987; Yuan et al., 2017a) or only during the very initial dissolution stage in a dilute water – feldspar system with a low flow rate from which the released solutes cannot be removed in time (Alekseyev et al., 1997; Zhu and Lu, 2009). Once the concentrations of Al^{3+}, $SiO_2(aq)$, K^+, or Na^+ exceed the concentrations needed for the saturation of secondary minerals (gibbsite, boehmite, kaolinite, illite, quartz), these minerals can precipitate, assuming that no kinetic barrier exists (Maher et al., 2009; Zhu and Lu, 2009; Zhu et al., 2010; Yuan et al., 2017a). Because the solute concentrations required for saturation differ for different minerals (Yuan et al., 2017a), the secondary minerals tend to form and break successively in a closed water-feldspar system with a low flow rate (Fig. 19) (Helgeson, 1979; Bjørkum and Gjelsvik, 1988; Bjørlykke and AAgaard, 1992; Glasmann, 1992; Bjørlykke and Jahren, 2012). In the diagenetic zone (generally $T < 200$ °C), the secondary mineral sequence in a closed K-feldspar-water system is probable gibbsite at the initial dissolution stage, followed by kaolinite, kaolinite + quartz, and then illite (muscovite) + quartz as the water-rock interactions proceed (Helgeson, 1979; Bjørkum and Gjelsvik, 1988) (Fig. 19 A–D). In an albite-water system or K-feldspar- NaCl water system with a high sodium concentration, the sequence is likely to be gibbsite, kaolinite, kaolinite + quartz, paragonite + quartz, and then albite, as the water-rock interactions proceed (Fig. 19 F, G) (Bjørlykke and AAgaard, 1992). When the temperature exceeds 200 °C, boehmite instead of gibbsite can be formed during the initial stage (Fig. 19 G–H) (Fu et al., 2009).

In a K-feldspar-H_2O-H^+ system at 100 °C, for example, the evolution of secondary minerals from the initial gibbsite to illite (muscovite) and quartz can be described by the following chemical reactions of Eq.

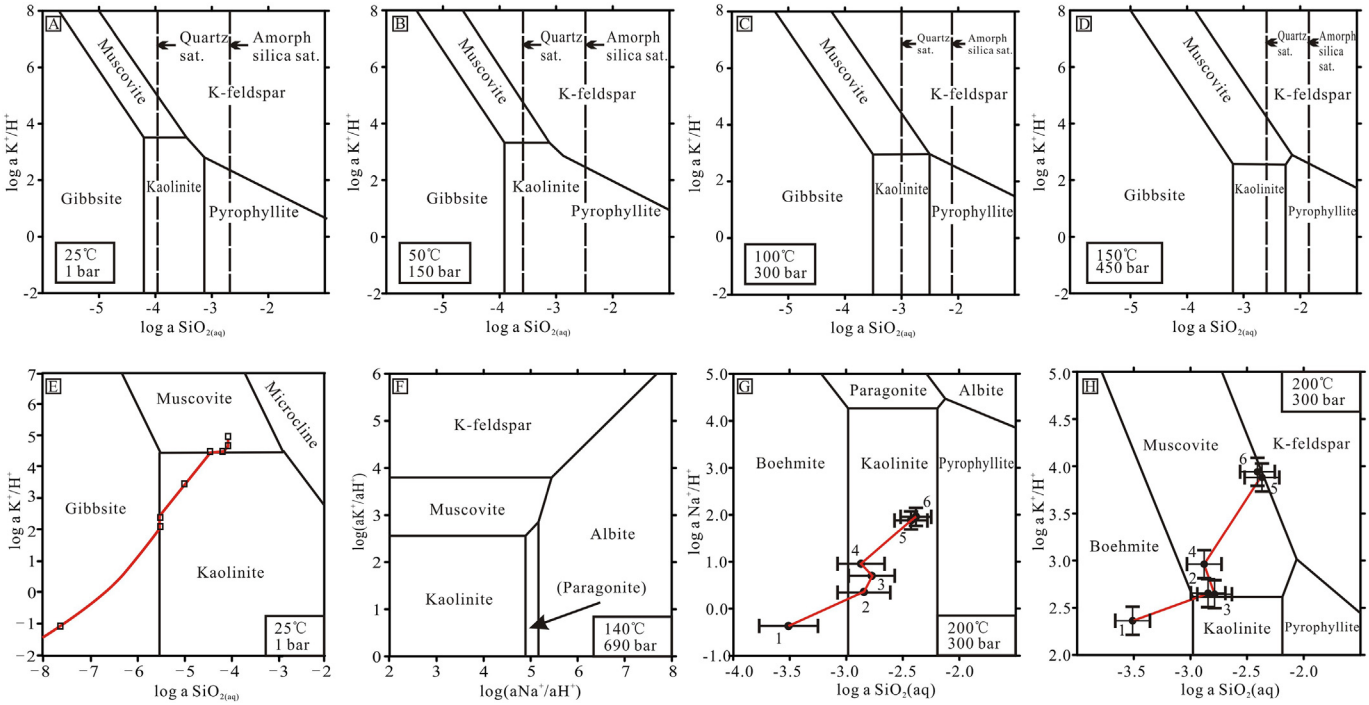

Fig. 19. (A, B) Logarithmic activity diagrams in the K_2O-SiO_2-Al_2O_3-H_2O system. For 25 °C, 1 bar (A) and 50 °C, 150 bars (B), when log *asio₂* is higher than the triple point (muscovite-K-feldspar-kaolinite), authigenic K-feldspar and authigenic kaolinite may form simultaneously in a closed system by degradation of muscovite. At a lower degree of silica supersaturation (less than the triple point), authigenic illite (muscovite) and quartz may form by degradation of K-feldspar and kaolinite. (C) For $T > 100$ °C and 300 bars, K-feldspar and kaolinite are an unstable mineral association independent of the silica activity, and K-feldspar and kaolinite react to form illite (muscovite) and quartz cement. (D) At 150 °C and 450 bars, kaolinite and K-feldspar do not form a stable mineral assemblage, and we expect illite (muscovite) and quartz cement to form by degradation of K-feldspar and kaolinite. (after Helgeson, 1979). (E) Equilibrium activity–activity diagram showing the reaction path of the dissolution of microcline in pure water at 25 °C (after Zhu and Lu, 2009). (F) Mineral variations in logarithmic activity diagrams of $\log(aNa^+/aH^+)$ vs. $\log(aK^+/aH^+)$ (Bjørlykke and AAgaard, 1992). (G-H) Mineral phase diagrams in the Na_2O–Al_2O_3–SiO_2–H_2O–HCl (G) and K_2O–Al_2O_3– SiO_2–H_2O–HCl (H) system at 200 °C and 300 bars with experimental data showing time series change of aNa^+/aH^+ and aK^+/aH^+, respectively, with $aSiO_2(aq)$ in alkali-feldspar dissolution experiment (78-day) at same conditions (after Fu et al., 2009).

17–25 (Fig. 20) (Helgeson, 1979; Giles and Boer, 1990; Zhu et al., 2010). Similar chemical reactions can be written to describe the water-rock interactions in other various feldspar-water geochemical systems.

During the initial stage, after the Al^{3+} concentration reaches a specific value, gibbsite is precipitated according to Eq. 17. Generally, this stage lasts a short time (< 1–2 days) in laboratory experiments with batch systems.

$$Al^{3+} + 3H_2O = Al(OH)_3(gibbsite) + 3H^+ \quad (17)$$

As the reaction continues, with an increase in the $SiO_2(aq)$ concentration, kaolinite is formed instead of gibbsite, which is represented by Eq. 18. The consumed Al^{3+} and $SiO_2(aq)$ may originate from the dissolution of the early formed gibbsite (reverse reaction of Eq. 17), residual K-feldspar (Eq. 16) or both; the corresponding integrated reactions can be represented by Eq. 19, Eq. 20 and Eq. 21, respectively.

$$Al^{3+} + SiO_2(aq) + 2.5H_2O = 0.5Al_2Si_2O_5(OH)_4(kaolinite) + 3H^+ \quad (18)$$

$$Al(OH)_3(gibbsite) + SiO_2(aq) = 0.5Al_2Si_2O_5(OH)_4(kaolinite) + 0.5\,H_2O \quad (19)$$

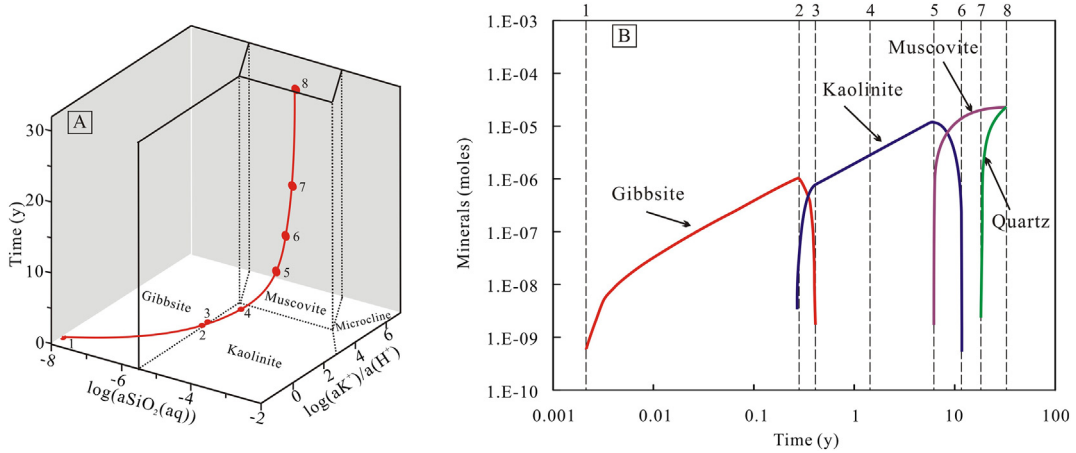

Fig. 20. (A) Equilibrium activity–activity diagram showing the reaction path evolution of the dissolution of microcline in pure water at 25 °C with time. (B) Secondary mineral abundance versus time in the dissolution experiment of microline in pure water at 25 °C (after Zhu and Lu, 2009).

$$Al(OH)_3(gibbsite) + KAlSi_3O_8(K\text{-feldspar}) + H^+ = Al_2Si_2O_5(OH)_4(kaolinite) + SiO_2(aq) + K^+ \quad (20)$$

$$KAlSi_3O_8(K\text{-feldspar}) + H^+ + 0.5H_2O = 0.5\ Al_2Si_2O_5(OH)_4(kaolinite) + 2SiO_2(aq) + K^+ \quad (21)$$

When the fluid becomes saturated or oversaturated with respect to quartz, authigenic quartz can be formed:

$$SiO_2(aq) = Quartz \quad (22)$$

As the system reaches a steady state among the fluids, K-feldspar, kaolinite and quartz, and the early formed gibbsite has been consumed totally, K-feldspar would be dissolved to form kaolinite and quartz directly with suitable solute concentration (Eq. 21). These chemical reactions should be common, because authigenic kaolinite and (or) quartz can be identified in most subsurface feldspar-rich sandstones at temperatures < 120–130 °C (Giles and Boer, 1990; Glasmann, 1992; Bjørlykke et al., 1995; Yuan et al., 2015a; Yuan et al., 2017a).

With the accumulation of K^+ in the fluid, high potassium level actively promote illitization reactions of kaolinite and feldspars, which are represented by Eq. 23–25.

$$Al_2Si_2O_5(OH)_4(kaolinite) + 0.667\ K^+ = H_2O + 0.667KAl_3Si_3O_{10}(OH)_2(illite/muscovite) + 0.667H^+ \quad (23)$$

$$Al_2Si_2O_5(OH)_4(kaolinite) + KAlSi_3O_8(K\text{-feldspar}) = KAl_3Si_3O_{10}(OH)_2(illite/muscovite) + 3SiO_2(quartz) + H_2O \quad (24)$$

$$KAlSi_3O_8(K\text{-feldspar}) + H^+ = 0.5\ KAl_3Si_3O_{10}(OH)_2(illite/muscovite) + 3SiO_2(quartz) + K+ \quad (25)$$

As the system reaches a steady state among the fluid, K-feldspar, illite, and quartz, and the early formed kaolinite has been entirely consumed, K-feldspar should be dissolved to form illite and quartz directly with suitable solute concentration (Eq. 25). These chemical reactions should also be common because authigenic illite and quartz exist in most deeply buried feldspar-rich sandstones at temperatures higher than 120–130 °C (Bjørlykke et al., 1995; Franks and Zwingmann, 2010; Hövelmann et al., 2010; Lander and Bonnell, 2010; Yuan et al., 2015a).

Under suitable conditions, the in-situ replacement of K-feldspars by albite occurs (Wilkinson et al., 2001; Hövelmann et al., 2010; Yuan et al., 2017a), and this process is represented by:

$$KAlSi_3O_8(K\text{-feldspar}) + Na^+ = NaAlSi_3O_8(Albite) + K^+ \quad (26)$$

4.2. Diagenetic mineral assemblages in subsurface reservoirs

Many petrographic studies in natural feldspar-rich sandstones, soils and laboratory experiments have reported diagenetic mineral assemblages (MA) of three end-members relating to feldspar alteration reactions, regarding the amount of leached feldspars and associated secondary minerals (gibbsite, kaolinite, illite and quartz) (Emery et al., 1990; Giles and Boer, 1990; Hayes and Boles, 1992; Taylor et al., 2010; Bjørlykke and Jahren, 2012; Yuan et al., 2015a; Yuan et al., 2017a; Yuan et al., 2017b).

(1) The first end-member (MA-1) is extensively leached feldspars coupled with few secondary mineral but enhanced secondary pores in an open system (Fig. 21A). On a thin section to a sandstone bed scale, quantitative data from thin sections indicate that the amount of secondary minerals is much less than the feldspar porosity (Yuan et al., 2017a). Giles and Boer (1990), Hayes and Boles (1992), and Bjørlykke and Jahren (2012) reported this MA-1 in surficial and shallow sandstones.
(2) The second end-member (MA-2) is extensively leached feldspars with massive authigenic kaolinite (gibbsite) and minor quartz cement (Fig. 21B). Gibbsite can be identified in surface soil (Bates, 1962; Vazquez, 1981; Taboada and García, 1999) or weathered claypan on top of an unconformity, but not common in shallow sands beneath the soils or claypan (Emery et al., 1990; Huang et al., 2003). On a thin section scale, the quantitative data from thin sections demonstrates a positive correlation between the amount of feldspar porosity and that of kaolinite, while the amount of quartz cement is much smaller than the feldspar porosity (Emery et al., 1990; Bjørlykke and Jahren, 2012; Yuan et al., 2017a).
(3) The third end-member (MA-3) is extensively leached feldspars with massive authigenic clays (kaolinite or illite) and quartz cements. MA-3 can be subdivided into two types including the kaolinite MA-3 (Fig. 21C, D) and the illite MA-3 (Fig. 21E, F) (Giles and Boer, 1990; Chuhan et al., 2000; Higgs et al., 2007; Yuan et al., 2015a). On a thin section scale, quantitative data from thin sections demonstrates positive relationships between the amount of feldspar porosity and that of secondary minerals (Yuan et al., 2017a).

4.3. Geological conditions for various mineral assemblages

The observed mineral and textural relationships, which indicate the significance of feldspar alteration, are controlled by integrated physicochemical processes including feldspar dissolution, secondary mineral precipitation, and transfer of Al^{3+}, $SiO_2(aq)$ and cations in chemical weathering, diagenesis, and hydrothermal alteration of sandstones (Giles and Boer, 1990; Thyne et al., 2001; Fu et al., 2009; Maher et al., 2009; Bjørlykke and Jahren, 2012; Lu et al., 2013; Farquhar et al., 2015; Yuan et al., 2017a). In combination with our previous work and studies from other geologists, we propose the favorable geological conditions for occurrence of the various mineral assemblages (Fig. 22).

MA-1 assemblage (extensively leached feldspars with small amounts of authigenic kaolinite and quartz cement) probably occurs in shallow sandstones at low temperatures (< 40–50 °C) and high flow rates (Giles, 1987) or in moderately-deeply buried sandstones where faults develop and meteoric freshwater is available (Yuan et al., 2017a; Yuan et al., 2017b). Hayes and Boles (1992) reported an example of MA-1 assemblage (1–3% feldspar porosity with only 0.1–0.2% kaolinite in thin sections) in meteoric-zone Vedder sandstones with temperature of 30–50 °C, and suggested that the feldspars were dissolved by fresh meteoric water at shallow depth. Yuan et al. (2017a, 2017b, 2018) reported an example of MA-1 assemblage (1–4.5% feldspar porosity with only 0.1–0.5% kaolinite in thin sections) in Eocene sandstones buried deeper than 3000 m, and suggested that feldspars were mainly dissolved by fresh meteoric water transferred by widely developed faults during the uplift stage when the distance of the sandstones to the sea surface was < 1000–1500 m.

MA-2 assemblage (extensively leached feldspars with large amount of authigenic kaolinite/gibbsite and minor quartz cement) may occur in subsurface sandstones at moderate temperature (40–80 °C), in soil or claypan on top of unconformity, in shallow sandstones where meteoric freshwater is limited, or in deeply buried sandstones with some faults serving as freshwater conduits (Yuan et al., 2017a). Glasmann (1992) reported that feldspar dissolution was accompanied by the precipitation of massive kaolinite but minor quartz cement (MA-2) in Brent Group sandstones of the North Sea, with a burial depth from 1000 m to 2000 m and temperatures ranging from 40 °C to 80 °C. Similarly, in many other sandstones with large amounts of feldspars, homogeneous temperature of aqueous fluid inclusions in authigenic quartz suggested the precipitation of quartz cements when temperatures exceeded 80–90 °C (Walderhaug, 1990; Grant and Oxtoby, 1992; Higgs et al., 2007; Guo et al., 2010). However, isotopic data of authigenic kaolinite in these sandstones suggested that the precipitation of kaolinite started in a relatively shallow burial diagenetic stage with low temperatures (40–50 °C), and generally in the presence of meteoric water (Bird and Chivas, 1988; Longstaffe and Ayalon, 1990; Bjørlykke and Jahren,

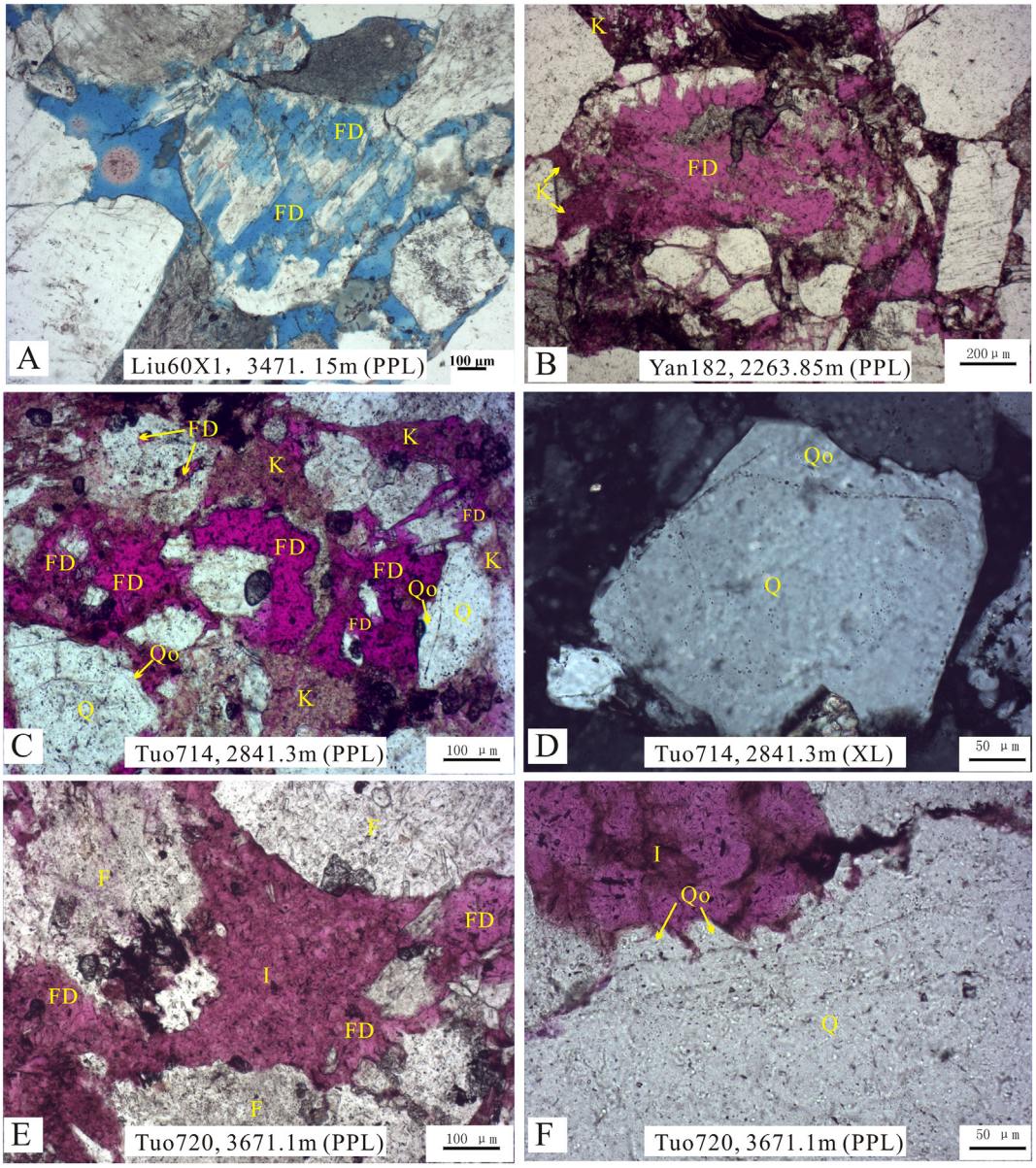

Fig. 21. Micropetrographic evidences of the three types of mineral assemblages of leached feldspars, authigenic kaolinite and quartz cement in the Eocene Shahejie sandstones from two different sub-basins of the Bohai Bay Basin. (A) Extensively leached feldspars with a very small amount of authigenic kaolinite and quartz cements, thin section at 3475.15 m of well Liu60X1 in the Gaoliu area of the Nanpu Sub-basin; (B) Extensively leached feldspars with large amount of authigenic kaolinite and minor quartz cement, thin section at 2263.85 m of well Yan182 in the Minfeng area of the Dongying Sub-basin; (C–D) Extensively leached feldspars with large amount of authigenic kaolinite and quartz, thin section at 2841.3 m of well Tuo714 in the Shengtuo area of the Dongying Sub-basin;. (E–F) Extensively leached feldspars with large amount of authigenic illite and quartz, thin section at 3671.1 m of well Tuo720 in the Shengtuo area of the Dongying Sub-basin. FD-secondary pores formed by feldspar dissolution, Qo-quartz overgrowth; K-kaolinite, Q-quartz, F-feldspar, R-aluminosilicate rock fragment.

2012).

MA-3 (extensively leached feldspars with a large amount of authigenic clays and quartz cements) probably occurs in subsurface sandstones with great depth (> 2000 m), high temperature (> 80 °C), low flow rate, and without widely developed faults (Yuan et al., 2017a). The kaolinite MA-3 probably occurs in subsurface sandstones with temperature from 80 °C to 125–130 °C, while the illite MA-3 probably occurs in subsurface K-feldspar-rich sandstones with temperature exceeding 125–130 °C (Franks and Zwingmann, 2010; Lander and Bonnell, 2010; Yuan et al., 2015a). Early hydrocarbon emplacement with high oil saturation may preserve the kaolinite to a high temperature during deep burial by isolation of K^+ in pore water with kaolinite (Hancock and Taylor, 1978; Jourdan et al., 1987; Glasmann et al., 1989). The ratio of K-feldspar to kaolinite in sandstones at the transitional zone (125–130 °C) also affects the final mineral assemblage during deeper burial (Fig. 23) (Chuhan et al., 2000), because the illitization of kaolinite needs potassium (Eq. 23).

5. Significance of feldspar alteration

5.1. Impact on rock porosity and permeability

Although the redistribution of secondary minerals and the impact of feldspar dissolution on porosity and permeability is still a matter of debate, most recent studies have reached a consensus (Giles and Boer, 1990; Taylor et al., 2010; Bjørlykke and Jahren, 2012; Bjørlykke, 2014; Yuan et al, 2015a). In accordance with the diagenetic mineral assemblages, the feldspar dissolution occurred mainly in open geochemical

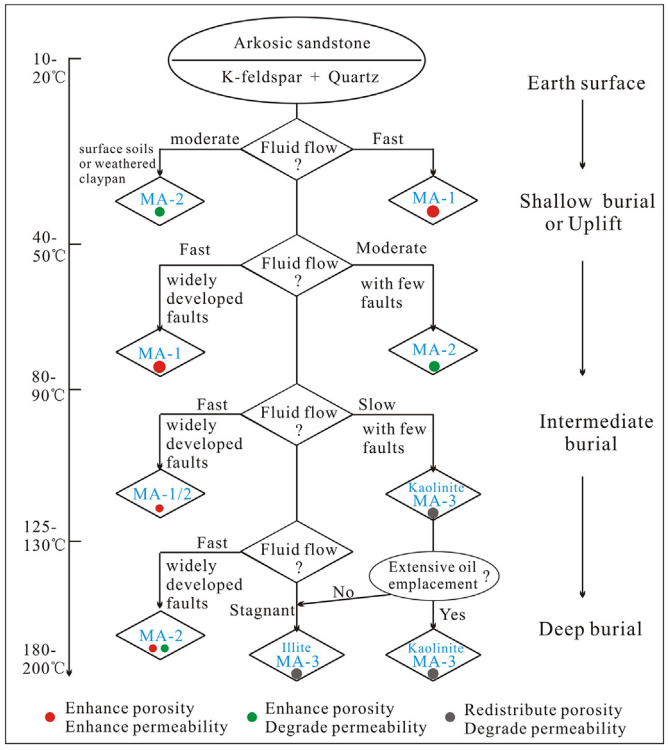

Fig. 22. Flow diagram show the formation of different mineral assemblages in different geological environments from shallow to deep burial in a sedimentary basin.

systems (e.g., sandstones at shallow depth, sandstones beneath unconformities, sandstones close to fault systems) generate enhanced secondary pores to increase the rock porosity and the permeability (Giles, 1987; Giles and Boer, 1990; Hayes and Boles, 1992; Yuan et al., 2015a; Yuan et al., 2017a). While feldspar dissolution may occur in a relative closed geochemical system (e.g., middle-deep buried sandstones) thereby generating redistributional secondary pores. In such a case, the associated secondary minerals (clay minerals and quartz) precipitated in existing pores and throats probably block the flow pathway, resulting in a reduction of the reservoir permeability (Chuhan et al., 2000; Yuan et al., 2015a). However, the quantitative relationship between the decrease in permeability and the amount of feldspar secondary pores in different types of reservoirs requires further attention. For example, Giles et al. (1990) suggested that a gain of < 10% porosity due to feldspar dissolution has little impact on the permeability, while Yuan et al (2015a) verified that even 1–2% authigenic clay mineral growth originating from feldspar dissolution in a closed system degrades the reservoir permeability extensively. Anyhow, secondary porosity generated by dissolution of feldspars and other aluminosilicate minerals may dominate the reservoir spaces in the deep and ultra-deep layers (Dutton and Loucks, 2010).

5.2. Impact on rock wettability

Feldspars can display mixed wettability (Barclay and Worden, 2009). Unweathered feldspar is a water-wet mineral, but the presence of partially co-ordinated aluminum ions along the surface can form various aluminum-organic complexes according to adsorption of wettability-altering polar compounds (Ehrenberg et al., 1995; Barclay and Worden, 2009). This kind of partially co-ordinated aluminum ions relates to feldspar alteration. In addition, feldspar alterations can lead to the precipitation of clay coating on the feldspar surface. The wettability altering compounds are electrostatically attracted to the negatively charged clay surfaces (Ehrenberg et al., 1995), which alter the wettability of reservoirs form water-wet to oil-wet. Meanwhile, the by-products of feldspar dissolution, especially the vermicular kaolinites, are typical oil-wet minerals (Barclay and Worden, 2009), formed in situ or allopatrically, and promote the wettability alteration (Giles and

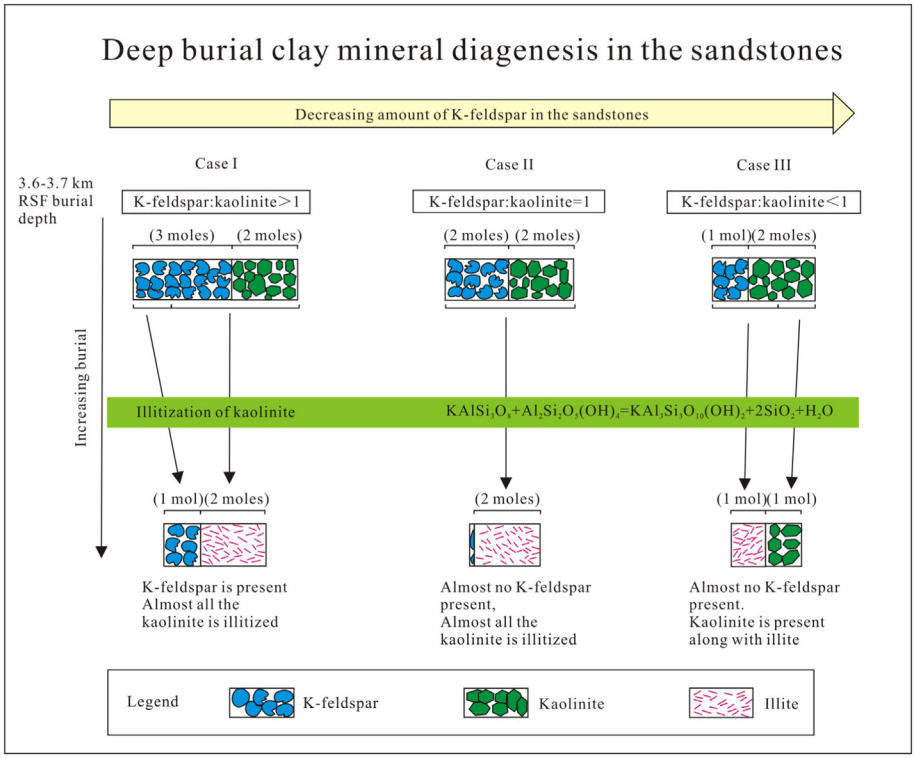

Fig. 23. Model illustrating the effect of primary K-feldspar variation in sandstones on late diagenetic illitization of kaolinite. (after Chuhan, 2000)

Boer, 1990; Barclay and Worden, 2009). The wettability evolution of the rocks from water-wet to oil-wet by feldspar alteration can probably enhance oil migration and accumulation in the reservoirs (Xi et al., 2018).

5.3. Impact on subsurface microorganisms and hydrocarbon degradation

Feldspar diagenesis is ubiquitous in hydrocarbon reservoirs before and after oil charging (van Berk et al., 2013; Yuan et al., 2018; Yuan et al., 2019). As aforementioned, biodegradation of hydrocarbon may promote feldspar alteration in reservoirs (Ehrenberg and Jakobsen, 2001). In turn, leached feldspars have been verified to provide inorganic nutrient (e.g., phosphorus) (Rogers et al., 1998; Rogers and Bennett, 2004) to promote microbial activity and further promote the biodegradation of hydrocarbons (Lee et al., 1996; Weise et al., 1999; Head et al., 2003). The promotion of the biodegradation by mineral alteration can be used for the clean-up of oil spills (Lee et al., 1996; Weise et al., 1999).

Thermal degradation of hydrocarbon also promotes feldspar alteration in reservoirs. However, the impact of feldspar alteration on thermal degradation of hydrocarbon has never been explored much in natural hydrocarbon reservoirs or in pyrolysis experiments (Yuan et al., 2019). Some pyrolysis experiments using oil (plus water and/or minerals) (Pan et al., 2010; Xiao et al., 2010) have been conducted to analyze the catalytic or retardant effects of water and selected minerals (illite, montmorillonite, calcite, quartz) on hydrocarbon degradation. Here, we suggest that such pyrolysis experiments using oil plus water and feldspars are required to test the impact of feldspar alteration on hydrocarbon degradation (Yuan et al., 2019).

5.4. Promotion of illitization in rocks

Sandstones are often interbedded with mudstones in most sedimentary sequences, and are composed of different minerals, leading to various diagenetic reactions in these rocks (Boles and Franks, 1979; Gluyas and Coleman, 1992; Thyne, 2001; Thyne et al., 2001).

K-feldspar dissolution releases K^+, SiO_2(aq), and Al^{3+}, and most SiO_2(aq) and Al^{3+} can be retained in sandstones through the precipitation of quartz and kaolinite at temperatures lower than 125 °C (Bjørlykke and Jahren, 2012; Yuan et al., 2015a). As sandstones may contain large amounts of feldspars and few percentages of detrital smectite clays and illite-smectite clays, few K^+ is consumed by illitization of detrital smectite or mixed illite-smectite in the sandstone beds, leading to a relative high concentration of K^+ in the sandstone pore water (Boles and Franks, 1979; Thyne, 2001). As interbedded mudstones generally contain few percentage of feldspars and large amounts of detrital clays, illitization reactions consume large amount of K^+ and result in a relatively low concentrations of K^+ in the mudstone pore water. The K^+ concentration differences lead to a diffusion transfer of K^+ from the sandstones to the mudstones, promoting the illitization reactions in the mudstones. In turn, the consumption of K^+ by the illitization reactions may promote an intensified feldspar dissolution in the sandstones. This mutual interrelationship between the K-feldspar dissolution in sandstones and the illitization in mudstones has been verified in both natural rocks and numerical simulations (Boles and Franks, 1979; Thyne, 2001). However, the diffusive transfer of K^+ from sandstones to mudstones occurs at a relatively small scale from centimeters to several meters and generally close to the mudstone-sandstone interfaces (Thyne, 2001). The illitization reactions in the central part of thick mudstone beds are probably supported by some other internal K^+ sources in the mudstones or some unknown transfer mechanisms that can move the K^+ from the sandstones to the mudstones on a large scale.

When temperature exceeds 125 °C, K-feldspar dissolution in the sandstones leads to the formation of illite and quartz cements, and K^+ released by the feldspar dissolution is consumed by the illitization of early formed authigenic kaolinite directly in the sandstones (Chuhan et al., 2000; Yuan et al., 2015a). In such a case, little K^+ is likely to be transferred to the mudstones to promote illitization reactions (Yuan et al., 2015a).

5.5. Promotion of CO_2 sequestration

The injection and storage of CO_2 in geological formations including depleted oil and gas reservoirs and saline aquifers is a promising method to maintain the atmospheric CO_2 concentration at a reasonable level (Bertier et al., 2006; Liu et al., 2011; Wigley et al., 2013; Farquhar et al., 2015; Tutolo et al., 2015). CO_2 injected into deep formations can be stored based on two processes: (1) in the pore space, as a supercritical phase and/or dissolved in the pore fluid, and (2) through mineral trapping, i.e., the formation of stable carbonate minerals (Bachu et al., 1994; Hitchon, 1996; Hangx and Spiers, 2009). The dissolution of aluminosilicate minerals (e.g., feldspars) is crucial for the long-term fate of the injected CO_2 because it consumes acidity to produce alkalinity, thereby increasing the saturation index of the carbonate phases, and potentially resulting in a permanent storage of CO_2 in carbonate minerals (Bickle, 2009; Wigley et al., 2013). At the same time, the precipitation of secondary minerals following feldspar dissolution also support the capture of carbon dioxide.

Many laboratory experiments, numerical simulations and natural analogue analyses have been conducted to study the promotion effect of feldspar dissolution on CO_2 sequestration (Xu et al., 2005; Bertier et al., 2006; Hangx and Spiers, 2009; Lu et al., 2013; Tutolo et al., 2015; Yuan et al., 2015b). In short term batch laboratory experiments (several days to several years) in CO_2-water-feldspar systems, secondary minerals including boehmite, hydrotalcite kaolinite, illite, muscovite and paragonite have been identified using scanning electron microscopy energy-dispersive spectroscopy (SEM-EDS), X-ray diffraction (XRD), TEM, or field-emission gun (FEG) microscopy methods (Lu et al., 2013). The initial water chemistry has a significant impact on the secondary mineral types: (i) the presence of a K^+-rich solution promotes the precipitation of illite and muscovite, (ii) the presence of a Na^+-rich aqueous fluid enables paragonite precipitation, and (iii) the presence of a Mg^{2+}-rich solution may promote the precipitation of carbonate (magnesite) (Hangx and Spiers, 2009). Boehmite and kaolinite can be identified in all batch experiments at the initial stage (few days to few weeks), depending on the conditions and solution composition. Long-term predictions of the fluid-mineral reactions in CO_2-brine-rock systems have been applied to interpret the reaction processes, although more kinetic and themodynamic data on feldspar dissolution and relevant secondary precipitation in a CO_2-charged feldspar-rich system are required. In numerical calculations simulating thousands to millions of years, various secondary minerals including clays (kaolinite, illite, chlorite), quartz, and carbonates (siderite, calcite, magnesite, dawsonite) can be expected following feldspar dissolution, depending on the mineral composition and water chemistry (Lu et al., 2013; van Berk et al., 2013; Wigley et al., 2013; Tutolo et al., 2015).

Most natural subsurface hydrocarbon reservoirs contain some percent of CO_2 originating from kerogen maturation or deep hot fluids as these rocks have experienced millions of years of fluid-rock interactions, and thus are considered the best natural laboratories for feldspar dissolution and relevant CO_2 sequestration (Smith and Ehrenberg, 1989; Seewald, 2003; Xu et al., 2005; van Berk et al., 2013; Yuan et al., 2015b). Compared to quartz-rich sandstones, most feldspar-rich rocks contain large amounts of various carbonate cements (calcite, dolomite, ankerite and ferrocalcite) (Fig. 15) (Baines and Worden, 2004), indicating that large amounts of carbon have been stored in these reservoirs by carbonate mineral trapping. These natural feldspar-rich analogs provide excellent evidences that feldspar dissolution can buffer the pore water to a suitable pH that promotes CO_2 sequestration by carbonate precipitation over geological time scales (Xu et al., 2005; Yuan et al., 2015b).

6. Conclusions

Feldspar alteration is ubiquitous from shallow aquifers to deep hydrocarbon reservoirs. There has been a vast amount of work over the past half-century on dissolution mechanisms, kinetic rate laws, diagenetic mineral assemblages, and the significance of feldspar alteration, using laboratory experiments, natural rock samples, and numerical modellings. Such activities were basically often driven by soil science, environmental issues, or questions related to oil and gas exploration. What is evident is that feldspar dissolution probably occurs through different mechanisms under different geochemical conditions. Additionally, factors including the crystal structure, Al/Si ordering, temperature, pH, surface area, organic acids, chemical affinity, and precipitation rates of secondary minerals affect the feldspar dissolution rates.

The rate inconsistency between laboratory experiments and field observations may be attributed to the armoring effects of secondary mineral coating on feldspar surfaces, the possible effects of leached layers, the approach to saturation with respect to feldspars, the inhibition by absorbed Al^{3+} on feldspar surface, or the inhibition by simultaneous slow clay precipitation rates. However, more physiochemical processes from feldspar dissolution to secondary formation and the precipitation and re-dissolution of a series of secondary minerals in a close to equilibrium geochemical system may affect the feldspar dissolution rate. Thus, the true feldspar dissolution rate may be obtained by a combination of laboratory experiments and relevant reactive transport modeling.

Inorganic meteoric water generally leaches feldspar at relatively shallow depth, leading to the development of MA-1 and MA-2 mineral assemblages and elevates the reservoir porosity and permeability. While organic original CO_2 and organic acids generally dissolve feldspars at middle-deep depths (> 2000 m), the MA-3 mineral assemblage develops. The authigenic clay formation leads to a redistribution of primary and secondary porosity and thus to a decrease in permeability. While authigenic clays (e.g., kaolinite) form following feldspar dissolution, the reservoir wettability alters and affects the charging and production of hydrocarbons. In addition, feldspar alteration may promote hydrocarbon degradation by promoting bioactivity or by consuming low molecular organic acids, and, it can furthermore promote CO_2 sequestration by H^+ consumption and pH buffering.

Acknowledgments

This study was funded by the Natural Science Foundation of China Project (No. 41602138 , 41872140), National Science and Technology Special Grant of China (No. 2016ZX05006-007; No. 2016ZX05006-003), and the Fundamental Research Funds for the Central Universities, China (18CX07007A). Prof. Andrew Aplin at Durham University, United Kingdom is sincerely thanked for his help. We also sincerely thank Dr. F.K. Crundwell and another anonymous reviewer for reviewing our work, they have provided great advices and constructive comments for this review work.

References

Aagaard, P., Helgeson, H.C., 1982. Thermodynamic and kinetic constraints on reaction rates among minerals and aqueous solutions; I, Theoretical considerations. Am. J. Sci. 282 (3), 237–285.
Alekseyev, V.A., Medvedeva, L.S., Prisyagina, N.I., Meshalkin, S.S., Balabin, A.I., 1997. Change in the dissolution rates of alkali feldspars as a result of secondary mineral precipitation and approach to equilibrium. Geochim. Cosmochim. Acta 61 (6), 1125–1142.
Bachu, S., Gunter, W.D., Perkins, E.H., 1994. Aquifer disposal of CO_2 hydrodynamic and mineral trapping. Energy Convers. Manag. 35 (4), 269–279.
Baines, S.J., Worden, R.H., 2004. The long-term fate of CO_2 in the subsurface: natural analogues for CO_2 storage. Geol. Soc. Lond., Spec. Publ. 233 (1), 59–85.
Barclay, S.A., Worden, R.H., 2009. In: Worden, R.H., Morad, S. (Eds.), Effects of Reservoir Wettability on Quartz Cementation in Oil FieldsQuartz Cementation in Sandstones, pp. 103–117 Special Pubilication.
Barth, T., Bjørlykke, K., 1993. Organic acids from source rock maturation: generation potentials, transport mechanisms and relevance for mineral diagenesis. Appl. Geochem. 8 (4), 325–337.
Barth, T., Borgund, A.E., Hopland, A.L., 1988. Volatile organic acids produced during kerogen maturation– amounts, composition and role in migration of off. Org. Geochem. 13 (1–3), 461–465.
Barth, T., Andresen, B., Iden, K., Johansen, H., 1996. Modelling source rock production potentials for short-chain organic acids and CO_2—a multivariate approach. Org. Geochem. 25 (8), 427–438.
Bates, T.F., 1962. Halloysite and gibbsite formation in Hawaii. In: Proceedings of the National Conference on Clays and Clay Mineralogy, pp. 315–328.
Beig, M.S., Lüttge, A., 2006. Albite dissolution kinetics as a function of distance from equilibrium: implications for natural feldspar weathering. Geochim. Cosmochim. Acta 70 (6), 1402–1420.
Berg, A., Banwart, S.A., 2000. Carbon dioxide mediated dissolution of Ca-feldspar: implications for silicate weathering. Chem. Geol. 163 (1), 25–42.
Berner, R.A., Holdren, G.R., 1979. Mechanism of feldspar weathering-II. Observations of feldspars from soils. Geochim. Cosmochim. Acta 43 (8), 1173–1186.
Bertier, P., Swennen, R., Laenen, B., Lagrou, D., Dreesen, R., 2006. Experimental identification of CO_2–water–rock interactions caused by sequestration of CO_2 in Westphalian and Buntsandstein sandstones of the Campine Basin (NE-Belgium). J. Geochem. Explor. 89 (1–3), 10–14.
Bevan, J., Savage, D., 1989. The effect of organic acids on the dissolution of K-feldspar under conditions relevant to burial diagenesis. Mineral. Mag. 53, 415–425.
Bickle, M.J., 2009. Geological carbon storage. Nat. Geosci. 2 (12), 815.
Bird, M.I., Chivas, A.R., 1988. Stable-isotope evidence for low-temperature kaolinitic weathering and post-formational hydrogen-isotope exchange in Permian kaolinites. Chem. Geol. Isot. Geosci. Sect. 72 (3), 249–265.
Bjørkum, P.A., Gjelsvik, N., 1988. An isochemical model for formation of authigenic kaolinite, K-feldspar and illite in sediments. J. Sediment. Res. 58 (3), 506–511.
Bjørlykke, K., 1984. Formation of Secondary Porosity: How Important Is It. Clastic Diagenesis: Part 2 Aspects of Porosity Modification. pp. 277–286.
Bjørlykke, K., 1993. Fluid flow in sedimentary basins. Sediment. Geol. 86 (1–2), 137–158.
Bjørlykke, K., 2014. Relationships between depositional environments, burial history and rock properties. Some principal aspects of diagenetic process in sedimentary basins. Sediment. Geol. 301, 1–14.
Bjørlykke, K., AAgaard, P., 1992. Clay minerals in North Sea Sandstones. In: Origin, Diagenesis and Pelrophysics of Clay Minerals in Sandstones. Vol. 47. SEPM Special Publication, pp. 65–79.
Bjørlykke, K., Jahren, J., 2012. Open or closed geochemical systems during diagenesis in sedimentary basins: constraints on mass transfer during diagenesis and the prediction of porosity in sandstone and carbonate reservoirs. AAPG Bull. 96 (12), 2193–2214.
Bjørlykke, K., Aagaard, P., Egeberg, P.K., 1995. Geochemical constraints from formation water analyses from the North Sea and the Gulf Coast Basins on quartz, feldspar and illite precipitation in reservoir rocks. Geol. Soc. Lond., Spec. Publ. 86 (1), 33–50.
Blake, R.E., Walter, L.M., 1999. Kinetics of feldspar and quartz dissolution at 70–80 °C and near-neutral pH: effects of organic acids and NaCl. Geochim. Cosmochim. Acta 63 (13), 2043–2059.
Blum, A.E., Lasaga, A.C., 1991. The role of surface speciation in the dissolution of albite. Geochim. Cosmochim. Acta 55, 2193–2201.
Blum, A.E., Stillings, L.L., 1995. Feldspar dissolution kinetics. Rev. Mineral. Geochem. 31 (1), 291–351.
Boles, J.R., Franks, S.G., 1979. Clay diagenesis in Wilcox sandstones of Southwest Texas_implications of smectite diagenesis on sandstone cementation. J. Sediment. Res. 49 (1), 55–70.
Bove, D.J., Eberl, D.D., McCarty, D.K., Meeker, G.P., 2002. Characterization and modeling of illite crystal particles and growth mechanisms in a zoned hydrothermal deposit, Lake City, Colorado. Am. Mineral. 87 (11－12), 1546–1556.
Brantley, S.L., Mellott, N.P., 2000. Surface area and porosity of primary silicate minerals. Am. Mineral. 85, 1763–1783.
Brantley, S.L., Kubicki, J.D., White, A.F., 2008. Kinetics of Water-Rock Interaction. Springer, New York, pp. 151–210.
Burch, T.E., Nagy, K.L., Lasaga, A.C., 1993. Free energy dependence of albite dissolution kinetics at 80 °C and pH 8.8. Chem. Geol. 105 (1–3), 137–162.
Cao, Y., et al., 2014. Characteristics and origin of abnormally high porosity zones in buried Paleogene clastic reservoirs in the Shengtuo area, Dongying Sag, East China. Pet. Sci. 11 (3), 346–362.
Carothers, W.W., Kharaka, Y.K., 1978. Aliphatic acid anions in oil-field waters–implications for origin of natural gas. AAPG Bull. 62 (12), 2441–2453.
Carroll, S.A., Knauss, K.G., 2005. Dependence of labradorite dissolution kinetics on CO_2(aq), Al(aq), and temperature. Chem. Geol. 217 (3–4), 213–225.
Casey, W.H., Westrich, H.R., Arnold, G.W., 1988. Surface chemistry of labradorite feldspar reacted with aqueous solutions at pH = 2,3, and 12. Geochim. Cosmochim. Acta 52, 2795–2807.
Casey, W.H., Westrich, H.R., Arnold, G.W., Banfield, J.F., 1989. The surface chemistry of dissolving labradorite feldspar. Geochim. Cosmochim. Acta 53, 821–832.
Casey, W.H., Westrich, H.R., Holdren, G.R., 1991. Dissolution rates of plagioclase at pH = 2 and 3. Am. Mineral. 76, 1–2.
Chardon, E.S., Livens, F.R., Vaughan, D.J., 2006. Reactions of feldspar surfaces with aqueous solutions. Earth Sci. Rev. 78 (1), 1–26.
Chen, Y., Brantley, S.L., 1997. Temperature- and pH-dependence of albite dissolution rate at acid pH. Chem. Geol. 135, 275–290.
Chou, L., Wollast, R., 1984. Study of the weathering of albite at room temperature and pressure with a fluidized bed reactor. Geochim. Cosmochim. Acta 48 (11), 2205–2217.
Chou, L., Wollast, R., 1985. Steady-state kinetics and dissoluton mechanisms of albite.

Am. J. Sci. 285 (10), 963–993.
Chuhan, F.A., Bj Rlykke, K., Lowrey, C., 2000. The role of provenance in illitization of deeply buried reservoir sandstones from Haltenbanken and North Viking Graben, offshore Norway. Mar. Pet. Geol. 17 (6), 673–689.
Correns, C.W., 1940. Die chemische Verwitterung der Silikate. Naturwissenschaften 28 (24), 369–376.
Correns, C.W., 1963. Experiments on the decomposition of silicate and discussion of chemical weathering. Clay Clay Miner. 10 (1), 443–459.
Correns, C.W., Von, E.W., 1938. Neue Untersuchungen über die Verwitterung des Kalifeldspates. Naturwissenschaften 26 (9), 137–138.
Crundwell, F.K., 2015a. The mechanism of dissolution of the feldspars: part I. Dissolution at conditions far from equilibrium. Hydrometallurgy 151, 151–162.
Crundwell, F.K., 2015b. The mechanism of dissolution of the feldspars: part II dissolution at conditions close to equilibrium. Hydrometallurgy 151, 163–171.
Drever, J.I., Stillings, L.L., 1997. The role of organic acids in mineral weathering. Colloids Surf. A Physicochem. Eng. Asp. 120, 167–181.
Dutton, S.P., Loucks, R.G., 2010. Diagenetic controls on evolution of porosity and permeability in lower Tertiary Wilcox sandstones from shallow to ultradeep (200–6700 m) burial, Gulf of Mexico Basin, U.S.A. Mar. Pet. Geol. 27 (1), 69–81.
Ehrenberg, S.N., Jakobsen, K.G., 2001. Plagioclase dissolution related to biodegradation of oil in Brent Group sandstones (Middle Jurassic) of Gullfaks Field, northern North Sea. Sedimentology 48, 703–721.
Ehrenberg, S.N., Skjevrak, I., Gilje, A.E., 1995. Asphaltene-rich residues in sandstone reservoirs of Haltenbanken province, mid-Norwegian continental shelf. Mar. Pet. Geol. 12 (1), 53–69.
Emery, D., Myers, K.J., Young, R., 1990. Ancient subaerial exposure and freshwater leaching in sandstones. Geology 18, 1178–1181.
Farquhar, S.M., et al., 2015. A fresh approach to investigating CO_2 storage: experimental CO_2–water–rock interactions in a low-salinity reservoir system. Chem. Geol. 399, 98–122.
Fenter, P., Zapol, P., He, H., Sturchio, N.C., 2014. On the variation of dissolution rates at the orthoclase (001) surface with pH and temperature. Geochim. Cosmochim. Acta 141, 598–611.
Fitzpatrick, R.W., Schwertmann, U., 1982. Al-substituted goethite—an indicator of pedogenic and other weathering environments in South Africa. Geoderma 27 (4), 335–347.
França, A.B., Araújo, L.M., Maynard, J.B., Potter, P.E., 2003. Secondary porosity formed by deep meteoric leaching: Botucatu eolianite, southern South America. AAPG Bull. 87 (7), 1073–1082.
Franks, S.G., Zwingmann, H., 2010. Origin and timing of late diagenetic illite in the Permian–Carboniferous Unayzah sandstone reservoirs of Saudi Arabia. AAPG Bull. 94 (8), 1133–1159.
Fu, Q., et al., 2009. Coupled alkali-feldspar dissolution and secondary mineral precipitation in batch systems: 1. New experiments at 200 °C and 300 bars. Chem. Geol. 258 (3–4), 125–135.
Gautier, J.M., Oelkers, E.H., Schott, J., 1994. Experimental study of K-feldspar dissolution rates as a function of chemical affinity at 150°C and pH 9. Geochim. Cosmochim. Acta 58 (21), 4549–4560.
Giles, M.R., 1986. Constraints on the development of secondary porosity in the subsurface: re-evaluation of processes. Mar. Pet. Geol. 3 (3), 243–255.
Giles, M.R., 1987. Mass transfer and problems of secondary porosity creation in deeply buried hydrocarbon reservoirs. Mar. Pet. Geol. 4 (3), 188–204.
Giles, M.R., Boer, R., 1990. Origin and significance of redistributional secondary porosity. Mar. Pet. Geol. 7.
Glasmann, J.R., 1992. The fate of feldspar in Brent Group reservoirs, North Sea: a regional synthesis of diagenesis in shallow, intermediate, and deep burial environments. Geol. Soc. Lond., Spec. Publ. 61 (1), 329–350.
Glasmann, J.R., Clark, R.A., Larter, S., Briedis, N., Lundegard, P.D., 1989. Diagenesis and hydrocarbon accumulation, Brent sandstone (Jurassic), Bergen High Area, North Sea. AAPG Bull. 37 (11), 1341–1360.
Gluyas, J., Coleman, M., 1992. Material flux and porosity changes during sediment diagenesis. Nature 356 (6364), 52–54.
Gluyas, J.G., Robinson, A.G., Primmer, T.P., 1997. Rotliegend Sandstone Diagenesis: A Tale of Two Waters, Geofluids II'97–Extended Abstract Volume. pp. 291–294.
Gómez-Alarcón, G., Muñoz, M.L., Flores, M., 1994. Excretion of organic acids by fungal strains isolated from decayed sandstone. Int. Biodeterior. Biodegrad. 34 (2), 169–180.
Gout, R., Oelkers, E.H., Schott, J., Wick, A., 1997. The surface chemistry and structure of acid-leached albite: new insights on the dissolution mechanism of the alkali feldspars. Geochim. Cosmochim. Acta 61 (14), 3013–3018.
Grant, S.M., Oxtoby, N.H., 1992. The timing of quartz cementation in Mesozoic sandstones from Haltenbanken, offshore mid-Norway: fluid inclusion evidence. J. Geol. Soc. 149, 479–482.
Gruber, C., Zhu, C., Georg, R.B., Zakon, Y., Ganor, J., 2014. Resolving the gap between laboratory and field rates of feldspar weathering. Geochim. Cosmochim. Acta 147, 90–106.
Gruber, C., Kutuzov, I., Zakon, Y., Ganor, J., 2017. What is the real ΔGr Function of Albite Dissolution? Proc. Earth Planet. Sci. 17, 148–152.
Guo, X., et al., 2010. Oil generation as the dominant overpressure mechanism in the Cenozoic Dongying depression, Bohai Bay Basin, China. AAPG Bull. 94 (12), 1859–1881.
Habermehl, M.A., 1980. The great Artesian Basin, Australia, BMR. J. Aust. Geol. Geophys. 5, 9–37.
Hancock, N.J., Taylor, A.M., 1978. Clay mineral diagenesis and oil migration in the Middle Jurassic Brent Sand Formation. J. Geol. Soc. 135 (1), 69–72.
Hangx, S.J.T., Spiers, C.J., 2009. Reaction of plagioclase feldspars with CO_2 under hydrothermal conditions. Chem. Geol. 265 (1–2), 88–98.
Harrison, W.J., Thyne, G.D., 1994. Geochemical Models of Rock-Water Interactions in the Presence of Organic Acids[M]//Organic Acids in Geological Processes. Springer, Berlin Heidelberg, pp. 355–397.
Hayes, M.J., Boles, J.R., 1992. Volumetric relations between dissolved plagioclase and kaolinite in sandstones: implications for aluminum mass transfer in the San Joaquin basin, California. In: Origin, Diagenesis and Pelrophysics of Clay Minerals in Sandstones. Vol. 47. SEPM Special Publication, pp. 111–123.
Head, I.M., Jones, D.M., Larter, S.R., 2003. Biological activity in the deep subsurface and the origin of heavy oil. Nature 426, 344–352.
Helgeson, H.C., 1971. Kinetics of mass transfer among si&ates and aqueous solutions. Geochim. Cosmochim. Acta 35, 421–469.
Helgeson, H.C., 1972. Kinetics of mass transfer among silicates and aqueous solutions_ Correction and clarification. Geochim. Cosmochim. Acta 36, 1067–1070.
Helgeson, H.C., 1979. Summary and critique of the thermodynamic properties of rock-forming minerals. Am. J. Sci. A 287, 1–229.
Helgeson, H.C., Murphy, W.M., Aagaard, P., 1984. Thermodynamic and kinetic constraints on reaction rates among minerals and aqueous solutions. II. Rate constants, effective surface area, and the hydrolysis of feldspar. Geochim. Cosmochim. Acta 48 (12), 2405–2432.
Hellevang, H., Pham, V.T.H., Aagaard, P., 2013. Kinetic modelling of CO_2–water–rock interactions. Int. J. Greenh. Gas Control 15, 3–15.
Hellmann, R., 1994a. A leached layer hydrolysis model: a better way to understanding feldspar dissolution at elevated temperatures and pressures. Mineral. Mag. A 58, 400–401.
Hellmann, R., 1994b. The albite-water system: part I. The kinetics of dissolution as a function of pH at 100, 200 and 300 C. Geochim. Cosmochim. Acta 58 (2), 595–611.
Hellmann, R., Tisserand, D., 2006. Dissolution kinetics as a function of the Gibbs free energy of reaction: an experimental study based on albite feldspar. Geochim. Cosmochim. Acta 70 (2), 364–383.
Hellmann, R., Penisson, J.M., Hervig, R.L., Thomassin, J.H., Abrioux, M.F., 2003. An EFTEM/HRTEM high-resolution study of the near surface of labradorite feldspar altered at acid pH: evidence for interfacial dissolution-reprecipitation. Phys. Chem. Miner. 30 (4), 192–197.
Hellmann, R., Daval, D., Tisserand, D., 2010. The dependence of albite feldspar dissolution kinetics on fluid saturation state at acid and basic pH: progress towards a universal relation. Compt. Rendus Geosci. 342 (7–8), 676–684.
Hellmann, R., et al., 2012. Unifying natural and laboratory chemical weathering with interfacial dissolution–reprecipitation: a study based on the nanometer-scale chemistry of fluid–silicate interfaces. Chem. Geol. 294–295, 203–216.
Hellmann, R., et al., 2015. Nanometre-scale evidence for interfacial dissolution–reprecipitation control of silicate glass corrosion. Nat. Mater. 14 (3), 307–311.
Hiebert, F.K., Bennett, P.C., 1992. Microbial control of silicate weathering in organic-rich ground water. Science 258 (5080), 278–281.
Higgs, K.E., Zwingmann, H., Reyes, A.G., Funnell, R.H., 2007. Diagenesis, porosity evolution, and petroleum emplacement in tight gas reservoirs, Taranaki Basin, New Zealand. J. Sediment. Res. 77 (12), 1003–1025.
Hill, R.J., Tang, Y., Kaplan, I.R., 2003. Insights into oil cracking based on laboratory experiments. Org. Geochem. 34, 1651–1672.
Hitchon, B., 1996. Aquifer Disposal of Carbon Dioxide: Hydrodynamic and Mineral Trapping-Proof of Concept.
Hövelmann, J., Putnis, A., Geisler, T., Schmidt, B.C., Golla-Schindler, U., 2010. The replacement of plagioclase feldspars by albite: observations from hydrothermal experiments. Contrib. Mineral. Petrol. 159 (1), 43–59.
Hower, J., Eslinger, E.V., Hower, M.E., Perry, E.A., 1976. Mechanism of burial metamorphism of argillaceous sediment: 1. Mineralogical and chemical evidence. Geol. Soc. Am. Bull. 87 (5), 725–737.
Huang, W.H., Kiang, W.C., 1972. Laboratory dissolution of plagioclase feldspars in water and organic-acids at room-temperature. Am. Mineral. 57 (11 − 1), 1849–1859.
Huang, W.L., Bishop, A.M., Brown, R.W., 1986. The effect of fluid/rock ratio on feldspar dissolution and illite formation under reservoir conditions. Clay Miner. 21 (4), 585–601.
Huang, S.J., Wu, W.H., Liu, J., Shen, L.C., Huang, C.G., 2003. Generation of secondary porosity by meteoric water during time of subaerial exposure: an example from Yanchang Formation sandstone of Triassic of Ordos Basin. Earth Sci./Diqiu Kexue 28 (4), 419–424.
Hutcheon, I., Abercrombie, H., 1990. Carbon dioxide in clastic rocks and silicate hydrolysis. Geology 18, 541–544.
Hutcheon, I., Shevalier, M., Abercrombie, H.J., 1993. pH buffering by metastable mineral-fluid equilibria and evolution of carbon dioxide fugacity during burial diagenesis. Geochim. Cosmochim. Acta 57, 1017–1027.
Jourdan, A., et al., 1987. Diagenesis as the control of the Brent sandstone reservoir properties in the Greater Alwyn area (East Shetland Basin). Petrol. Geol. North West Eur. 2, 951–961.
Kampman, N., Bickle, M., Becker, J., Assayag, N., Chapman, H., 2009. Feldspar dissolution kinetics and Gibbs free energy dependence in a CO_2-enriched groundwater system, Green River, Utah. Earth Planet. Sci. Lett. 284 (3–4), 473–488.
Knauss, K.G., Wolery, T.J., 1986. Dependence of albite dissolution kinetics on ph and time at 25 °C and 70 °C. Geochim. Cosmochim. Acta 50, 2481–2497.
Lagache, M., 1965. Contribution a letude de lalteration des feldspaths dans leau, entre 100 et 200 °C sous diverses pressions de CO_2 et application a la synthese des mineraux argileux. Bulletin De La Societe Francaise Mineralogie Et De Cristallographie 88 (2), 223–253.
Lagache, M., Wyart, J., Sabatier, G., 1961a. Dissolution Des Feldspaths Alcalins Dans Leau Pure Ou Chargee De CO_2 A 200 Degrees C. GAUTHIER-VILLARS/EDITIONS ELSEVIER 23 RUE LINOIS, 75015 PARIS, FRANCE. pp. 2019.

Lagache, M., Wyart, J., Sabatier, G., 1961b. Mechanisme de la dissolution des feldspaths alcalins dans l'eau pure ou charg. ee de CO_2 a 200 CCR Seances Acad. Sci. Ser. 2 (253), 2296–2299.
Land, L.S., Macpherson, G.L., 1992. Origin of saline formation waters, cenozoic section, Gulf of Mexico Sedimentary Basin (1). AAPG Bull. 76 (9), 1344–1362.
Lander, R.H., Bonnell, L.M., 2010. A model for fibrous illite nucleation and growth in sandstones. AAPG Bull. 94 (8), 1161–1187.
Lasaga, A.C., 1984. Chemical Kinetics of Water-Rock Interactions. J. Geophys. Res. Solid Earth 89 (B6), 4009–4025.
Lasaga, A.C., Luttge, A., 2001. Variation of crystal dissolution rate based on a dissolution stepwave model. Science 291 (5512), 2400–2404.
Lasaga, A.C., Soler, J.M., Ganor, J., Burch, T.E., Nagy, K.L., 1994. Chemical weathering rate laws and global geochemical cycles. Geochim. Cosmochim. Acta 58 (41), 2361–2386.
Lee, K., Weise, A.M., St-Pierre, S., 1996. Enhanced oil biodegradation with mineral fine interaction. Spill Sci. Technol. Bull. 3 (4), 263–267.
Lewan, M.D., 1997. Experiments on the role of water in petroleum formation. Geochim. Cosmochim. Acta 61 (17), 3691–3723.
Lian, B., Wang, B., Pan, M., Liu, C., Teng, H.H., 2008. Microbial release of potassium from K-bearing minerals by thermophilic fungus Aspergillus fumigatus. Geochim. Cosmochim. Acta 72, 87–98.
Liu, F., Lu, P., Zhu, C., Xiao, Y., 2011. Coupled reactive flow and transport modeling of CO_2 sequestration in the Mt. Simon sandstone formation, Midwest U.S.A. Int. J. Greenh. Gas Control 5 (2), 294–307.
Longstaffe, F., Ayalon, A., 1990. Hydrogen-isotope geochemistry of diagenetic clay minerals from Cretaceous sandstones, Alberta, Canada: evidence for exchange. Appl. Geochem. 5, 657–668.
Lu, P., et al., 2013. Coupled alkali feldspar dissolution and secondary mineral precipitation in batch systems – 2: new experiments with supercritical CO_2 and implications for carbon sequestration. Appl. Geochem. 30, 75–90.
Lundegard, P.D., Land, L.S., Galloway, W.E., 1984. Problem of secondary porosity_ Frio Formation (Oligocene)__ Texas Gulf Coast. Geology 12 (7), 399–402.
Macquaker, J.H.S., Taylor, K.G., Keller, M., Polya, D., 2014. Compositional controls on early diagenetic pathways in fine-grained sedimentary rocks: implications for predicting unconventional reservoir attributes of mudstones. AAPG Bull. 98 (3), 587–603.
Maher, K., Steefel, C.I., White, A.F., Stonestrom, D.A., 2009. The role of reaction affinity and secondary minerals in regulating chemical weathering rates at the Santa Cruz Soil Chronosequence, California. Geochim. Cosmochim. Acta 73 (10), 2804–2831.
Mahnheim, F.T., 1967. Evidence for submarine discharge of water on the Atlantic continental slope of the southern United States, and suggestions for further research. Transact. N. Y. Acad. Sci. 29, 839–853.
Manning, D.A.C., K, G., C, R.E.I., 1992. Feldspar dissolution in the presence of organic acid anions under diagenetic conditions: an experimental study. Org. Geochem. 19 (4–6), 483–492.
Mansurbeg, H., El-ghali, M.A.K., Morad, S., Plink-Björklund, P., 2006. The impact of meteoric water on the diagenetic alterations in deep-water, marine siliciclastic turbidites. J. Geochem. Explor. 89 (1–3), 254–258.
Meredith, W., Kelland, S.J., Jones, D.M., 2000. Influence of biodegradation on crude oil acidity and carboxylic acid composition. Org. Geochem. 31 (11), 1059–1073.
Milliken, K.L., 1992. Chemical behavior of detrital feldspars in mudrocks versus sandstones, Frio Formation (Oligocene), South Texas. J. Sediment. Res. (5), 62.
Milliken, K.L., McBride, E.F., Land, L.S., 1989. Numerical assessment of dissolution versus replacement in the subsurface destruction of detrital feldspars, Oligocene Frio Formation, South Texas. J. Sediment. Res. 59 (5), 740–757.
Molenaar, N., Felder, M., Bär, K., Götz, A.E., 2015. What classic greywacke (litharenite) can reveal about feldspar diagenesis: an example from Permian Rotliegend sandstone in Hessen, Germany. Sediment. Geol. 326, 79–93.
Muir, I.J., Nesbitt, H.W., 1991. Effects of aqueous cations on the dissolution of labradorite feldspar. Geochim. Cosmochim. Acta 58 (11), 3181–3189.
Muir, I.J., Michael Bancroft, G., Wayne Nesbitt, H., 1989. Characteristics of altered labradorite surfaces by SIMS and XPS. Geochim. Cosmochim. Acta 53 (6), 1235–1241.
Muir, I.J., Bancroft, G.M., Shotyk, W., Nesbitt, H.W., 1990. A SIMS and XPS study of dissolving plagioclase. Geochim. Cosmochim. Acta 54, 2247–2256.
Nesbitt, H.W., MacRae, N.D., Shotyk, W., 1991. Congruent and incongruent dissolution of labradorite in dilute, acidic, salt solutions. Author(s): H. W. Nesbitt, N. D. MacRae and W. Shotyk Source: The Journal of Geology, 99, No. 3 (May, 1991), pp. 429–442 Published by: The University of Chicago Press Stable URL: http://www.jstor.org/stable/30062626 Accessed: 14-03-2016 04:47 UTC. J. Geol. 99 (3), 429–442.
Nugent, M.A., Brantley, S.L., Pantano, C.G., Maurice, P.A., 1998. 8 (ng/l-1). Nature 395 (8), 588–591.
Oelkers, E.H., Schott, J., 1995. Experimental study of anorthite dissolution and the relative mechanism of feldspar hydrolysis. Geochim. Cosmochim. Acta 59 (24), 5039–5053.
Oelkers, E.H., Schott, J., 1998. Does organic acid adsorption affect alkali-feldspar dissolution rates? Chem. Geol. 151 (1), 235–245.
Onstott, T.C., Hinton, S.M., Silver, B.J., King Jr., H.E., 2010. Coupling hydrocarbon degradation to anaerobic respiration and mineral diagenesis: theoretical constraints. Geobiology 8 (1), 69–88.
Palandri, J.L., Kharaka, Y.K., 2004. A Compilation of Rate Parameters of Water-Mineral Interaction Kinetics for Application to Geochemical Modeling. Geological Survey, Menlo Park, CA.
Pan, C., Jiang, L., Liu, J., Zhang, S., Zhu, G., 2010. The effects of calcite and montmorillonite on oil cracking in confined pyrolysis experiments. Org. Geochem. 41, 611–626.
Parsons, I., Thompson, P., Lee, M.R., Cayzer, N., 2005. Alkali feldspar microtextures as provenance indicators in siliciclastic rocks and their role in feldspar dissolution during transport and diagenesis. J. Sediment. Res. 75 (5), 921–942.
Purvis, K., 1995. Diagenesis of lower Jurassic sandstones, Block 211/13 (Penguin Area), UK northern North Sea. Mar. Pet. Geol. 12 (2), 219–228.
Putnis, A., 2014. Why mineral interfaces matter. Science 343 (6178), 1441–1442.
Ribbe, P.H., 1994. The Crystal Structures of the Aluminum-Silicate FeldsparsFeldspars and Their Reactions. Springer, pp. 1–49.
Rogers, J.R., Bennett, P.C., 2004. Mineral stimulation of subsurface microorganisms: release of limiting nutrients from silicates. Chem. Geol. 203 (1–2), 91–108.
Rogers, J.R., Bennett, P.C., Choi, W.J., 1998. Feldspars as a source of nutrients for microorganisms. Am. Mineral. 83, 1532–1540.
Ruizagudo, E., King, H.E., Olópez, L.P., Putnis, C.V., Geisler, T., 2016. Control of silicate weathering by interface-coupled dissolution-precipitation processes at the mineral-solution interface. Geology 44 (7), 567–570.
Ruiz-Agudo, E., Putnins, C.V., Rodriguez-Navarro, C., Putnis, A., 2012. Mechanism of leached layer formation during chemical weathering of silicate minerals. Geology 40 (10), 947–950.
Ruiz-Agudo, E., et al., 2016. Control of silicate weathering by interface-coupled dissolution-precipitation processes at the mineral-solution interface. 44 (7), 567–570.
Schmidt, V., A, M.D., 1979. The role of secondary porosity in the course of sandstone diagenesis. SEPM Spec. Publ. 26, 175–207.
Schweda, P., 1990. Kinetics and Mechanisms of Alkali Feldspar Dissolution at Low Temperatures. Medd./Miner. Inst., Stockholm, pp. 99.
Schweda, P., 1989. Proceedings of the Sixth International Symposium on Water/Rock Interaction. In: Milne, D.L. (Ed.), A.A. Balkema, Rotterdam, pp. 609–612 (Data given in Crundwell (2015a)).
Seewald, J.S., 2001. Aqueous geochemistry of low molecular weight hydrocarbons at elevated temperatures and pressures: constraints from mineral buffered laboratory experiments. 65 (10), 1641–1664.
Seewald, J.S., 2003. Organic-inorganic interactions in petroleum-producing sedimentary basins. Nature 426 (6964), 327–333.
Seiffert, F., Bandow, N., Bouchez, J., von Blanckenburg, F., Gorbushina, A.A., 2014. Microbial colonization of bare rocks: laboratory biofilm enhances mineral weathering. Proc. Earth Planet. Sci. 10, 123–129.
Smith, J.T., Ehrenberg, S.N., 1989. Correlation of carbon dioxide abundance with temperature in clastic hydrocarbon reservoirs: relationship to inorganic chemical equilibrium. Mar. Pet. Geol. 6 (2), 129–135.
Steefel, C.I., Lasaga, A.C., 1994. A coupled model for transpot of multiple chemical species and kinetic precipitation dissolution reactions. Am. J. Sci. 294 (5), 529–592.
Steefel, C.I., Van Cappellen, P., 1990. A new kinetic approach to modeling water-rock interaction: the role of nucleation, precursors, and Ostwald ripening. Geochim. Cosmochim. Acta 54 (10), 2657–2677.
Steefel, C., Depaolo, D., Lichtner, P., 2005. Reactive transport modeling: an essential tool and a new research approach for the Earth sciences. Earth Planet. Sci. Lett. 240 (3–4), 539–558.
Stillings, L.L., Brantley, S.A., 1995. Feldspar dissolution at 25°C and pH 3: reaction stoichiometry and the effect of cations. Geochim. Cosmochim. Acta 59, 1483–1496.
Stoessell, R.K., D, P.E., 1990. Secondary porosity revisited_ the chemistry of feldspar dissolution by carboxylic acids and anions. AAPG Bull. 74 (12), 1795–1805.
Surdam, R.C., Crossey, L.J., 1987. Integrated diagenetic modeling: a process-oriented approach for clastic systems. Annu. Rev. Earth Planet. Sci. 15 (1), 141–170.
Surdam, R.C., Boese, S.W., Crossey, L.J., 1984. The Chemistry of Secondary Porosity: Part 2. Aspects of Porosity Modification. pp. 127–149.
Taboada, T., García, C., 1999. Pseudomorphic transformation of plagioclases during the weathering of granitic rocks in Galicia (NW Spain). Catena 35 (2), 291–302.
Tardy, Y., 1971. Characterization of the principal weathering types by the geochemistry of waters from some European and African crystalline massifs. Chem. Geol. 7 (4), 253–271.
Taylor, T.R., Land, L.S., 1996. Association of Allochthonous Waters and Reservoir Enhancement in Deeply Buried Miocene Sandstones: Picaroon Field, Corsair Trend, Offshore Texas. Siliciclastic Diagenesis and Fluid Row Concepts and Applications. Vol. 55. SEPM Special Publication, pp. 37–48.
Taylor, T.R., et al., 2010. Sandstone diagenesis and reservoir quality prediction: models, myths, and reality. AAPG Bull. 94 (8), 1093–1132.
Thyne, G., 2001. A model for diagenetic mass transfer between adjacent sandstone and shale. Mar. Pet. Geol. 18, 743–755.
Thyne, G., Boudreau, B.P., Ramm, M., Midtbø, R.E., 2001. Simulation of potassium feldspar dissolution and illitization in the Statfjord Formation, North Sea. AAPG Bull. 85 (4), 621–637.
Tian, H., Wang, Z., Xiao, Z., Li, X., Xiao, X., 2006. Oil cracking to gases: kinetic modeling and geological significance. Chin. Sci. Bull. 51 (22), 2763–2770.
Turchyn, A.V., Depaolo, D.J., 2011. Calcium isotope evidence for suppression of carbonate dissolution in carbonate-bearing organic-rich sediments. Geochim. Cosmochim. Acta 75, 7081–7098.
Tutolo, B.M., Luhmann, A.J., Kong, X., Saar, M.O., Seyfried, W.E., 2015. CO_2 sequestration in feldspar-rich sandstone: coupled evolution of fluid chemistry, mineral reaction rates, and hydrogeochemical properties. Geochim. Cosmochim. Acta 160, 132–154.
van Berk, W., Schulz, H., Fu, Y., 2013. Controls on CO_2 fate and behavior in the Gullfaks oil field (Norway): how hydrogeochemical modeling can help decipher organic-inorganic interactions. AAPG Bull. 97 (12), 2233–2255.
van Berk, W., Fu, Y., Schulz, H.M., 2015. Porosity Creation in Carbonate Reservoirs by Pre-Oil Charging With Source Rock-Derived Corrosive Fluids: One-Dimensional Reactive Mass Transport Modeling. Pet. Geosci. 21, 35–42.
Vazquez, F.M., 1981. Formation of gibbsite in soils and saprolites of temperate–humid zones. Clay Miner. 16 (1), 43–52.
Walderhaug, O., 1990. A fluid inclusion study of quartz cemented sandstones from

offshore mid-Norway possible evidence for continued quartz cementation during oil emplacement. J. Sediment. Petrol. 60 (2), 203–210.
Wang, T., Wang, H., Zhang, F., Xu, T., 2013. Simulation of CO_2–water–rock interactions on geologic CO_2 sequestration under geological conditions of China. Mar. Pollut. Bull. 76 (1–2), 307–314.
Weise, A.M., Nalewajko, C., Lee, K., 1999. Oil-mineral fine interactions facilitate oil biodegradation in seawater. Environ. Technol. 20, 811–824.
Welch, S.A., Ullman, W.J., 1993. The effect of organic acids on plagioclase dissolution rates and stoichiometry. Geochim. Cosmochim. Acta 57 (12), 2725–2736.
Welch, S.A., Ullman, W.J., 1996. Feldspar dissolution in acidic and organic solutions: compositional and pH dependence of dissolution rate. Geochim. Cosmochim. Acta 60 (16), 2939–2948.
Welch, S.A., Ullman, W.J., 2000. The temperature dependence of bytownite feldspar dissolution in neutral aqueous solutions of inorganic and organic ligands at low temperature (5–35 °C). Chem. Geol. 167, 337–354.
Wigley, M., Dubacq, B., Kampman, N., Bickle, M., 2013. Controls of sluggish, CO_2-promoted, hematite and K-feldspar dissolution kinetics in sandstones. Earth Planet. Sci. Lett. 362, 76–87.
Wilkinson, M., Milliken, K.L., Haszeldine, R.S., 2001. Systematic destruction of K-feldspar in deeply buried rift and passive margin sandstones. J. Geol. Soc. 158 (4), 675–683.
Williams, J.Z., Bandstra, J.Z., Pollard, D., Brantley, S.L., 2010. The temperature dependence of feldspar dissolution determined using a coupled weathering–climate model for Holocene-aged loess soils. Geoderma 156 (1–2), 11–19.
Wollast, R., 1967. Kinetics of the alteration of K-feldspar in buffered solutions at low temperature. Geochim. Cosmochim. Acta 31 (4), 635–648.
Xi, K., et al., 2018. Authigenic minerals related to wettability and their impacts on oil accumulation in tight sandstone reservoirs: an example from the lower cretaceous Quantou Formation in the southern Songliao Basin, China. J. Asian Earth Sci. https://doi.org/10.1016/j.jseaes.2018.04.025.
Xiao, Q., Sun, Y., Zhang, Y., 2010. The role of reservoir mediums in natural oil cracking: preliminary experimental results in a confined system. Chin. Sci. Bull. 55 (33), 3787–3793.
Xu, T., Apps, J.A., Pruess, K., 2005. Mineral sequestration of carbon dioxide in a sandstone–shale system. Chem. Geol. 217 (3), 295–318.
Yang, Y., Min, Y., Jun, Y.S., 2013. A mechanistic understanding of plagioclase dissolution based on Al occupancy and T–O bond length: from geologic carbon sequestration to ambient conditions. Phys. Chem. Chem. Phys. 15 (42), 18491–18501.
Yang, Y., Min, Y., Jun, Y., 2014a. Effects of Al/Si ordering on feldspar dissolution: part II. The pH dependence of plagioclases' dissolution rates. Geochim. Cosmochim. Acta 126, 595–613.
Yang, Y., Min, Y., Lococo, J., Jun, Y., 2014b. Effects of Al/Si ordering on feldspar dissolution: part I. Crystallographic control on the stoichiometry of dissolution reaction. Geochim. Cosmochim. Acta 126, 574–594.
Yuan, G., et al., 2015a. Feldspar dissolution, authigenic clays, and quartz cements in open and closed sandstone geochemical systems during diagenesis: typical examples from two sags in Bohai Bay Basin, East China. AAPG Bull. 99 (11), 2121–2154.
Yuan, G., et al., 2015b. Selective dissolution of feldspars in the presence of carbonates: the way to generate secondary pores in buried sandstones by organic CO_2. Mar. Pet. Geol. 60, 105–119.
Yuan, G., Cao, Y., Gluyas, J., Jia, Z., 2017a. Reactive transport modeling of coupled feldspar dissolution and secondary mineral precipitation and its implication for diagenetic interaction in sandstones. Geochim. Cosmochim. Acta 207, 232–255.
Yuan, G., Cao, Y., Zhang, Y., Gluyas, J., 2017b. Diagenesis and reservoir quality of sandstones with ancient “deep” incursion of meteoric freshwater——an example in the Nanpu Sag, Bohai Bay Basin, East China. Mar. Pet. Geol. 82, 444–464.
Yuan, G., Cao, Y., Gluyas, J., Cao, X., Zhang, W., 2018. Petrography, fluid inclusion, isotope and trace element constraints on the origin of quartz cementation and feldspar dissolution and the associated fluid evolution in arkosic sandstones. AAPG Bull. 102 (5), 761–792.
Yuan, G., et al., 2019. Coupled mineral alteration and oil degradation in thermal oil-water-feldspar systems and implications for organic-inorganic interactions in hydrocarbon reservoirs. Geochim. Cosmochim. Acta 248, 61–87.
Zhu, C., 2005. In situ feldspar dissolution rates in an aquifer. Geochim. Cosmochim. Acta 69 (6), 1435–1453.
Zhu, C., Lu, P., 2009. Alkali feldspar dissolution and secondary mineral precipitation in batch systems: 3. Saturation states of product minerals and reaction paths. Geochim. Cosmochim. Acta 73 (11), 3171–3200.
Zhu, C., Blum, A.E., Veblen, D.R., 2004. A new hypothesis for the slow feldspar dissolution in groundwater aquifers [C]. Geochim. Cosmochim. Acta 68 (11), A148 The Boulevard, Langford Lane, Kidlington, Oxford OX5 1GB, England: Pergamon-Elsevier Science Ltd.
Zhu, C., Lu, P., Zheng, Z., Ganor, J., 2010. Coupled alkali feldspar dissolution and secondary mineral precipitation in batch systems: 4. Numerical modeling of kinetic reaction paths. Geochim. Cosmochim. Acta 74 (14), 3963–3983.
Zhu, C., Liu, Z., Schaefer, A., Wang, C., Zhang, G., 2014. Silicon isotopes as a new method of measuring silicate mineral reaction rates at ambient temperature. Proc. Earth Planet. Sci. 10, 189–193.